Titre: Title:	Excimer laser-induced removal of particles from silicon surfaces
Auteur: Author:	Xioguang Wu
Date:	2000
Type:	Mémoire ou thèse / Dissertation or Thesis
Référence: Citation:	Wu, X. (2000). Excimer laser-induced removal of particles from silicon surfaces [Thèse de doctorat, École Polytechnique de Montréal]. PolyPublie. https://publications.polymtl.ca/27746/

UNIVERSITÉ DE MONTRÉAL

EXCIMER LASER-INDUCED REMOVAL OF PARTICLES FROM SILICON SURFACES

XIAOGUANG WU

DÉPARTEMENT DE GÉNIE PHYSIQUE ET DE GÉNIE DES MATÉRIAUX

ÉCOLE POLYTECHNIQUE DE MONTRÉAL

THÈSE PRÉSENTÉE EN VUE DE L'OBTENTION
DU DIPLÔME DE PHILOSOPHIAE DOCTOR (Ph.D.)
(GÉNIE PHYSIQUE)
MAY 1999

UNIVERSITÉ DE MONTRÉAL

ÉCOLE POLYTECHNIQUE DE MONTRÉAL

Cette thèse intitulée:

EXCIMER LASER-INDUCED REMOVAL OF PARTICLES FROM SILICON SURFACES

présentée par: WU Xiaoguang

en vue de l'obtention du diplôme de: Philosophiae Doctor

a été dûment acceptée par le jury d'examen constitué de:

M. YELON Arthur ,	Ph.D., président
M. MEUNIER Michel,	Ph.D., membre et directeur de recherche
M. SACHER Ed,	Ph.D., membre et co-directeur de recherche
M. ELLIS H. Thomas ,	Ph.D., membre
M. BUSNAINA Ahmed,	Ph.D., membre

To my wife Nan Zhang

and

the memory of my father

ACKNOWLEDGMENTS

The successful completion of this thesis critically depended on the countless contributions from people throughout my academic life, including my formative years as an undergraduate and graduate student at Shandong University. I am forever in debt to the many people who provided me with friendship and comradeship, whom I cannot acknowledge by name.

Of great benefit during my years in the Ph.D. program was having Michel Meunier and Ed Sacher as my research advisors. I admire their talent, ability, consideration, thoughtfulness, and integrity. It was a real boon to learn from them and to work with them. They have always been approachable, friendly, patient, and ready to discuss and advise with great insight. I am sincerely grateful to them and attribute what I have accomplished during my Ph.D. study to their supervision, support, and mentorship.

I am equally grateful to many current and former students and researchers who gave much needed assistance to this project. Samir Boughaba helped me familiarize myself with experimental equipment and procedures in my first year; Mingkun Shi and Félix Beaudoin made many important suggestions on processing details. In addition, Steve Guétré shared both time and cleaning of the clean room, and help me to translate the abstract and conclusion into French.

I am grateful to the staffs in the various laboratories, whose diligent efforts in maintaining and improving the performance of the lots of complicated equipment has been instrumental in the completion of this project. I would like to thank J. P. Lévesque for his technical assistance throughout this project, Kostas Piyakis for his aid in the design of the computer interface and in the analysis of the data, and Suzie Poulin for her help in analyzing surface properties by XPS and AFM.

I am also grateful to the Natural Sciences and Engineering Research Council of Canada for supporting my work.

I am grateful to jury Authur Yelon, Thomas H. Ellis and Ahmed Busnaina for reading this thesis and giving judicious comments.

I wish to thank my family, my mother, my sister, as well as my mother-in-law, for their unconditional love, patience, understanding and encouragement. They have helped me to take care of my children so I could spend more time on my studies.

Finally, my deep thanks must go to my wife, Nan; she has always been with me in love, and has comforted, motivated and energized me. In addition, my two sweet daughters, Mengyou and Mengya, cheered me on and made numerous adjustments so I could

accomplish this goal. It is very clear that I would not be where I am today without their love, encouragement, and affection. "Thanks," from my heart!

RESUMÉ

L'enlèvement de particules sous-micronique de la surface d'un semiconducteur est une tâche qui pose d'énormes défis à l'industrie de la micro-électronique. Le nettoyage laser démontre un grand potentiel pour accomplir cette tâche à cause de sa grande efficacité, sa simplicité, sa compatibilité au " cluster tools ", sa rapidité et son coût. Cette thèse explore les aspects théoriques et expérimentaux du nettoyage par laser excimer.

Un laser excimer pulsé KrF a été utilisé pour enlever plusieurs types de particules sous-microniques d'une surface de silicium hydrophile. Presque toutes les particules de polystyrène latex (PSL) et carboxylate-modifié latex (CML), de 0.1 micron et plus, sont enlevées des surfaces de silicium par nettoyage sec, l'énergie du substrat étant transféré directement aux particules. Pour des particules de SiO_2 et d'Al_2O_3, la plus grande efficacité de nettoyage est obtenue par nettoyage vapeur, l'énergie du laser étant transféré à une couche d'eau qui explose en vapeur. Les seuils de nettoyage sont déterminés pour tous ces types de particules pour un nettoyage sec et vapeur.

Une nouvelle technique, la thermophorésis, est utilisée pour prévenir la recontamination de la surface par les particule éjectées. Cette technique a grandement amélioré l'efficacité du nettoyage des particules de PSL. Elle est par rapport à d'autres techniques comme le flux laminaire, plus simple à utiliser et plus efficace.

Nous avons observé et expliqué la naissance d'ondes photo-acoustiques (PAW) pendant le nettoyage laser (sec et vapeur). Les résultats des mesures PAW etnettoyage laser démontrent que la région sent un pulse thermoélastique seulement et couplage énergie du pulse thermoélastique aux particules est la plus grante efficacité. L'enlevement de particules organiques pour le nettoyage sec fut limiteré dans le région sent; la pression causée par la création de bulles est dominant pour l'enlèvement des particules d'oxyde inorganique durant le nettoyage vapeur. Il existe dans le région sent seulement.

Plusieurs modèles sont développés pour calculer les forces d'adhésion entre la surface du substrat et les particules et les forces d'enlèvement induites par le pulse de laser. La force de van der Waals est dominante pour l'adhésion des particules organiques au substrat. La liaison hydrogène contribue principalement à l'adhésion des particules inorganiques à la surface du substrat. Pendant le nettoyage vapeur, ces deux forces d'adhésion sont grandement réduites par l'écrantage et par la rupture des chaînes de ponts hydrogène.

L'augmentation de la température du substrat induite par le laser est calculée à l'aide de l'équation de transfert de chaleur à 1 dimension. Les forces d'enlèvement provenant de l'expansion thermique rapide du substrat due à l'effet thermoélastique, et le choc de pression dû à la création de bulles dans le film d'eau condensé, sont calculés. Une situation avec des particules réelles (i.e. rugosité, formes irrégulières) est considérée.

L'analyse théorique inclue les effets d'aspérités en surface des particules et l'agrégation de celles-ci. Les résultats de ces calculs montrent que la rugosité de la surface d'une particule, qui est relativement petite par rapport à la dimension d'une particule, cause une réduction importante des forces d'adhésion et de l'effet thermoélastique, ce qui est consistant avec les observations expérimentales.

ABSTRACT

The efficient removal of submicron-sized particles from semiconductors surface is one of the most challenging tasks the microelectronics industry must face. Laser cleaning demonstrates a high potential for this task because of high efficiency, simplicity, conformability to cluster tools, speed and low cost. This thesis addresses both experimental and theoretical aspects of the excimer laser cleaning technique.

A pulsed KrF excimer laser was used to remove several types of submicron-sized particles from hydrophilic silicon surfaces. Almost all polystyrene latex (PSL) and carboxylate-modified latex (CML) particles, 0.1 μm and larger, were removed from silicon surfaces by dry laser cleaning, in which energy from the substrate is transferred directly to the particles. High cleaning efficiencies for SiO_2 and Al_2O_3 particles were obtained by steam laser cleaning, in which energy from the substrate is transferred to a coupling liquid. The laser cleaning thresholds were defined and measured for these kinds of particles during dry and steam cleaning.

A new technique, thermophoresis, was introduced to prevent the recontamination of emitted particles; this technique have greatly improved the cleaning efficiency of PSL particles during dry cleaning. Compared with other techniques, such as laminar flow, thermophoresis is simpler to establish and has a higher cleaning efficiency.

Photoacoustic wave (PAW) signals generated during laser dry and steam cleaning were monitored. The PAW measurement and laser cleaning results showed that only the irradiated area suffers a thermoelastic pulse. Energy coupling from the thermoelastic pulse to the particles is more efficient then, the removal of organic particles during dry cleaning was localized in the laser beam. The shock pressure induced by bubble generation is the dominant factor in the removal of inorganic oxide particles during steam cleaning, which also only occurred in the laser beam.

Several models have been developed to calculate the adhesion forces between the particles and substrate surfaces and the removal forces induced by the laser pulse. The van der Waals force with deformation is the dominant adhesion force holding organic particles to the surfaces. Hydrogen bonding is the major contributor to the adhesion of inorganic particles to substrate surfaces. During steam cleaning, these two adhesion forces are greatly reduced by both the shielding effect and hydrogen bond chain breaking.

The temperature increases in substrates, induced by the laser pulse, were calculated by the one-dimensional heat transfer equation. The removal forces arising from the rapid thermal expansion of the substrate due to the thermoelastic effect, and the pressure shock due to bubble generation in the condensed water film, were calculated. The situation of practical (i. e., rough, irregularly shaped) particles has been considered, and the

theoretical analysis includes the effects of both asperities on the particle surface and particle aggregation. The results of the calculations show that particle surface roughnesses which are small compared with the particle dimension can cause a large reduction in both adhesion and thermoelastic removal forces, consistent with the experimental observations.

CONDENSÉ EN FRANÇAIS

Dans le premier chapitre de cette thèse, nous avons présenté une vue d'ensemble des divers aspects de la contamination des gaufres de semiconducteurs : discussion des types de contaminants, leurs origines et les effets sur la qualité et le rendement des dispositifs semiconducteurs. Une compréhension des principes sous-jacents de ces divers disciplines est importante pour résoudre avec succès les problèmes de nettoyage de gaufres en laboratoires et en industries. Plusieurs technologies qui sont associées au nettoyage des gaufres sont brièvement commentées. Ces technologies incluent des méthodes chimiques et physiques. Leurs avantages et désavantages (ou limitations) ont également été présentés.

Le développement du nettoyage laser est revu dans ce chapitre. Les lasers Nd:YAG, Er:YAG, CO_2 et excimer pulsés ont été utilisés pour enlever, par nettoyage sec ou vapeur, des particules micronique et sous-micronique d'une surface solide. Ces lasers agissent sur différents matériaux, soit les particules, le substrat ou le film de liquide, selon la longueur d'onde du laser et l'absorption des matériaux. Parmi toutes ces techniques de nettoyage laser, le nettoyage vapeur avec laser excimer est la plus efficace pour nettoyer les plus petites particules. Une revue des études théoriques sur l'adhésion et l'enlèvement des particules est présentée. Les forces d'adhésion qui retiennent une particule à un substrat sont les forces de van der Waals, les forces électrostatiques, les

forces capillaires et les liens chimiques. On croît que les liens chimiques jouent un rôle important dans l'adhésion des particules sur une surface de silicium. Cependant, il y a peu d'analyses quantitatives sur l'adhésion des particules par liens chimiques. Pour le nettoyage vapeur, les forces d'enlèvement proviennent de l'effet thermoélastique et de l'explosion évaporatoire. Il y a peu de descriptions directes sur les forces d'enlèvement provenant de la création de bulles dans un film liquide. Nous détaillons également dans ce chapitre le but de cette recherche, qui est de développer une méthode expérimentale et des modèles théoriques pour comprendre l'adhésion des particules et son enlèvement durant le nettoyage laser.

Dans le deuxième chapitre, nous avons présenté les résultats de l'enlèvement, sur une surface de silicium, de particules de PSL de 0.1 μm, de CML de 0.2 μm et de particules de SiO_2 et d'Al_2O_3 de 0.1 μm par nettoyage sec et vapeur. Une efficacité remarquable est atteinte pour l'enlèvement, par nettoyage sec, des particules de PSL et de CML. Pour des particules de SiO_2, on observe une haute efficacité de nettoyage seulement avec un nettoyage vapeur car l'explosion évaporatoire du liquide déposé génère des forces d'enlèvement additionnelles. Une nouvelle technique est introduite, la thermophorésie, utilisée pour prévenir la recontamination de la surface par les particules éjectées. Des calculs théoriques montrent que la force themophorétique agissant sur des particules de 0.5 μm et moins est beaucoup plus grande que la gravité. De cette façon, on calcul que le

mécanisme de recontamination principale, la fluctuation de l'air, peut être vaincue et une majorité des particules ne pourront recontaminer la surface nettoyée. Les résultats expérimentaux ont vérifés ces prédictions théoriques; ceci permet une plus grande efficacité pour le nettoyage sec. Une comparaison est effectuée avec la technique du flux laminaire. La thermophorésie, qui est induite par une lampe infrarouge a l'avantage d'être simple a réaliser pour une grande efficacité de nettoyage.

Dans le troisième chapitre, des mesures PAW sont présentés en détail. Lors des mesures d'onde photoacoustique (PAW), les vibrations de surface induites par les pulses de laser sont étudiées. Ces mesures ont montré que le nettoyage vapeur génère des signaux PAW plus grand que le nettoyage sec. Ces résultats nous aident à comprendre les mécanismes du procédé de nettoyage laser. En variant la fluence du laser et la position de détection sur la gaufre, les résultats PAW suggèrent que le région sent un pulse thermoélastique seulement et couplage énergie du pulse thermoélastique aux particules est la plus grante efficacité, l'enlevement de particules organiques pour le nettoyage sec fut limiteré dans le région sent; la pression causée par la création de bulles est dominant pour l'enlèvement des particules d'oxyde inorganique durant le nettoyage vapeur. Il existe dans le région sent seulement.

Dans le quatrième chapitre, un bref calcul a montré que les forces de van der Waals entre des particules d'oxyde et la surface de silicium sont plus petite que celles des particules

de PSL à cause d'une surface de contact plus petite. Ceci est en contradiction avec les résultats expérimentaux de nettoyage sec et vapeur. Ainsi, nous croyons que le pont hydrogène entre les particules d'oxyde inorganique et une surface hydrophile de silicium sont très importants.

Dans la deuxième section, un modèle est développé pour calculer les forces d'adhésion dues au pont hydrogène, entre des particules inorganiques et une surface de silicium hydrophile. Dans ce modèle, les particules adhèrent à une surface soit directement par un seul pont hydrogène ou indirectement par une chaîne de liens hydrogènes. Pendant le nettoyage vapeur, une chaîne de liens hydrogènes peut être interrompu par des molécules d'eau, ce qui réduit considérablement les forces d'adhésion. Ce modèle explique bien les résultats expérimentaux où les particules de PSL s'enlève facilement par nettoyage sec mais où les particules de SiO_2 et d'Al_2O_3 sont seulement enlevées efficacement par nettoyage vapeur. Lorsque nous avons utilisé de l'alcool comme agent partiel de dispersion au lieu de l'eau, l'efficacité du nettoyage vapeur des particules de SiO_2 et de Al_2O_3 a été grandement réduite. L'alcool forme des onts hydrogène qui interagis sent plus fortement avec les particules et il est plus difficile de les interrompre par des molécules libres d'eau durant le nettoyage vapeur.

Dans la troisième section, nous présentons des résultats expérimentaux du nettoyage vapeur et sec de particules PSL, CML, SiO_2 et Al_2O_3 sous-micronique, sur une surface

de silicium hydrophile. Les seuils de nettoyage sont déterminés pour toutes ces particules. Pour des particules de PSL de 0.1 micron, le seuil du nettoyage sec est établies à 76 mJ/cm^2, beaucoup plus bas que les conditions optimales de nettoyage établies à 340 mJ/cm^2. Pour des particules d'Al_2O_3 et de SiO_2, le seuil est le même à 143 mJ/cm^2 pour un nettoyage vapeur. Cette valeur est très près des conditions optimales de nettoyage et correspond à la plus basse valeur de fluence laser qui induit une explosion évaporatoire du film de liquide.

De plus, dans cette section, plusieurs modèles sur l'adhésion d'une particule sont utilisés pour expliquer les résultats expérimentaux. La force d'adhésion principale pour les particules organiques comme le PSL est la force de van der Waals. Des ponts hydrogènes sont responsables de l'adhésion des particules d'oxyde métallique comme l'Al_2O_3. Il y a une réduction des forces d'adhésion en déposant un film d'eau à la surface du substrat. Ce film brise les liens hydrogènes et à un effet d'écrantage sur la force de van der Waals.

L'équation uni-dimensionelle du transfert de chaleur est utilisé pour calculer la distribution de température sur le substrat; l'augmentation de température des particules et la perte de chaleur par convection et radiation du substrat sont négligées. En effet, les particules absorbent peu d'énergie du laser excimer et les pertes de chaleur de la surface du substrat sont beaucoup plus petites que l'énergie du laser incident. L'effet

thermoélastique induit par les pulses de laser contribuent aux forces d'enlèvement pendant un nettoyage sec ou vapeur. Pour le nettoyage vapeur, une force additionnelle contribue à l'enlèvement de particules : la pression causée par la création de bulles. Un calcul montre que la force due à la création de bulles est plus grande que celle due à un effet thermoélastique.

Les agrégats de particules et les aspérités de surface d'une particule réduisent la force d'adhésion et d'enlèvement thermoélastique; cependant, ils n'ont pas d'effet sur la création de bulles. Le rayon effectif des particules, leur forme et les multiples points de contact sont pris en considération dans ce modèle. Il prédit que des particules avec différentes formes et rugosités de surface vont avoir une efficacité de nettoyage vapeur très différente. Les résultats de ces calculs montrent qu'il y a un bon accord avec les résultats expérimentaux.

Il résulte du travail contenu dans cette thèse les articles et les présentations suivantes:

(1) Boughaba S., Wu X., Sacher E. and Meunier M., Liquid Explosive Evaporation Removal of Submicron- sized particles from Silicon Surfaces, *Proc. 19th Annu. Mtg. Adhesion Soc.,* (Blacksburg, VA, 1996) p. 509.

(2) Boughaba S., Wu X., Sacher E. and Meunier M., Liquid Explosive Evaporation Removal of Submicron- sized particles from Silicon Surfaces, *J. Adhesion* **61**, 293 (1997).

(3) Wu X., Sacher E. and Meunier M., Excimer Laser Induced Removal of Particles from Silicon Surfaces: Effects of Photoacoustic Waves, *Proc. 21th Annu. Mtg. Adhesion Soc.,* (Blacksburg, VA, 1998) p. 309.

(4) Wu X., Sacher E. and Meunier M., Excimer Laser induced Removal of Particles from Hydrophilic Silicon Surfaces, *J. Adhesion* **70**, 167 (1999).

(5) Wu X., Sacher E. and Meunier M., Photoacoustic Waves Emission during Laser Enhanced Particle Removal, *Proc. 22th Annu. Mtg. Adhesion Soc.,* (Blacksburg, VA, 1999) p. 309.

(6) Invited talk, Wu X., Sacher E. and Meunier M., Photoacoustic Waves Emission during Laser Enhanced Particle Removal, Adhesion Sociaty Meeting, Panania City Beach, FL, Feb. 21-24, 1999.

(7) Wu X., Sacher E. and Meunier M., The Effects of Hydrogen Bonds on the Adhesion of Inorganic Oxide Particles On Hydrophilic silicon Surfaces, J. Appl. Phys., **86**, 1744 (1999).

(8) Wu X., Sacher E. and Meunier M., The Modeling of Excimer Laser Particle Removal from Hydrophilic Silicon Surfaces, J. Appl. Phys., submitted.

(9) Meunier M., Wu X., Sacher E., Beaudoin F., Simard-Normandin M., Excimer Laser Cleaning for Microelectronics: Modeling, Applications and Challenges, SPIE proceedings (Conference, San Jose, January 1999).

TABLE OF CONTENTS

DEDICATION iv

ACKNOWLEDGMENTS v

RESUMÉ viii

ABSTRACT xi

CONDENSÉ EN FRANÇAIS xiv

TABLE OF CONTENTS xxi

LIST OF TABLES xxv

LIST OF FIGURES xxvi

LIST OF SYMBOLS xxxiii

Chapter 1 INTRODUCTION 1

1.1 Importance of Cleaning Wafer Surfaces 1

1.2 Types, Origins and Effects of Contaminants 2

1.3 Traditional Cleaning Methods 4

1.3.1 Wet-chemical etching 4

1.3.2 Vapor-phase cleaning techniques 7

1.3.3 Brush scrubbing, fluid jet, and ultrasonic techniques 8

1.4 Laser Cleaning Techniques 9

1.4.1 Advantages of laser cleaning 9

1.4.2 Dry laser cleaning 11

1.4.3 Steam laser cleaning 12

1.5 Theoretical Models of Laser Cleaning 14

1.6 Objective of This Thesis 16

1.7 References 19

Chapter 2 EXCIMER LASER CLEANING SYSTEM AND RESULTS 23

2.1 Experimental System and Procedures of Excimer Laser Cleaning 23

2.1.1 Experimental setup 23

2.1.2 Pretreatment of the silicon wafer surface 26

2.1.3 Particle deposition 26

2.1.4 Particle measurement system 27

2.1.5 Selection of the liquid and the liquid film thickness measurement system 28

2.2 Experimental Results of Excimer Laser Cleaning 31

2.3 Thermophoresis: Applications for Preventing Particle Recontamination 32

2.3.1 Thermophoretic force 40

2.3.2 Thermophoresis and laminar flow experiments. 43

2.3.3 Results and discussion 44

2.4 References 47

Chapter 3 PHOTOACOUSTIC WAVE EMISSION DURING LASER-

ENHANCED PARTICULATE REMOVAL 49

3.1 Introduction 49

3.2 Experimental Arrangement and Procedure..... 49

3.3 Results and Discussion 51

3.4 References 56

Chapter 4 THEORETICAL MODELING OF EXCIMER LASER CLEANING 58

4.1 Introduction 58

4.1.1 Dominant adhesion forces between the particles and substrate surfaces 58

4.1.2 References 63

4.2 The Effects of Hydrogen Bonds on the Adhesion of Inorganic Oxide Particles on Hydrophilic Silicon Surfaces 65

4.2.1 Introduction 66

4.2.2 Experimental equipment and procedure 68

4.2.3 Laser cleaning results 69

4.2.4 Chemical bonds and adhesion forces 71

4.2.5 Conclusions 80

4.2.6 Acknowledgments 80

4.2.7 References 80

4.3 The Modeling of Excimer Laser Particle Removal from Hydrophilic

Silicon Surfaces 84

4.3.1 Introduction 85

4.3.2 Summary of excimer laser cleaning results and photoacoustic wave Measurements 87

4.3.3 Laser cleaning thresholds 90

4.3.4 Theoretical models of an ideal spherical particle on a smooth surface 91

4.3.4.1 Adhesion model 91

4.3.4.2 Model for dry laser cleaning 95

4.3.4.3 Model for steam laser cleaning 102

4.3.5 Theoretical models of practical particles on a practical silicon 109

4.3.5.1 Surface roughness and particle aggregation 109

4.3.5.2 Modified adhesion and laser cleaning models 112

4.3.6 Conclusions 117

4.3.7 Acknowledgment 118

4.3.8 References 118

Chapter 5 Conclusions and Future Directions 123

BIBLIOGRAPHY 132

Appendix Physical and chemical Properties of Si, SiO_2, Al_2O_3 and PSL 147

LIST OF TABLES

Chapter 1

1.1 The yield killers: killer density per critical mask level for 70% IC (chip) yield 2

1.2 Forms and types of contaminants 3

1.3 Sources of particles and contaminant films 4

1.4 Effects of contaminants 5

Chapter 2

2.1 Liquid properties 28

Chapter 4

4.1 The adhesion forces of 0.2 μm PSL and SiO_2 particles on the silicon surface 71

4.2 Laser cleaning thresholds for PSL, SiO_2 and Al_2O_3 particles and Damage threshold during dry and steam cleaning 90

4.3 The adhesion and removal forces for a 0.1 μm irregular Al_2O_3 or SiO_2 particles attached on silicon surface during steam cleaning with a laser flux of 150 mJ/cm^2 115

LIST OF FIGURES

Chapter 2

2.1 Experimental setup for excimer laser cleaning 23

2.2 Laser intensity distribution (a) before and (b) after the rectangular aperture 24

2.3 Optical interference setup 29

2.4 Interference photomicrographs of water vapor condensed onto a hydrophilic silicon surface after surface chemical pretreatment for (a) 10 min (b) two hours. The vapor burst duration was 0.1 second 30

2.5 PSL particle distribution maps (a) before and (b) after dry laser cleaning. (c) PSL particle densities before and after dry laser cleaning. The laser energy flux was 326 mJ/cm^2, 2 cleaning cycles 33

2.6 CML particle distribution maps (a) before and (b) after dry laser cleaning. (c) CML particle densities before and after dry laser cleaning. The laser energy flux was 363 mJ/cm^2, 1 cleaning cycles 34

2.7 SiO_2 particle distribution maps (a) before and (b) after dry laser cleaning. (c) SiO_2 particle densities before and after dry laser cleaning. The laser energy flux was 314 mJ/cm^2, 4 cleaning cycles 35

2.8 Al_2O_3particle distribution maps (a) before and (b) after dry laser cleaning. (c) Al_2O_3 particle densities before and after dry laser

cleaning. The laser energy flux was 326 mJ/cm^2, 4 cleaning cycles 36

2.9 SiO_2 particle distribution maps (a) before and (b) after steam laser cleaning. (c) SiO_2 particle densities before and after dry laser cleaning. The laser energy flux was 180 mJ/cm^2, 5 cleaning cycles 37

2.10 Al_2O_3particle distribution maps (a) before and (b) after steam laser cleaning. (c) Al_2O_3 particle densities before and after dry laser cleaning. The laser energy flux was 154 mJ/cm^2, 4 cleaning cycles 38

2.11 Distribution maps of unknown particle on as-received silicon wafer surface. (a) before and (b) after dry laser cleaning. The laser energy flux was 154 mJ/cm^2, 4 cleaning cycles 39

2.12 The thermophoretic force acting on 0.1 μm PSL particles at 60 °C as a function of the temperature gradient. (b) The thermophoretic force (solid line) and gravity (dash line) acting on PSL particles as a function of the particle diameter. The particles are at 60 °C and the temperature gradient is 10 K/cm 42

2.13 Schematic of the experimental system for thermophoresis during laser cleaning 43

2.14 Schematic of the experimental system for laminar flow during laser cleaning 44

2.15 The densities of 0.2 μm CML particles before and after dry laser cleaning: (a) the laser flux was 363 mJ/cm^2, 1 cleaning cycle, the temperature of wafer front surface was 62 °C and the 0.2 μm particle density was 410 cm^{-2}; (b) the laser flux was 363 mJ/cm^2, 4 cleaning cycles, the wafer was not heated, and the 0.2 μm particle density was 374 cm^{-2} 45

2.16 The densities of 0.2 μm CML particles before and after laser cleaning. The laser flux was 357 mJ/cm^2, 3 cleaning cycles. The nitrogen flow was 4223 ml/min. The 0.2 μm particle density was 420 cm^{-2} 47

Chapter 3

3.1 Experimental arrangement to demonstrate PAW generation and detection, and removal of PSL and Al_2O_3 particles by dry and steam cleaning 50

3.2 The photoacoustic wave signals : (a) dry laser cleaning at a laser energy flux of 195 mJ/cm^2; (b) steam laser cleaning at a flux of 187 mJ/cm^2; (c) dry laser cleaning at a flux of 310 mJ/cm^2 54

3.3 The peak-to-peak amplitude of PAW signal as a function of incident laser fluxes during dry and steam cleaning 55

3.4 The peak-to-peak amplitude of PAW signal as a function of the distance between the laser beam and the transducer located at the backside of the silicon wafer during dry cleaning with laser flux of 321 mJ/cm^2 55

Chapter 4

4.1 XPS spectra of C^{1s} peak, PSL particles deposited on hydrophilic silicon surfaces. (a) before laser cleaning, the concentration of C^{1s} is 25.26 % (b) after laser cleaning, laser flux is 220 mJ/cm^2, the concentration of C^{1s} is 21.57% 61

4.2 0.1 μm PSL, SiO_2 and Al_2O_3 particle densities before (gray bar) and after (white bar) laser cleaning. (a) During dry laser cleaning, the laser energy fluxes were 326, 314 and 326 mJ/cm^2, respectively, and 2, 4 and 4 cleaning scanning cycles, respectively were used. (b) During steam cleaning, the laser energy fluxes were 180 and 154 mJ/cm^2, respectively, and 5 and 4 cleaning scanning cycles were used, respectively 69

4.3 0.1 μm SiO_2 and Al_2O_3 particle densities before (gray bar) and after (white bar) steam laser cleaning, using methanol and ethanol instead of DI water during particle deposition. The laser energy flux was 204 mJ/cm^2, and 5 cleaning scanning cycles were used 70

4.4 Several examples of water hydrogen bonded to hydroxylated

surfaces. The dashed lines are hydrogen bonds 74

4.5 Indirect (a) and direct (b) hydrogen bonding between particle and substrate surfaces. The dashed lines are hydrogen bonds 74

4.6 $F_{H\text{-}bond}$ and $F_{van\ der\ Waals}$ as a function of particle diameters for SiO_2 and Al_2O_3 particles on the silicon surface during dry and steam cleaning 78

4.7 Postulated ways in which alcohol molecules may form hydrogen bonds with hydroxyl groups on SiO_2 and Al_2O_3 surfaces 79

4.8 Particle densities before (gray bar) and after (white bar) laser cleaning. During dry laser cleaning, the laser energy fluxes for PSL, SiO_2, Al_2O_3 and CML were 326, 314, 326 and 353 mJ/cm^2, respectively, and 2, 4, 4 and 2 cleaning scanning cycles were used, respectively. During steam cleaning, the laser energy fluxes for SiO_2 and Al_2O_3 were 180 and 154 mJ/cm^2, respectively, and 5 and 4 cleaning scanning cycles were used, respectively 88

4.9 The peak-to-peak amplitude of the PAW signal as a function of incident laser flux during dry and steam cleaning 89

4.10 The peak-to-peak amplitude of the PAW signal as a function of the distance between the laser beam and the the transducer located at the backside of the silicon wafer during dry cleaning with laser flux of 321 mJ/cm^2 90

4.11 Adhesion forces (van der Waals F_v and hydrogen bonding F_{chem}) of PSL and Al_2O_3 particles on hydrophilic silicon surface during dry and steam cleaning, as a function of particle diameter 96

4.12 Surface temperature of silicon substrate as a function of laser energy density. Points **a** and **b** give the laser damage thresholds for dry and steam cleaning, respectively 99

4.13 Thermal removal forces F_{them} and dominant adhesion forces (van der Waals F_v and hydrogen bonding F_{chem}) as a function of particles diameter for PSL and Al_2O_3 particles during dry cleaning at laser flux 320 mJ/cm^2 and 76 mJ/cm^2 (dry cleaning threshold for PSL particles) 101

4.14 Thermal removal force F_{them}, bubble removal force F_{bubble} and dominant adhesion force F_{chem} as functions of the particle diameter, for Al_2O_3 particles during steam cleaning with a laser flux of 150 mJ/cm^2 106

4.15 The bubble generation cleaning forces of Lu's and explosion models for 0.1 μm particle as function of the vapor pressure 107

4.16 Photomicrographs of 0.1 μm particles after deposition: (a) Al_2O_3 by SEM, (b) SiO_2 by SEM, (c) PSL by TEM 110

4.17 Particle densities before and after steam laser cleaning. (a) SiO_2 particles, laser energy flux of 180 mJ/cm^2, 5 cleaning cycles. (b)

Al_2O_3 particles, laser energy flux of 154 mJ/cm^2, 4 cleaning cycles 111

4.18 SEM photomicrographs of 0.1 μm colloidal SiO_2 particles 115

4.19 Colloidal SiO_2 particle densities before and after steam laser cleaning with laser energy flux 215 mJ/cm^2, 6 cleaning cycles 116

LIST OF SYMBOLS

A	Deformation contact radius of the particle on the surface (μm)
A	Chip area (cm^2)
B	Probability of the particle and the surface forming a hydrogen bond.
c	Transmit speed of the stress wave (m/s)
C_p	Specific heat (J/gK)
d_{bond}	Dissociation distance of a chemical bond (Å)
D	Density of OH group (OH/cm^2)
D_C	Diameter of the chamber (mm)
E	Young's modulus (GPa)
E_{bond}	Hydrogen bonding energy (eV)
E_{total}	Total chemical bond energy (eV)
f	Volume fraction of the vapor
F	Laser flux (mJ/cm^2)
F_{bubble}	Removal force due to bubble generation (mdyn)
F_c	Capillary force (mdyn)
F_{dl}	Double layer forces (mdyn)
F_{ei}	Electrostatic image force (mdyn)
$F_{H\text{-}bond}$, F_{chem}	Adhesion force due to hydrogen bonding (mdyn)
F_g	Gas flow (l/min)

F^G	Gravity (N)
F^T	Thermophoretic force (N)
$F_{thermal}$	Thermoelastic removal force (mdyn)
F_{vdw}, F_V,	Van der Waals force (mdyn)
$F^V{}_0$	Van der Waals force without deformation (mdyn)
$F^V{}_{deformation}$	Van der Waals force with deformation (mdyn)
H	Height of the chamber (mm)
h_c	Unit thermal conductance (W/m^2K).
$h\varpi_{132}$	Lifshitz-van der Waals constant (eV)
$I_0(t)$	Incident laser intensity (W/cm^2)
J_{conv}	Power flux lost convection with the ambient air (W/m^2)
J_{in}	Power flux flowing into the substrate (W/m^2)
J_{rad}	Power flux lost by radiation (W/m^2)
N	Average number of contact points between particle and surface
P_{atm}	Atmospheric pressure (KPa)
P_{over}	Overpressure (MPa)
$P_{reflect}$	Reflected pressure (MPa)
P_{shock}	Shock-generated pressure (MPa)
$P_v(T)$	Vapor pressure at temperature T (MPa)
$P_v(T_0)$	Ambient liquid pressure (MPa)
P_∞	Ambient liquid pressure (MPa)

R	Surface reflectivity
R_e	Reynolds number
r_p	Radius of the particle (μm)
r_e	Effective radius of the particles (asperity radius) (μm)
S	Total interaction area between particle and substrate (μm^2)
T	Time (μs)
T	Temperature (K)
T_0	Room temperature (K)
Δt	Time delay of PAW signal for two detection points (μs)
$(\nabla T)_\infty$	Temperature gradient over large distances (K/cm)
U	Zeta potential (V)
V	Average velocity of the gas flow (m/s)
V_{PAW}	Velocity of PAW signal (m/s)
W	Work of adhesion (eV)
Δx	Distance between two detection points (mm)
Y	Product yield
z	Cartesian coordinate normal to the substrate surface (μm)
z_0	Separation distance between particle and substrate (Å)
Δz	Height near the contact point of particle and substrate surface (Å)
α	Optical absorption coefficient (cm^{-1})

α_C	Angle between the point vertically from the center of the particle to the point of the liquid film contact with the particle
$\varepsilon 0$	Dielectric constant of free space
ε	Relative dielectric constant
γ	Linear thermal expansion coefficient (K^{-1})
γ^S	Surface free energy (eV)
η	Viscosity (Kg/sm)
κ	Thermal conductivity (W/mK)
κ_g, κ_s	Thermal conductivity of the gas and the sphere (W/K)
ν	Poisson's ratio
θ	Contact angle of the liquid on the particle
ρ	Density (g/cm^3)
σ_{liquid}	Liquid surface tension (mN/cm)
τ	Duration of laser pulse (ns)

Chapter 1

INTRODUCTION

1.1 Importance of Cleaning Wafer Surfaces

The importance of cleaning substrate surface during the fabrication of semiconductor microelectronics devices has been recognized since the dawn of solid-state device technology in the 1950s. It is well known that device performance, reliability and the product yield of silicon circuits are critically affected by chemical contaminants and particulate impurities present on the wafer or device surface. More than 50% of yield losses in integrated circuit fabrication are due to microcontamination caused by chemical impurities and particles [1]. The device yield decreases dramatically as chip area and defect density increase [2]. Effective techniques for cleaning silicon wafers, initially and after oxidation and patterning, are now more important than ever before because of the extreme sensitivity of the semiconductor surface and the submicron sizes of the device features. As a consequence, the preparation of ultraclean silicon wafers has become one of the key technologies in the fabrication of ULSI silicon circuits, such as 64MB, 256MB, and beyond, DRAM devices [3]. Table 1.1 shows the density of yield killer particles per critical mask level for manufacturing DRAM ICs from the 1MB device level to the 1GB device level, based on an IC chip yield of 70% [3]. The last column

shows that the defect density, or contamination must be reduced ~ 1000 times from 1MB device to 1GB device.

Table 1.1 The yield killers: killer density per critical mask level for 70% IC (chip) yield [3].

DRAM bits	**1MB**	**4MB**	**16MB**	**64MB**	**256MB**	**1GB**
Mask levels	12	14	16	18	20	22
IC area (cm^2)	0.60	0.90	1.50	2.45	3.85	6.10
CD (μm)	1.25	0.80	0.60	0.40	0.25	0.15
D (cm^2 per level) (size > 0.1 × CD)	0.05	0.028	0.015	0.008	0.0045	0.0025
D (cm^2 per level) (particle size > 0.125μm)	0.05	0.012	0.0035	0.0008	0.00018	0.000036

1.2 Types, Origins and Effects of Contaminants

Contaminants on semiconductor wafer surfaces occur in essentially three forms: contaminant films, discrete particles or clusters (groups of particles) and adsorbed gases. Surface contaminant films and particles can be classified as molecular compounds, ionic materials, and atomic species, as summarized in Table 1.2 [4].

The sources of contaminants are listed in Table 1.3 [4] and are seen to be manifold. Static charge built up on the wafers and carriers is a powerful mechanism of particle deposition, but is often overlooked and not properly dealt with.

The effects of contaminants on semiconductor materials and dielectrics during wafer processing, and the effects on the finished semiconductor devices, are complex and depend on the nature and quantity of a specific type of contaminant. A brief summary of contaminant effects is presented in Table 1.4 [4].

Table 1.2 Forms and types of contaminants [4].

Forms	Films, discrete particles, clusters, micro-droplets, vapors and gases	
Type	**Molecular**	Condensed organic vapors from lubricants, greases, photoresist, solvent residues, components from plastic storage containers, and metal oxides or hydroxides
	Ionic	Physically adsorbed and chemically bonded cations and anions from inorgnics; e.g. Na^+, Cl^-, SO_4^{-2}, fluoride species
	Atomic	Elemental metal films and particles; e.g. electrochemically plated Au, Ag, Cu films; particles of Si, Fe, Ni
	Gaseous	Adsorbed gases and vapors; generally of little practical consequence

Adsorbed gases and moisture have much less serious effects, but they can cause problems by outgasing in vacuum systems and affecting the quality of deposited films.

Table 1.3 Sources of particles and contaminants films [4]

	Mechanical	Gas piping
Equipment	Deposition systems	Metal tweezers
	Ion implanters	Liquid-containers
Humans	Factory operators	
	Process engineers	
	Liquid chemicals	Photoresists
Materials	Etchants	Air
	D.I. water	Gases
Processes	Combinations of all sources above	

1.3 Traditional Cleaning Methods

Many techniques for cleaning silicon wafers have been tried over the years, with various degrees of success. Some techniques are useful only for specific applications or may introduce undesirable side effects. For example, glow discharge techniques [5] such as plasma etching, effectively strip photoresist film but leave inorganic contaminants and metals behind. Various types of sputter-etching [5] can cause surface damage. The principal methods that the literature claims will remove particles that are less than 10 μm in diameter are given in following sections.

1.3.1 Wet-chemical etching

It is a chemical cleaning method that consists of dissolving unwanted substances on a surface [6]. The most common combination of chemicals used to etch the surface is the

RCA cleaning process [7]; it is still the dominant cleaning technique in use today. In the first treatment step, the mixture H_2O:H_2O_2:NH_4OH (5:1:1), known as "RCA standard clean 1 or SC-1", is used to remove organic surface contaminants by oxidative breakdown and dissolution. In the second treatment step, the solution known as "RCA standard clean 2 or SC-2", H_2O:H_2O_2: HCl (6:1:1) is used to remove metallic contaminants.

Table 1.4 Effects of contaminants [4]

Molecular types	Block and mask operations Reduce adhesion Form deleterious decomposition products Nucleate defects in films
Ionic types	Diffuse on surface, in bulk, at interfaces Cause electrical device defects Degrade device performance and yield Cause crystal defects Lower oxide breakdown field
Atomic types	Can diffuse readily Cause surface conduction Decrease minority-carrier lifetime Degrade electrical device performance Lower product yield Nucleate crystal defects Particles short-out conductor lines

The original RCA cleaning process was based on a simple immersion technique. Several different and improved variants have been introduced over the years. One is *Centrifugal Spray Cleaning* [8]. Hot SC-1, SC-2 and DI water are, in turn, pressure-fed into a mixing manifold and then directed as a dispersed spray onto the spinning wafers. The spin-rinsed wafers are dried by high-speed spinning in heated nitrogen. The cleaning efficiency for particles is higher than that of the immersion process. Another process is *Megasonic Cleaning* [9 – 12]. The wafers are submerged in the cleaning solution. Particles ranging in size from several micrometers down to 0.3 μm can be efficiently removed by acoustic streaming, resulted from the interaction of a 0.8 – 1.0 MHz megasonic wave with the cleaning solution of propagation or with a boundary layer near the wafer surface. The total input power is 150 W.

Wet-chemical cleaning has a number of inherent shortcoming which may limit its effectiveness in the fabrication of at least some future generation integrated circuits. First, a clear incompatibility exists between wet wafer cleaning operations and process integration in full-scale cluster tool processing [13]. Second, there are problems associated with the wet processing of high aspect ratio structures. The complications stem not from the difficulty of getting liquid into small openings, as this problem can be dealt with by using surfactants, but from the difficulty of getting it out [14]. Next, there is the difficulty of controlling particles during wafer treatments in liquid chemical and rinse/dry cycles. Finally, the cost of high-purity chemicals and DI water, problems with

water usage and hazardous waste disposal, and the abandonment of chlorofluorocarbons (CFCs), forced by government mandate, are causes for considering new cleaning technologies in the semiconductor and electronics industries.

1.3.2 Vapor-phase cleaning techniques

Vapor-phase cleaning is often called dry cleaning in contrast with wet cleaning, since cleaning processes are carried out in the gas or vapor phase. It has many actual and potential advantages over liquid cleaning methods in the fabrication of advanced semiconductor devices. Its development for commercial application is, as a consequence, being pursued vigorously. In this section, some basic approaches for the removal of various groups of contaminant types are presented. More details have been included in the literature review in reference [15].

Organic contaminants can be removed, depending on their composition, by one of the following methods: volatilization in vacuum at elevated temperature, oxidative degradation by UV/O_3 reaction, $NO/HCl/N_2$ thermal reaction, remote or downstream oxygen plasma treatment, and plasma glow discharge reaction.

Native and chemical thin films of oxides and silicate glasses require chemical etching or physical sputter etching for their removal. The latter can lead to erosion of the semiconductor surface. Techniques include anhydrous HF, $HF-H_2O$, reduction annealing

in H_2 under UHV at high temperature, low-energy ECR plasma etching in Ar or NF_3, and thermal desorption at high temperatures.

Physisorbed and chemisorbed ions and deposited elemental metals require chemical processes to remove them from the semiconductor or oxide surface. Typical examples are the removal of metallic impurities by remote microwave plasma or by UV-generated chlorine radicals. The key requirement is the formation of volatilizable species by reaction at low temperatures, followed by their elimination at elevated temperatures and low pressures.

Removal of particles in a vacuum system compatible with a dry cleaning sequence is technologically a great deal more difficult. Safety problem, hazardous waste disposal and the cost of high-purity gas still exist in vapor-phase cleaning processes.

1.3.3 Brush scrubbing, fluid jet, and ultrasonic techniques

The removal of particles larger than 1 μm has been accomplished since the early days with wafer scrubbing machines that dislodge particles hydrodynamically with brushes made of a hydrophilic material while DI water or isopropyl alcohol is applied to the surface [16]. The difficulty is in brush maintenance.

High-pressure fluid jet cleaning consists of a high-velocity jet of liquid sweeping over the surface at pressures up to 4000 psi [14, 15]. The liquid can be DI water or organic solvents. The shear force effectively dislodges submicron particles and can penetrate into dense topography, but damage to the wafer can result with improperly adjusted pressures.

1.4 Laser Cleaning Techniques

1.4.1 Advantages of laser cleaning

The traditional cleaning techniques, mentioned in the previous section, show that wet-chemical cleaning is incompatible with cluster tool and has the difficulties of chemical material purify and disposal. Vapor-phase cleaning processes lack efficiency in particle removal. The traditional cleaning processes are also prone to damage delicate parts because they rely on mechanical contact forces and chemical reaction [17, 18].

"Laser cleaning" is a new approach for particle removal by using short-pulse laser irradiation of the surface. It has been shown to be a potentially promising means of meeting highly demanding cleaning needs [19-27]. This novel technique, capable of removing submicron sized particles and adsorbed hydrocarbon films. Because laser cleaning of a surface is performed by scanning with one or more laser pulses, if there is enough laser energy, cleaning of whole 8 inch silicon wafer will just need less than one second, it is a very quick process. Selective cleaning, i.e., cleaning of a designated spot,

can make the cleaning process fast, avoid the redundant cleaning of cleaned area, render the cleaning of large objects possible, and reduce the possibility of damage of sensitive parts or surface structure. Consequently, laser cleaning can be implemented at any stage of the manufacturing process. It also eliminates the use of toxic chemicals and the problems of liquid contamination and waste disposal. Because laser cleaning works in atmosphere or in vacuum, the process may be compatible with cluster tools. Nonchemical, solvent-free cleaning by laser is of interest in a variety of fields, and can be applied not only to microscopic removal in microelectronic industry but also to macroscopic scale removal, such as paint stripping from airplanes and graffiti removal [28, 29]. In addition, in the field of optics, a thorough cleaning of high-power optical lenses and mirrors is mandatory to provide prolonged lifetime and enhanced reliability since the slight contamination of an optical surface is known to cause a dramatic increase on damage probability.

Up to date, laser cleaning techniques can remove certain kinds of material and particles, and high laser energy may damage the substrate surface. These are the reasons that laser cleaning techniques are limited in laboratory today. As we know, laser cleaning of silicon wafer back side have been used in industry in order to reduce ion iron diffusion.

Two general types of laser cleaning, dry cleaning and steam cleaning, have recently been reported in the literatures, relying on the pulsed laser heating of the surface with or

without the presence of a thin liquid coating. Further classifications are possible, depending on whether the laser wavelength is chosen to be strongly absorbed by the substrate, particle, or liquid. These different approaches to laser cleaning are summarized below.

1.4.2 Dry laser cleaning

There are two extreme cases of "dry laser cleaning" in which the laser wavelength is chosen to be strongly absorbed by the substrate only, or by the particles only. The explanation of this particle ejection by dry laser cleaning is keyed to the sudden expansion of the substrate surface, or particle, or both, depending on which is rapidly heated by the laser pulses. As an example of the first case, Kelley *et al* [30] demonstrated that 20 ns pulsed Nd:YAG laser irradiation at a fluence of 0.65 J/cm^2 results in 95% removal of micron-sized tungsten particles from a lithium niobate substrate after 100 pulses. However, this technique is obviously lacking in generality; it is very selective in its capability for particle removal. For example, only 5% cleaning efficiency could be achieved with epoxy particles under otherwise identical experimental conditions. This was obviously due to the weak absorption by epoxy at the Nd:YAG wavelength. Consequently the approach of strong particle absorption/weak substrate absorption is suited only to remove certain, well defined particulate contamination. As an example of the second case, strong substrate absorption was used, to be independent of the kind of particle material to be removed. Using an excimer laser pulse of 20 ns

duration at 248 nm wavelength with a fluence of typically 350 mJ/cm^2, 0.3 to 1.5 μm alumina particles can be removed from silicon surface, even from grooves and trenches [19, 23].

1.4.3 Steam laser cleaning

For certain sensitive (device) surfaces, it is obligatory to restrict irradiation to low fluence levels. Tam *et al* [19, 23] observed that the deposition of certain thin liquid films, covering over particle and substrate, during short-pulse irradiation can provide highly efficient particle removal, even at the desired reduced laser fluences. Water and water mixture are the preferred choice of film material. The highest cleaning efficiency for silicon wafer surfaces was observed experimentally for excimer laser irradiation. This kind of approach is called "steam laser cleaning". The main mechanism of steam laser cleaning is proposed to be the momentum transfer from the laser-heated, and explosively evaporating, liquid film to the particles on the surface. Given a silicon surface contaminated with particles and covered with a water film of several microns in thickness, the laser wavelength can be chosen to provide three distinctly different ways to heat the thin water film:

(1) UV excimer laser radiation penetrates the water film, and is essentially absorbed within the top 0.1 μm layer of the silicon surface. During a time interval of some 10 ns, thermal energy diffuses 1 μm into the silicon and only 0.1 μm into the water film, which

give sufficient laser energy to cause the water to explode at the interface. 0.1μm Al_2O_3 and 0.2 μm gold particles could be removed from silicon surfaces by a KrF excimer laser at a fluence 120 mJ/cm^2, with a 16 ns pulse duration [19, 23].

(2) CO_2 laser radiation at 10.6 μm has an absorption length of about 10 μm in water, and is only weakly absorbed in the silicon wafer. Water films of a few micrometers in thickness will, therefore, be fairly homogeneously heated directly by the laser radiation. For efficient explosion of the entire water film and, thus, ejection of the particles from the surface, the water film thickness must therefore be well controlled because thicker water film cannot be heated sufficiently down to the water/silicon interface The advantage of using CO_2 laser irradiation is that it is independent of the substrate material. This method was first used by Allen and co-workers [19, 20]. Great improvements have been made in our group: 0.1 μm polystyrene latex, alumina and silica particles could be successfully removed from silicon wafer surfaces at a fluence of 1 J/cm^2, with a 0.2 μs pulse duration [26, 27].

(3) Er:YAG lasers emit at 2.94 μm wavelength, which is close to the strongest water absorption peak. The light penetration depth in water is about 0.8 μm. Therefore, only the top surface sheet of the water film is heated by laser and caused to explode. Strong liquid-film absorption did not remove off 0.2 μm gold particles as well as strong substrate absorption did because the peak temperature occurs at the top liquid surface in the former case, and at the interface in the latter case [23].

1.5 Theoretical Models of Laser Cleaning

Particle adhesion is important in a variety of science and engineering applications. A great number of studies, carried out to unravel the interactions that occur during particle adhesion, were reviewed by Krupp [31], Bowling [32] and Ranade [33]. Interactions between solids, which bring about adhesion, can be classed into several groups. Group I includes long-range attractive interactions which act to bring the particle to the surface and establish the adhesive contact area. These include van der Waals forces, electrostatic forces, and magnetic attractions. Group II includes other forces which, along with group I forces, establish the adhesive area. This group of interfacial reactions includes sintering effects, such as diffusion and condensation, diffusive mixing, and mutual dissolution and alloying at the interface. This category also includes the establishment of liquid and solid bridges between particle and surface, and the consequential capillary forces associated with these phenomena. Group III is made up of very short range interactions which can add to adhesion only after the establishment of an adhesive contact area. It includes chemical bonds of all types, and intermediate bonds, such as hydrogen bonds [31, 34].

The quantitative analyses of group II and III adhesive forces are very difficult because they are primarily specific to each case, being dependent upon the particle and surface materials. However, chemical bonds were believed that to play an important role in

particle adhesion on silicon surface [31, 32]. The primary forces which act to bring particles to a surface and then hold them there are van der Waals forces and electrostatic forces. Electrostatic forces predominate for large particles, *i.e.*, greater that about 50 μm diameter. Van der Waals forces, however, predominate for smaller particles [32]. Electrostatic forces are comprised of two types of forces, excess charge image forces and electrostatic contact potentials, also known as electrical double layer forces. Wet systems can have an additional capillary force acting to hold the particles, and immersed systems may experience a shielding of each of these forces so that the total force holding the particles is reduced.

The early simplified model by Kelley and Hovis [35] for pulsed laser-induced thermal detachment of small particles was based on the idea that an absorbing particle is heated and expands. The expansion lifts the center of mass and accelerates the particle. This analytical thermal expansion model is used to explain the experimental results on tungsten and epoxy particles removed from the antireflection-coated lithium niobate surface by a Q-switched Nd:YAG laser [35]. Recently, Lu and co-workers [36-38] proposed other laser cleaning models. By using quartz substrates and a KrF excimer laser at a wavelength of 248 nm, the thermal expansion of the substrate can be ignored. The temperature distribution of an aluminum particle during laser pulse irradiation was simplified by an aluminum semi-infinite substrate. The thermal expansion removal force was obtained from the relationship between stress and strain in the particle. The

calculation results can explain the difference between cleaning efficiencies between front and back laser irradiation [36]. An extended model was established to explain the experimental results for removing quartz particles from a silicon surface [37]. The removal forces during steam cleaning were modeled by the bubble pressure which is deduced from the velocity of bubble growth, the energy of the stress wave, and energy conservation. The model was used to explain the experimental results for the removal of alumina particles from a nickel-phosphorus surface with an isopropyl alcohol thin film by excimer laser pulse irradiation [38].

1.6 Objective of This Thesis

As mentioned in previous sections, a great number of experimental and theoretical studies have been carried out on laser cleaning, but many questions still remain. First of all, there are few quantitative particle cleaning data being reported. The laser cleaning threshold is not clearly defined and experimental data are lacking. Second, many papers mention that chemical bonding plays an important role in particle adhesion on silicon surface, although there are few calculations of chemical adhesion forces. Next, most photoacoustic wave measurements were not performed under real cleaning situations. Finally, the effect of asperities on particle and substrate surfaces was not included in the calculation of adhesion and removal forces during laser cleaning.

The objective of this thesis is to develop experimental methods and theoretical models for a necessary fundamental understanding of laser cleaning. In preliminary studies, we reported that several kinds of submicron-sized particles could be removed during steam cleaning by a CO_2 laser [26, 27]. At the CO_2 laser wavelength (10.6 μm), the laser energy is strongly absorbed by the water film and partially absorbed by the silicon wafer. In this thesis, we have used a KrF excimer laser because, at the wavelength used (248 nm), water is transparent and the silicon substrate has a very short optical penetration length (5.5 nm) so less laser energy is required to heat the substrate surface. During steam cleaning, explosive vaporization of the liquid layer occurs at the liquid/substrate interface, giving high cleaning efficiency. The excimer laser operates in multiple modes, it has poor spatial coherence, which virtually eliminates diffraction and interference effects, giving an uniform laser beam.

In chapter 2, the excimer laser cleaning experimental system is presented. Procedural details of the removal of 0.1 μm polystyrene latex (PSL), Al_2O_3 and SiO_2 particles from hydrophilic silicon surface by dry and steam laser cleaning are given. Methods and principles of measuring particles on the wafer surface are described. Particle distribution maps on the wafer surface and particle densities before and after laser cleaning are presented. Part of this work has been published in the Journal of Adhesion **70**, 167 (1999). A new technique to prevent particle recontamination after removal is

demonstrated: a thermal gradient established between the silicon wafer surface and surrounding ambient atmosphere can greatly improve the cleaning efficiency.

Photoacoustic waves (PAW), detected by a piezoelectric transducer, are used to monitor the surface vibrations induced by the laser pulses. Relationships between the amplitude of the PAW signal and the laser flux, and the distance of the transducer from laser beam have been obtained. This work has been published in the Proc. 22nd Annu. Mtg. Adhesion Soc. (Adhesion Society, Blacksburg, VA, 1999), p.277.

In chapter 4, we develop the theoretical models for the interactions between particles and surfaces during laser cleaning. The effects of hydrogen bonds on the adhesion of inorganic particles are presented in the first part. A quantitative analysis of adhesion forces due to hydrogen bonds between inorganic oxide particles and the silicon surface has been carried out, and is used to interpret the efficiencies of removing PSL, SiO_2 and Al_2O_3 particles from a hydrophilic silicon surface by excimer laser cleaning. This work has been published in the Journal of Applied Physics, **86**, 1744 (1999). The modeling of excimer laser cleaning is presented in the second part. First, dry and steam laser cleaning results are summarized, and cleaning thresholds for both methods are obtained. Based upon these experimental results, adhesion forces between particles and substrate surfaces are discussed. The dominant adhesion force for organic particles is the van der Waals force, and for inorganic oxide particles is the hydrogen bonding force. The

temperature distributions in particle and substrate are discussed and calculated, using the semi-infinite one-dimensional heat transfer equation and an implicit finite difference algorithm. The particle removal forces, which come from rapid thermal expansion of the substrate due to the thermoelastic effect, and the pressure shock due to bubble generation in the condensed water film, are analyzed. The situation of practical (i. e., rough, irregularly shaped) particles has been considered, and the theoretical analysis includes the effects of both asperities on the particle surface and particle aggregation. This work has been submitted to the Journal of Applied Physics. In the final chapter, the conclusions and suggestions for future research are given.

1.7 References

[1] Kern W., *J. Electrochem. Soc.* **137,** 1887 (1990).

[2] Hattori T., *Solid State Tech.* July, S1 (1990).

[3] Tolliver D., in *Handbook of Semiconductor Wafer Cleaning Technology.* Kern W., ed. (Noyes Publications, Park Ridge, New Jersey, 1993), pp. 68-69.

[4] Kern W., in *Handbook of Semiconductor Wafer Cleaning Technology.* Kern W., ed. (Noyes Publications, Park Ridge, New Jersey, 1993), pp. 6-8.

[5] Vossen J. L., *J. Phys. E: Scientific Instrum.*, **12**, 159 (1979).

[6] Stowers I. F. and Patton H. G., in *Surface Contamination: Genesis, Detection, and Control*, Mittal K. L., ed. (Plenum Press, New York, 1979), Vol. 1, pp. 341-349.

[7] Kern W. and Puotinen D., *RCA Rev.*, **32**, 187 (1970).

[8] Burkman D., *ibid.*, **4**, 103 (1981).

[9] Mayer A. and Shwartzman S., *J. Electron. Mater.*, **8**, 885 (1979).

[10] Shwartzman S., Mayer A. and Kern W., *RCA Rev.*, **46**, 81 (1985).

[11] Busnaina A. A. Kashkoush I. I. And Gale G. W., *J. Electrochem. Soc.*, **142**, 2812 (1995).

[12] Gale G. W. and Busnaina A. A., *J. Particulate Sci. Tech.*, 13, 197 (1995).

[13] Moslehi M. M., Chapman R. A., Wong M., Paranipe A., Najm H. N., Kuene J., Yeakley R. L. and Davis C. J., *IEEE Trans. Electron Dev.*, **39**, 4 (1992).

[14] Tipton C. M. and Bowlig R. A., in *Proc. First Intern. Symp. On Cleaning Technol. In Semicond. Dev. Manufacturing, Pennington, N. J. 1992*, Ruzyllo J. and Novak R., eds, pp.170-178.

[15] Kern W., ed. *Handbook of Semiconductor Wafer Cleaning Technology.* (Noyes Publications, Park Ridge, New Jersey, 1993), Part III.

[16] Burggraaf P. S., *Semicond. Int.*, **4**, 17 (1981).

[17] Bardina J., in *Particles on Surface 1: detection, Adhesion, and Removal*, Mittal K. L., ed. (Plenum Press, New York, 1988), pp. 329.

[18] Menon V. B., Michaels L. D., Donovan R. P., and Ensor D. S., *Solid State Technol.*, Mar. S7 (1989).

[19] Zapka W., Ziemlich W., and Tam A. C., *Appl. Phys. Lett.*, **58**, 2217 (1991).

[20] Magee T. J. and Leung C. S.. in *Particles on Surfaces 3*, Mittal K. L. ed. (Plenum Press, New York, 1991).

[21] Imen K., Lee S. J., and Allen S. D., *Appl. Phys. Lett.*, **58**, 203 (1991).

[22] Lee S. J., Imen K., and Allen S. D., *Appl. Phys. Lett.*, **61**, 2314 (1992).

[23] Tam A. C., Leung W. P., Zapka W., and Ziemlich W., *J. Appl. Phys.*, **71**, 3515 (1992).

[24] Zapka W., Ziemlich W., Leung W. P., and Tam A. C., *Microelectron. Eng.*, **20**, 171 (1993).

[25] Park H. K., Grigoropoulos C. P., Leung W. P., and Tam A. C., *IEEE Trans. Com. Pack. Manuf. Technol.*, A17, 631 (1994).

[26] Heroux J. B., Boughaba S., Ressejac I., Sacher E., and Meunier M., *J. Appl. Phys.*, **79**, 2857 (1996).

[27] Boughaba S., Wu X., Sacher E., and Meunier M., *J. Adhesion,* **61**, 293 (1997).

[28] Frank A. M. and Lovoi P. A., U. S. Patent No. 4588885, 1986.

[29] Liu K. X., Garmire E., and Fathe L., *Amer. Phys. Soc. Bull.*, 38, 1731 (1993).

[30] Kelley J. D., Stuff M. I., Hovis F. E., and Linford G. J., *SPIE Proc.* **1415**, 211 (1991).

[31] Krupp H., *Advan. Colloid Interface Sci.,* **1**, 111 (1967).

[32] Bowling R. A., *J. Electrochem. Soc.,* **132**, 2209 (1985).

[33] Ranade M. B., *Aerosol Sci. Tech.*, **7**, 161 (1987).

[34] Bhattacharya S. and Mittal K. L., *Surf. Technol.*, **7**, 413 (1978).

[35] Kelley J. D. and Hovis F. E., *Microelectronic Engineering*, **20**, 159 (1993).

[36] Lu Y. F., Song W. D., Ang B. W., Hong M. H., Chan D. S. H., and Low T. S., *Appl. Phys.*, **A65**, 9 (1997).

[37] Lu Y. F., Song W. D., Ye K. D., Lee Y. P., Chan D. S. H., and Low T. S., *Jpn. J. Appl. Phys.*, **36**, L1304 (1997).

[38] Lu Y. F., Zhang Y., Song W. D., and Chan D. S. H., *Jpn. J. Appl. Phys.*, **37**, L1330 (1998).

Chapter 2

EXCIMER LASER CLEANING SYSTEM AND RESULTS

2.3 Experimental Systems and Procedures of Excimer Laser Cleaning

2.1.1 Experimental setup

The experimental setup for excimer laser cleaning is shown schematically in Figure 2.1. Optical pulses from an MPB Technologies, Inc., AQX-150 excimer laser, operating at the KrF wavelength of 248 nm, with a 22 ns pulse width at half maximum (FWHM) and

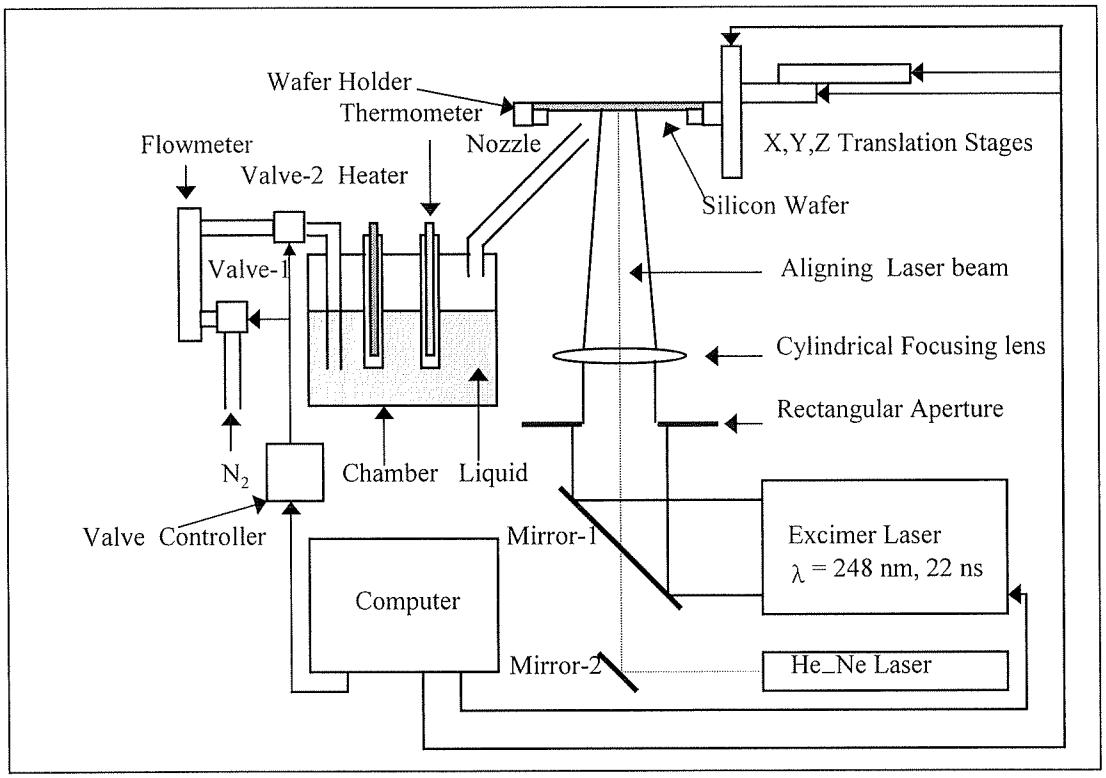

Figure 2.1 Experimental setup for excimer laser cleaning.

200 mJ of pulse energy, were directed onto a 6 mm × 18 mm aperture which was imaged onto the wafer using a 100 mm focal length lens. This rectangular aperture greatly improved the intensity homogeneity of the laser beam. The intensity distributions of the laser beam before and after the aperture are shown in Figure 2.2. The energy fluence of

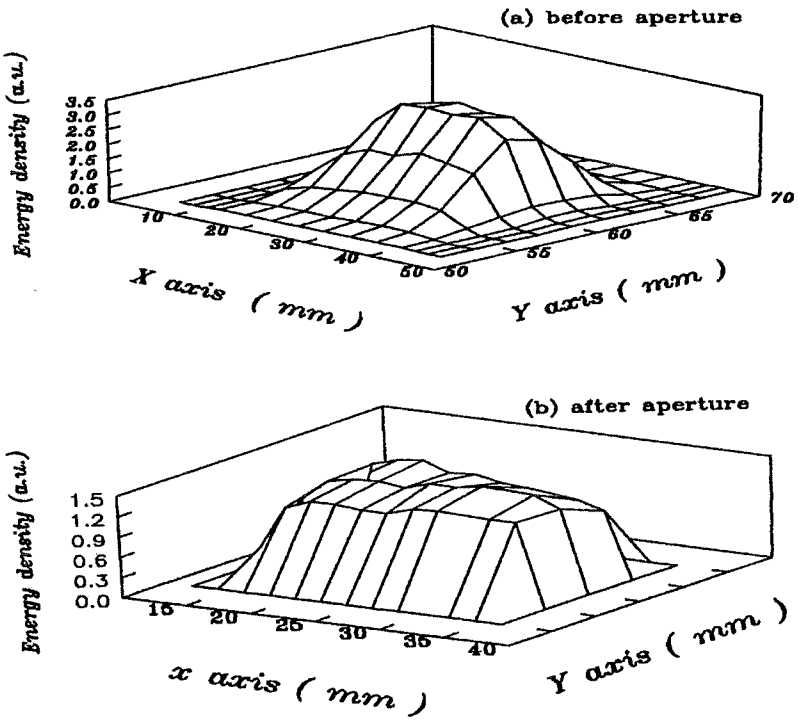

Figure 2.2 Laser intensity distribution (a) before and (b) after the rectangular aperture.

the laser pulse was monitored by using a beam splitter and a joulemeter in front of mirror 1. The wafer sample was mounted face down on a computer-controlled XYZ stage so that the area irradiated by the laser could be varied by scanning in the XY directions, and laser energy densities on the wafer surface could be varied, in the range

50 – 1000 mJ/cm^2, by changes in the Z axis position. A He-Ne laser was used to align the excimer laser beam and indicate the correct deposition position of liquid film.

During dry laser cleaning, the liquid deposition system, in the left middle part of Fig. 2.1, was not used. During steam laser cleaning, a specially designed liquid film deposition system was used to coat the sample at the irradiation location prior to laser exposure. This system utilized a burst of nitrogen gas into a stainless steel chamber half-filled with deionized (DI) water typically kept at 40 °C by a stainless steel isolated heater; the water temperature was measured by a stainless steel isolated thermometer.

The nitrogen gas input of 4700 ml/min entrained a controlled volume of water vapor, which was directed toward the wafer surface by a stainless steel nozzle, kept at 45 °C. Gas valves controlled by computer were opened for 0.2 seconds, and water vapor condensed as a thin liquid film, several microns thick, on the colder wafer surface. Three laser pulses, separated by 0.1 second, were triggered 0.1 second after the deposition of the water vapor. During laser cleaning, the wafer was linearly stepped after each water vapor burst, with the beam overlap kept at ~10%. The laser beam scanning whole cleaning area is called one cleaning cycle. We used multiple cleaning cycles in order to cover the gaps between previous step scans and to remove any recontaminating particles. The laser energy flux was carefully maintained below the silicon surface damage

threshold we determined, at about 380 mJ/cm^2 for dry cleaning and at 200 mJ/cm^2 for steam cleaning. The time needed to clean whole wafer is about 3 to 5 minutes, depending upon the laser energy density on the surface and the total laser energy output.

2.1.2 Pretreatment of the silicon wafer surface

The samples were 100 mm <100> silicon wafers, whose surfaces were cleaned and made hydrophilic using a modified RCA recipe [1]. This consisted of (i) SC1, 80 °C, 10 min; (ii) SC2, 80 °C, 10 min (iii) 0.5% HF etch, 2 min; (iv) boiling isopropyl alcohol, 2 min; (v) SC1, 80 °C, 10 min; (vi) DI water rising, 10 min; (vii) dry by high speed spinner. Here, SC1 (standard clean 1) refers to NH_4OH:H_2O_2:H_2O (0.05:1:5) and SC2, to HCl:H_2O_2:H_2O (1:1:6); SC1 is used to remove particles and organic contaminants and SC2, to remove metals.

2.1.3 Particle deposition

The particles used to artificially contaminate the surface were Particle Measuring Systems, Inc. 0.1 μm polystyrene latex (PSL) and 0.2 μm carboxylate modified latex (CML) particles; Beta Diamond Corp. 0.1 μm SiO_2 and Al_2O_3. The particles were deposited onto the wafer surface using a Particle Measuring Systems, Inc., particle generator. Filtered air was driven through a nebulizer with the desired particles suspended in DI water. The droplets so generated were carried through a tube and a

drying chamber, resulting in particle-laden dry air. This air exited through a nozzle which could be manually moved over the wafer surface. To avoid any cross-contamination, a set of liquid containers, dedicated nebulizers, drying tubes and chambers was used for each type of contaminant particle.

2.1.4 Particle measurement system

A Particle Measuring Systems, Inc., SAS 3600 XP laser scanning surface inspection system was used to count the particles on the wafer surface. The measurement principle is based on the detection of the light scattered by small, laser illuminated particles/defects. The particle is simultaneously illuminated by two plane polarized He-Ne laser beams, one "P" polarized with respect to the wafer surface and operating at 594 nm wavelength, required to measure the particles over 0.3 μm in diameter, and the other "S" polarized with respect to the wafer surface and operating at 633 nm wavelength, required to measure the particles below 0.3 μm in diameter. The SAS 3600 XP system operates similarly to an optical disk drive. The wafer spins on a vacuum chuck driven by a brushless DC motor, and the optical stage mechanically steps radially, generating concentric tracks at 200 microns separation. The surface illuminated is imaged and the resulting pixel image format is converted to Cartesian coordinates for display. A seven-color display is used for color-coding particle sizes in both the image and histogram display formats. Before measuring the particle distribution on the wafer surface during

laser cleaning, the SAS 3600 XP system was carefully calibrated using monodispersed polystyrene latex particles distributed on a bare virgin silicon wafer.

2.1.5 Selection of the liquid and the liquid film thickness measurement system

During steam laser cleaning, the properties, quality and thickness of the liquid film directly affect the cleaning efficiency. The liquid required should have the following properties: a high critical pressure, giving greater cleaning force; a low surface tension, having better wettability on substrate surface; a suitable vapor pressure, depositing easily; non-toxicity and residue-free. In Table 2.1, some kinds of liquid commonly used are listed. Because the substrate surface is a hydrophilic silicon surface, most kinds of liquid can completely wet it. Therefore, in this work, we selected the DI water which has the highest critical pressure and is the safest of those given in the Table 2.1.

Table 2.1 Liquid properties

Liquid	Surface tension (mJ/m^2)	Vapor pressure (mmHg, 20 °C)	Critical pressure (Mpa)	Maximum allowed value (ppm)
Water	72.75	17.38	22.06	
Methanol	22.61	97.3	8.09	200
Ethanol	22.75	44	6.13	1000
1-propanol	23.78	14.81	5.17	200
2-propanol	21.7	30.82	4.76	400

The liquid film thickness can be controlled by changing the liquid temperature, the pressure and the nitrogen gas flow into the liquid deposition system, the opening time of the gas valve and the time delay between the liquid film deposition and the arrival of laser pulse.

Using an optical interference set-up, as shown in Figure 2.3, similar to that reported in ref. [2], and a water vapor supply unit similar to that used in Figure 2.1, the wettablity and the thickness of the liquid can be monitored and measured. A He-Ne laser beam is expanded and reflects on the substrate surface with the liquid film, and then projected

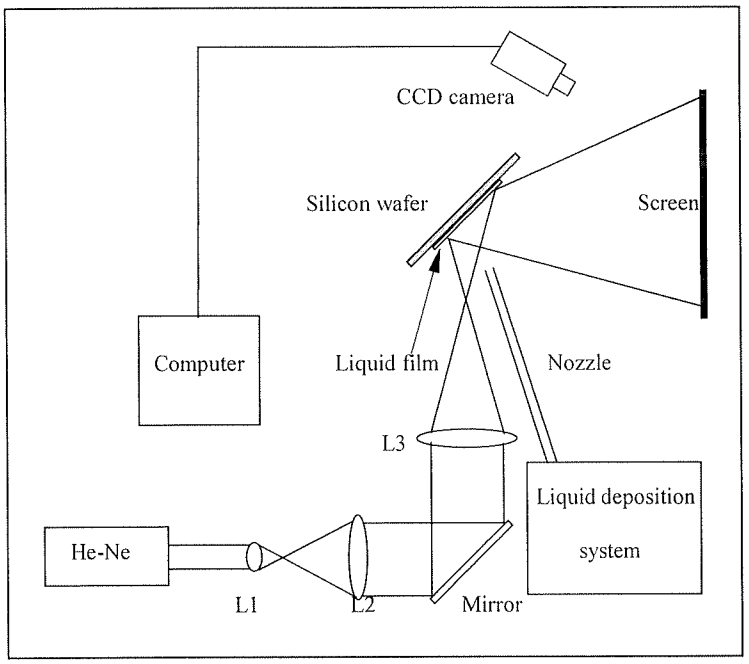

Figure 2.3 Optical interference setup.

onto a screen. A CCD camera takes the picture on the screen and sends it to computer. The interference fringes show that the film becomes thinner from the center toward the edge. Dry spots were observed within the water film; these spots first appeared as localized points , as shown in Figure 2.4 (a), enlarging and increasing in number with time, in Figure 2.4 (b). These spots, not present on initial cleaning, are certainly due to

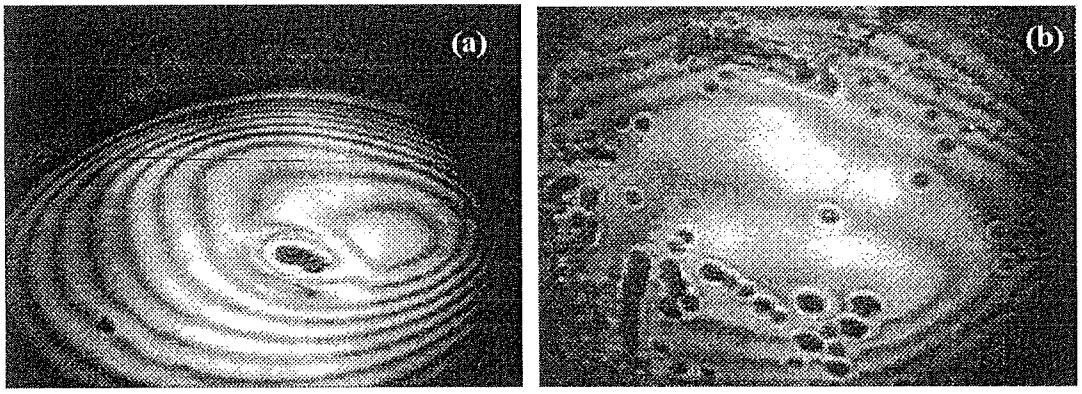

Figure 2.4 Interference Photomicrographs of water vapor condensed onto a hydrophilic silicon surface after surface chemical pretreatment for (a) 10 min (b) two hours. The vapor burst duration was 0.1 second.

hydrocarbon contamination, which results in a decrease in the surface tension to the point where wettability is lost (water has a surface tension of ~ 72 mJ/m^2, while that of a hydrocarbon surface is ~ 34 mJ/m^2). The difference in thickness between two point on the liquid film, separated by ***m*** fringes, is given by:

$$\Delta d = (\lambda/n_l)(m + 0.5) \quad (2.1)$$

where λ is the wavelength of He-Ne laser and n_l is the refractive index of liquid. In our cleaning conditions, the thickness of the liquid film is a few microns.

2.2 Experimental Results of Excimer Laser Cleaning

The evaluation of the removal efficiency was carried out in a 30 mm circle inside a 50 mm × 50 mm cleaned square. We used the particle density remaining after cleaning to quantify the cleaning efficiency. For every cleaning condition, several experiments have been repeated. The error of cleaning efficiencies were less than 5%, mainly induced by different initial particle densities. The typical particle distribution maps and particle densities as a function of their size distributions, for PSL, CML, SiO_2 and Al_2O_3 on the hydrophilic silicon wafer surface, before and after dry and steam laser cleaning, are shown in Figures 2.5 – 2.10. Almost all the PSL and CML particles ≥ 0.1 μm were removed by dry cleaning at 326 mJ/cm^2 but the dry cleaning of SiO_2 and Al_2O_3 particles was inefficient. However, using steam cleaning with a laser energy flux reduced to 180 mJ/cm^2, most of the SiO_2 and Al_2O_3 particles ≥ 0.1 μm were removed; it was not necessary to use steam cleaning to remove PSL and MCL particles from the silicon surface because they were essentially completely removed by dry cleaning. Any particles remaining after cleaning may be due to several sources: strongly adhering original particles, recontamination by the ejected particles near the surface, a transfer from

adjacent uncleaned areas and contamination by the steam cleaning liquid deposition system. Some kinds of unknown particles on as-received wafer surface could be almost completely removed by dry laser cleaning, as shown in Figure 2.11. The detail discussion for excimer laser cleaning results will be given in chapter 4. The main results of excimer laser cleaning have been published in Journal of Adhesion, **70**, 167 (1999).

2.3 Thermophoresis: Applications for Preventing Particle Recontamination

Contaminant particle deposition onto product surfaces during manufacturing is a major cause of low product yields in the microelectronics industry. Despite a controlled, filtered environment during production, it is not possible to achieve completely particle-free conditions in the vicinity of the product. The same problem exists during laser cleaning processes. During laser cleaning, the viscous drag force of the atmosphere slows down the velocities of ejected particles and causes the particles to be suspended in the air a few centimeters above the cleaned surface [3]. These particles may re-contaminate the cleaned surface.

The mechanisms which determine the transport of these particles are convection, diffusion, gravitational settling, inertia, electrical force, thermophoretic force and turbulence. The Brownian diffusivity of an aerosol particle is very small, much smaller than any of the gas diffusivities, owing to the massive size of a particle in comparison with a gas molecule. For example, for spherical particles of 0.05–1.0 μm diameter in air,

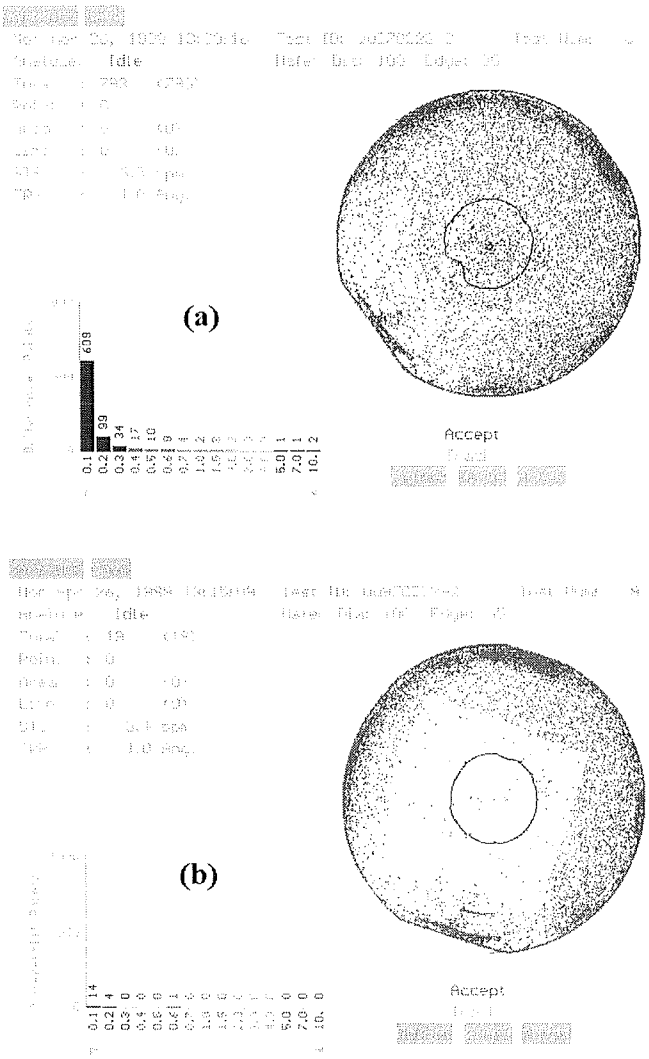

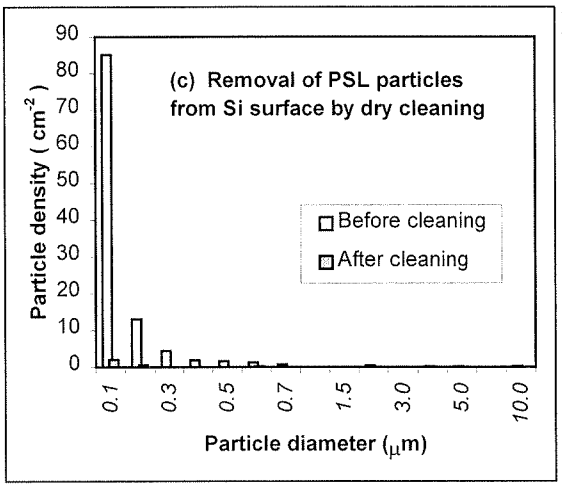

Figure 2.5 PSL particle distribution maps (a) before and (b) after dry laser cleaning. (c) PSL particle densities before and after dry laser cleaning. The laser energy flux was 326 mJ/cm^2, 2 cleaning cycles.

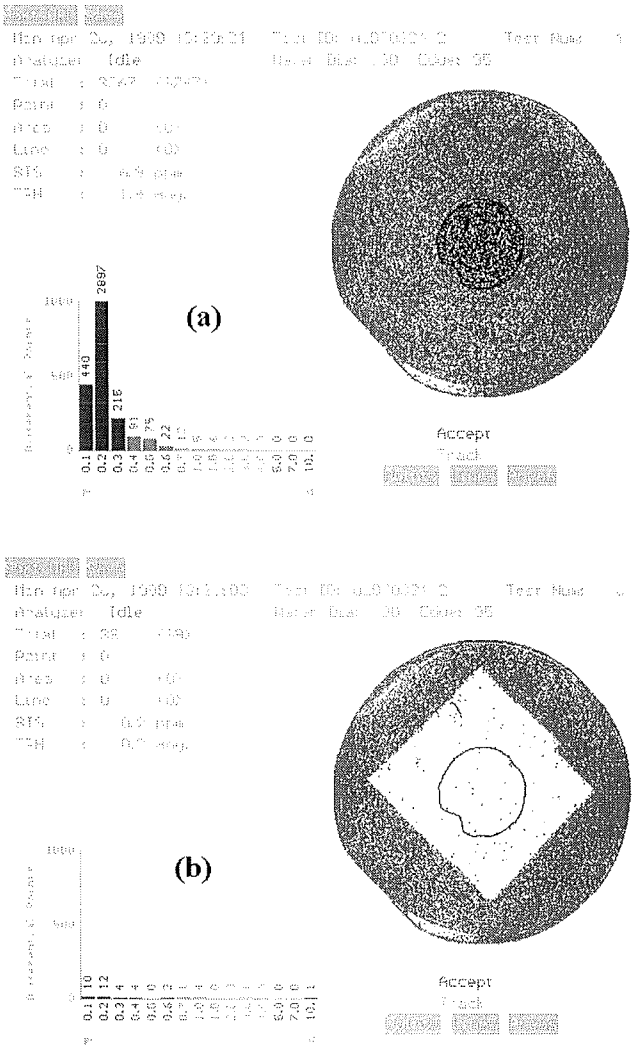

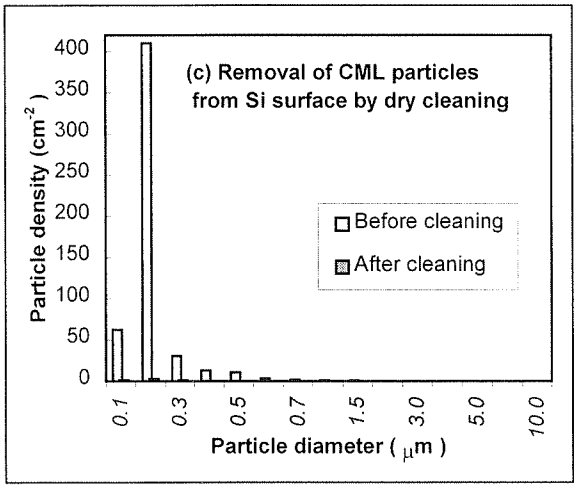

Figure 2.6 CML particle distribution maps (a) before and (b) after dry laser cleaning. (c) CML particle densities before and after dry laser cleaning. The laser energy flux was 363 mJ/cm^2, 1 cleaning cycles.

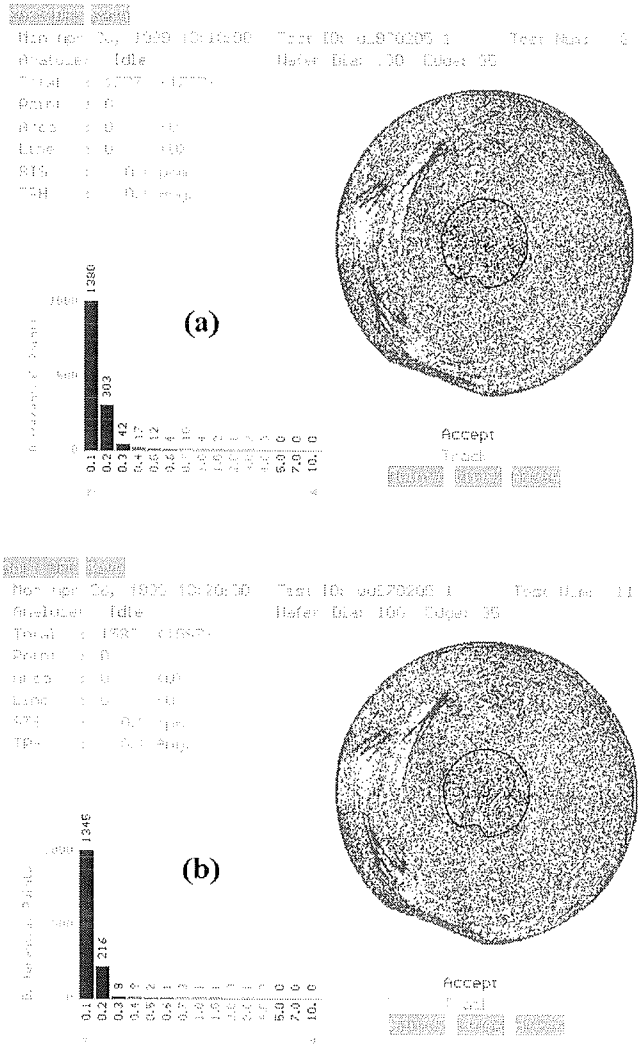

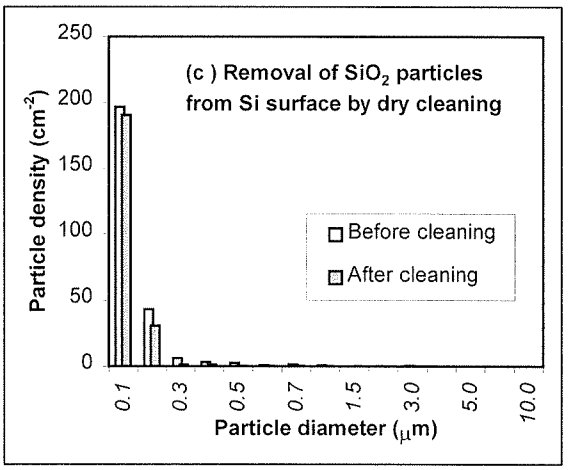

Figure 2.7 SiO_2 particle distribution maps (a) before and (b) after dry laser cleaning. (c) SiO_2 particle densities before and after dry laser cleaning. The laser energy flux was 314 mJ/cm^2, 4 cleaning cycles.

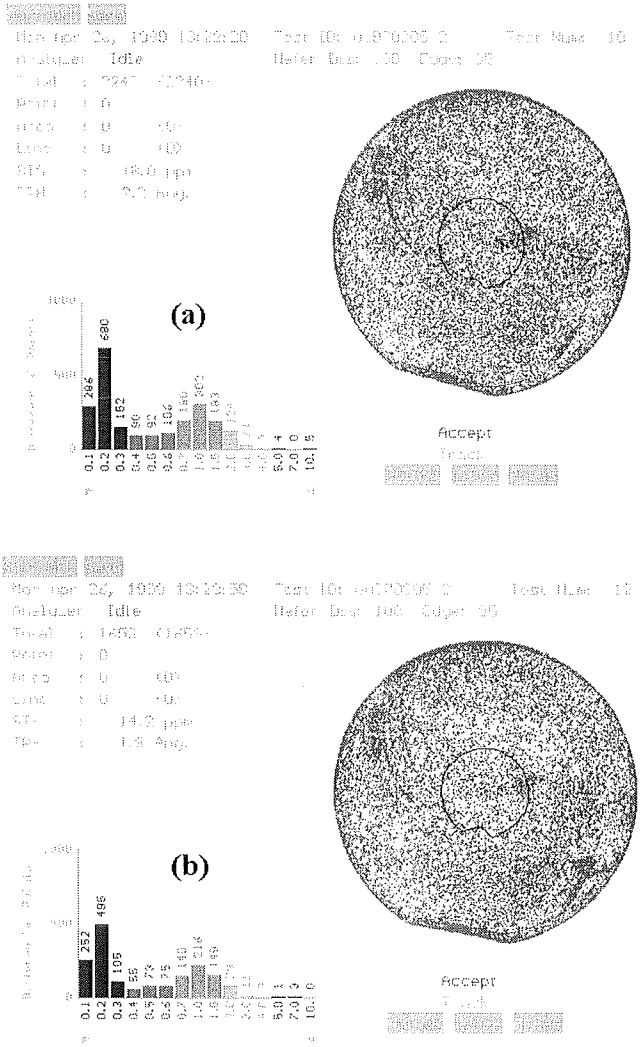

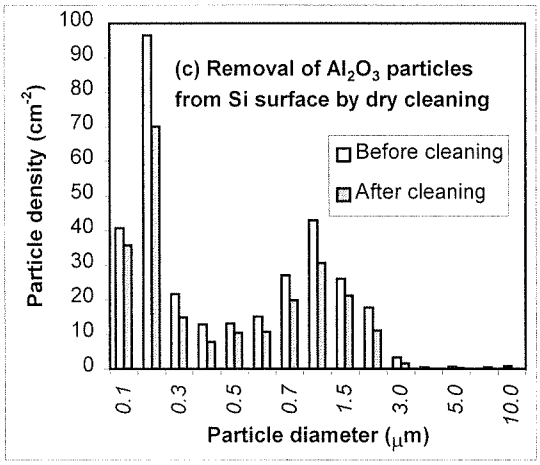

Figure 2.8 Al_2O_3 particle distribution maps (a) before and (b) after dry laser cleaning. (c) Al_2O_3 particle densities before and after dry laser cleaning. The laser energy flux was 326 mJ/cm^2, 4 cleaning cycles.

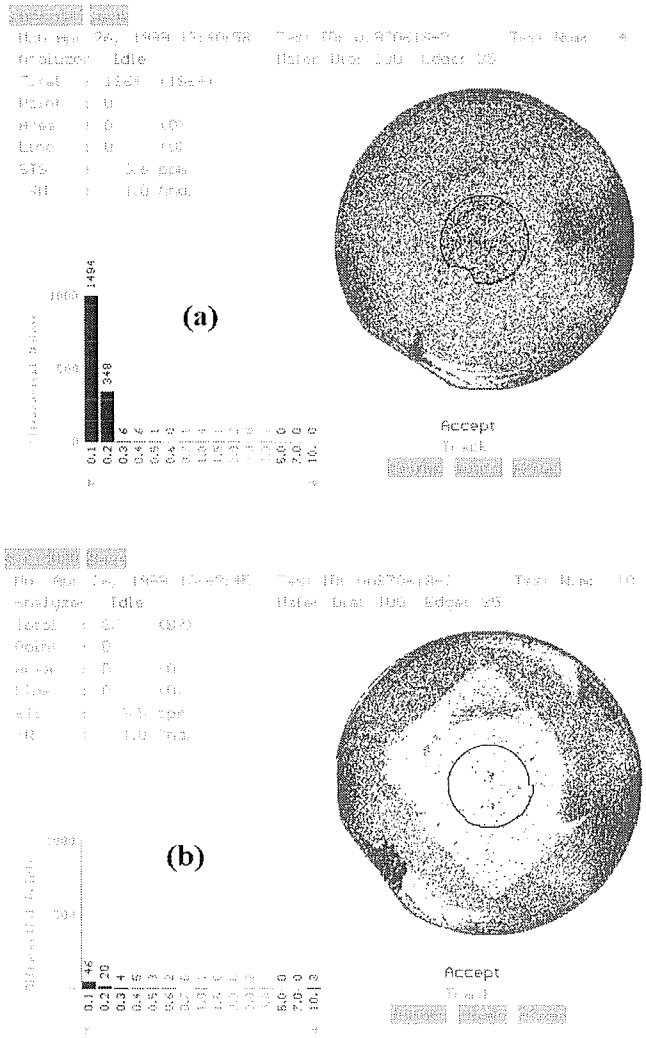

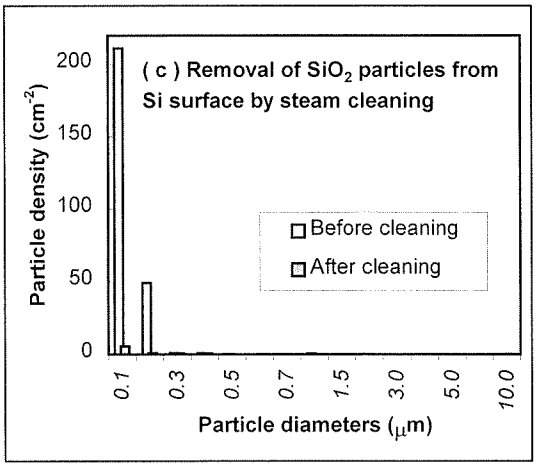

Figure 2.9 SiO_2 particle distribution maps (a) before and (b) after steam laser cleaning. (c) SiO_2 particle densities before and after steam laser cleaning. The laser energy flux was 180 mJ/cm^2, 5 cleaning cycles.

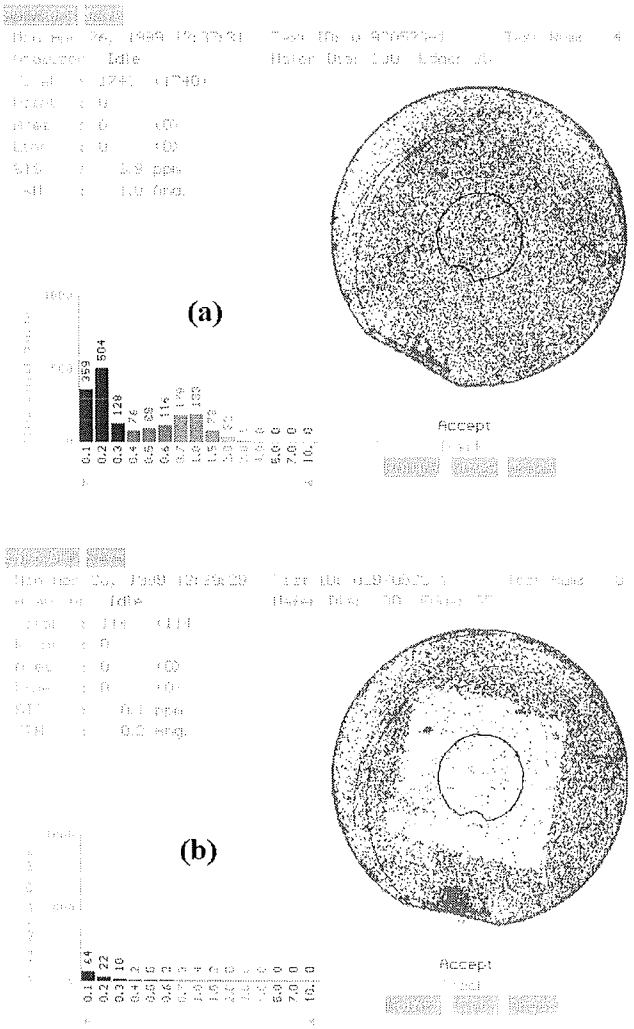

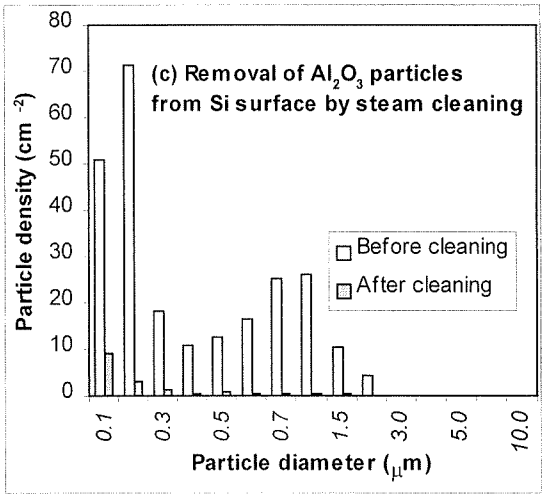

Figure 2.10 Al_2O_3 particle distribution maps (a) before and (b) after steam laser cleaning. (c) Al_2O_3 particle densities before and after dry laser cleaning. The laser energy flux was 154 mJ/cm^2, 4 cleaning cycles.

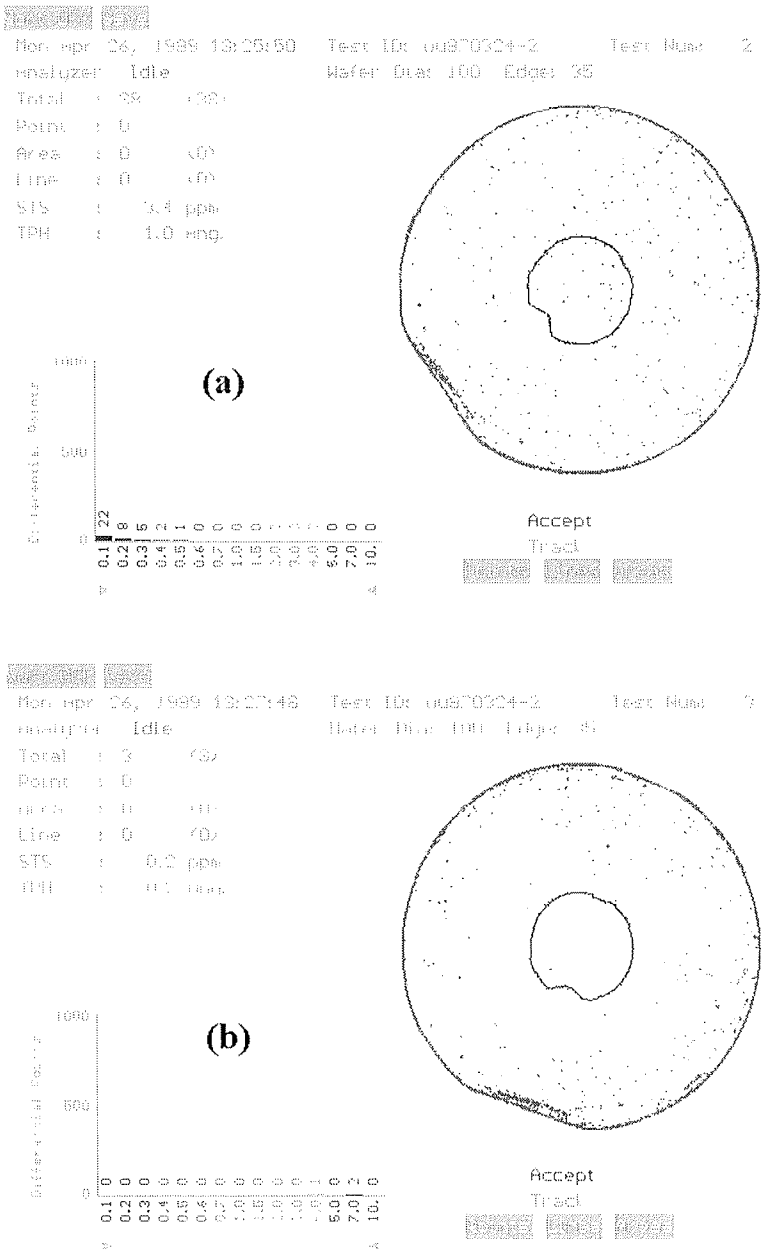

Figure 2.11 Distribution maps of unknown particle on as-received silicon wafer surface. (a) before and (b) after dry laser cleaning. The laser energy flux was 363 mJ/cm^2, 1 cleaning cycle.

diffusivities range from 2.4×10^{-3} to 2.8×10^{-5} m^2/s [4]. The effects of particle diffusion can normally be neglected. The electrical force can, depending on the polarity between the particle and the surface, either increase or decrease the possibility of particle re-contamination. In our clean room, there are several air-filtered fans hanging from the ceiling. Air flow fluctuations exist almost everywhere there; the air flow has the features of unsteady laminar flow but is different from the turbulence in a tube flow at high Reynolds numbers because of its much lower velocity, weaker diffusion and dissipation of eddy energy, and larger scale. Air flow fluctuations are the primary reason for particle recontamination.

There are several techniques for preventing particle re-contamination during laser cleaning. The simplest one is to place the wafer to be cleaned face down [5,6]; the particles removed can be drawn away from the surface by gravity and inertia. Another technique is to use a laminar gas flow [7]; a laminar flow maintains a stable, non-flowing boundary layer with a thickness modified by the choice of gas or by varying the pressure. Once the contaminant passes through the boundary layer, it becomes entrained in the bulk gas flow. The laminar flow technique is not compatible with cluster tools.

2.3.1 Thermophoretic force

The force arising from a temperature gradient acting on particles suspended in a gas has long been the subject of theoretical and experimental investigations [8-15]. This

thermophoretic force experienced by a particle is produced by the greater kinetic energy of gas molecules on the higher temperature side of the particle, thereby driving the particle to the region of lower temperature. The thermophoretic force is directly proportional to the local temperature gradient and is given by the following equation for an isolated sphere [16]:

$$F^{T} = -\frac{9\pi\eta r_p}{\rho T}\frac{k_g}{k_s + 2k_g}(\nabla T)_\infty \tag{2.2}$$

where the symbols mean the following: η is the viscosity of the gas; ρ is the density of the gas; T is the absolute temperature of the particle; k_g and k_s are the thermal conductivities of the gas and the sphere, respectively; r_p is the radius of the sphere and $(\nabla T)_\infty$ is the overall temperature gradient in the gas at large distances from the sphere. During laser cleaning, the gas environment is air. We calculated the thermophoretic forces acting on 0.1 μm PSL particles as a function of the temperature gradients, as shown in Figure 2.12 (a). In the calculation, we assume the particles to be spheres and the particle temperature is taken to be 60 °C, the same as the temperature of the front wafer surface. By taking a typical temperature gradient of 10 K/cm, which is easily obtained experimentally, the thermophoretic force and gravity as a function of particle diameter are given in Figure 2.12 (b) for comparison. For particles smaller than 0.5 μm, the thermophoretic force is greater than gravity and the difference between them increases dramatically with decreasing particle diameter. Thus, the thermophoretic force is much stronger than gravity in pulling the free sub-micron sized particle away from the

surface, and greatly reduces the possibility of particles recontamination by air flow fluctuations. For large particles, more than a few microns in diameter, their greater inertia and gravity pull them from the surface. They are not easily influenced by air flow fluctuations. These predictions have been verified in our experimental work. To our knowledge, we are first to use thermophoresis during laser cleaning to decrease particle re-contamination.

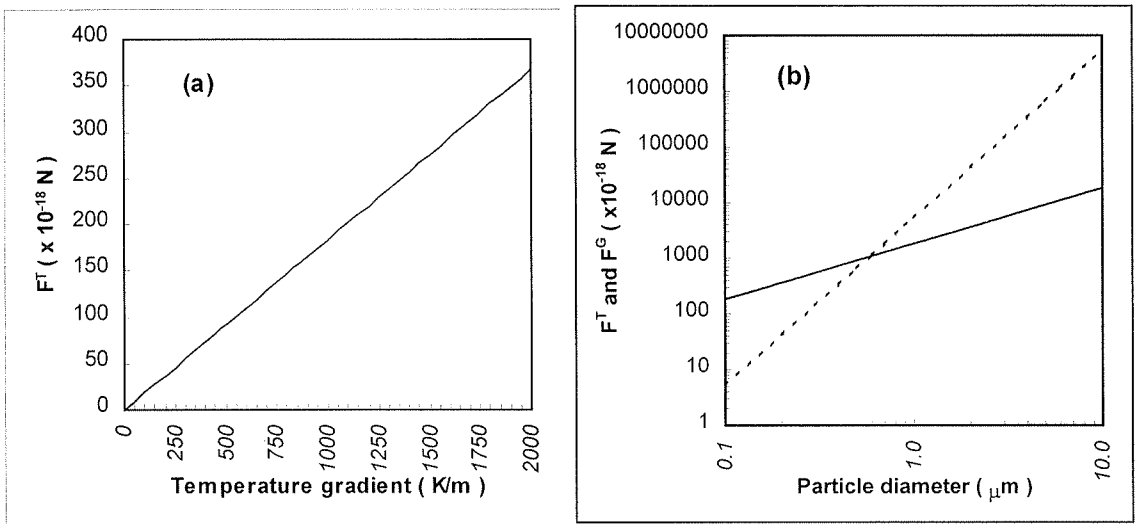

Figure 2.12 (a) The thermophoretic force acting on 0.1 μm PSL particles at 60 °C as a function of the temperature gradient. (b) The thermophoretic force (solid line) and gravity (dash line) acting on PSL particles as a function of the particle diameter. The particles are at 60 °C and the temperature gradient is 10 K/cm.

2.3.2 Thermophoresis and laminar flow experiments

The laser cleaning experimental setup is the same as that shown in section 2.1, except for the added heating, as shown in Figure 2.13. An infrared lamp was used to heat the backside of the silicon wafer. A thermocouple contacted the backside of the wafer and the temperature, controlled by a transformer, was shown on a meter. The temperature at the front side was about 8 °C lower than that of the backside. Before laser cleaning, the wafer temperature reached 60 °C in a few minutes, establishing the 10 K/cm temperature gradient. Another way to form the temperature gradient was put a circular cell below the wafer. The cell had a hole to let the laser beam pass through and was filled with liquid nitrogen. 0.2 μm carboxylate modified latex (CML) particles and 0.3 μm Al_2O_3 particles were used during dry and steam cleaning.

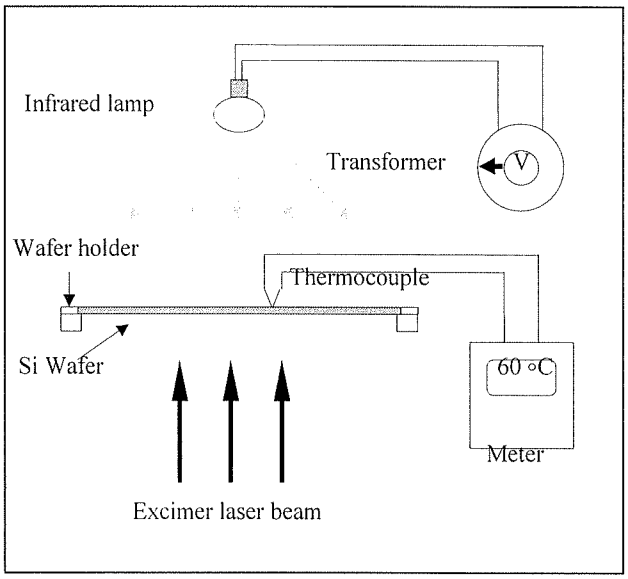

Figure 2.13 Schematic of the experimental system for thermophoresis during laser cleaning

Laminar flow experiments were also carried out, in order to compare with thermophoresis. The wafer was put in a specially designed chamber, as shown in Figure 2.14. Nitrogen was introduced into the chamber and the gas flow was controlled by a flowmeter.

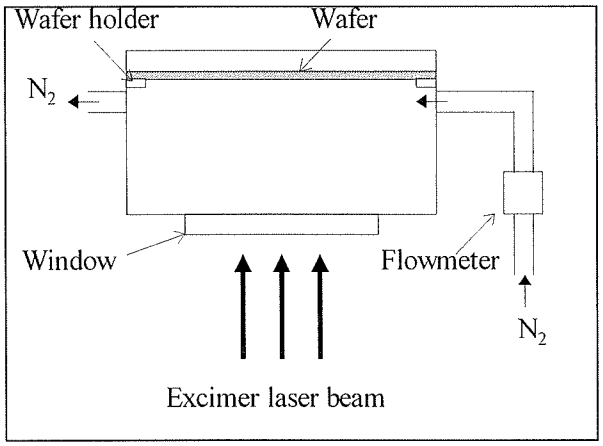

Figure 2.14 Schematic of the experimental system for laminar flow during laser cleaning.

2.3.3 Results and discussion

First, during dry laser cleaning, we used identical laser cleaning conditions with and without thermophoresis. The substantial difference in laser cleaning efficiencies for these two processes, using 0.2 μm CML particles, is shown in Figure 2.15. We can see that the recontamination of sub-micron sized CML particles was greatly reduced by thermophoresis. The smaller the particle, the more obvious this phenomenon is. For Al_2O_3 particles, thermophoresis did not improve the dry laser cleaning efficiency because Al_2O_3 particles can not be removed by dry cleaning.

During steam cleaning, we found that thermophoresis did not help much. The cleaning efficiencies for Al_2O_3 particles with and without thermophoresis was almost the same. There are two reasons for these results: first, particles obtain much higher speeds from explosive evaporation of the liquid film and their removal distance is greater; thus, the

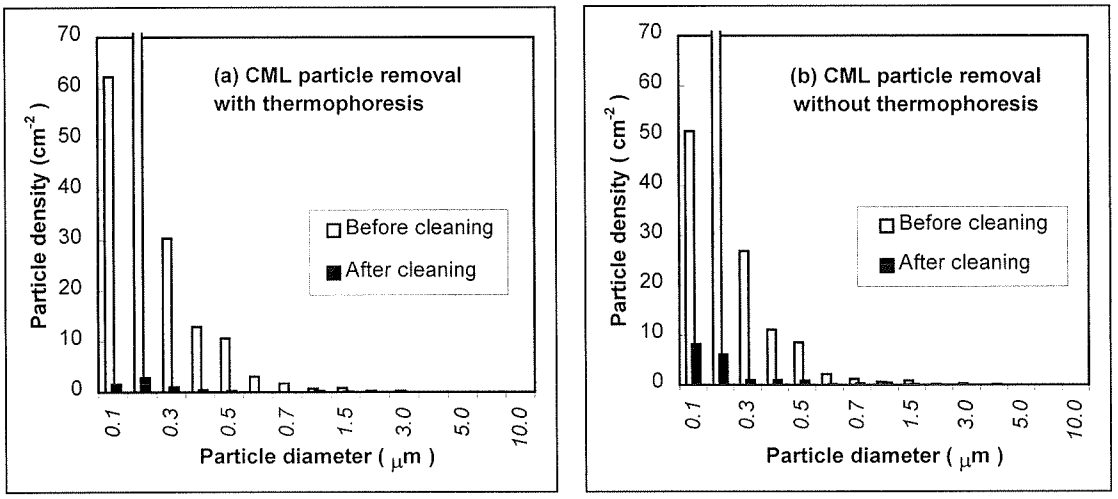

Figure 2.15 The densities of 0.2 μm CML particles before and after dry laser cleaning: (a) the laser flux was 363 mJ/cm^2, 1 cleaning cycle, the temperature of wafer front surface was 62 °C and the 0.2 μm particle density was 410 cm^{-2}; (b) the laser flux was 363 mJ/cm^2, 4 cleaning cycles, the wafer was not heated, and the 0.2 μm particle density was 374 cm^{-2}.

possibility of particle recontamination is smaller, compared with dry cleaning. Second, when the wafer is heated, it is very difficult to control the condensation of vapor on the

wafer surface. If the uniformity of the liquid film on the wafer surface is not good, the cleaning efficiency will be lower.

We also used an aluminum cell, filled with liquid nitrogen, to establish a temperature gradient near the wafer front surface. During dry cleaning, the cleaning efficiency was greater than that without thermophoresis, but lower than that using an infrared lamp to heat the wafer. One possible reason is the fog of water droplets, condensed from water vapor in the air surrounding the cell, influencing the homogeneity of the laser beam. During steam cleaning, the cleaning efficiency in this case was again not greatly improved in this situation.

In the laminar flow experiment, the gas flow was 4223 ml/min; the Reynolds number $\boldsymbol{R}_e$ in the chamber was approximated by [17]

$$R_e = \rho V D_C / \eta \qquad (2.3)$$

where ρ (1.25 Kg/m^3) and η (1.79× 10^{-5} Kg/m/s) are the density and the viscosity of nitrogen, respectively, $\boldsymbol{D}_c$ (100 mm) is the diameter of the chamber, $\boldsymbol{V}$ is the average velocity of the gas flow, which can be calculated by $\boldsymbol{V = F_g / D_c h}$, where $\boldsymbol{h}$ (15 mm) is the height of the chamber, and $\boldsymbol{F}_g$ is the gas flow of nitrogen. Thus, under our conditions, $\boldsymbol{N}_R$ is about 328, which is much smaller than the critical Reynolds number of 2000 [17]. This means that there was a stable, laminar flow, and a boundary layer at the front wafer

surface. In Figure 2.16, the density of 0.2 μm CML particles before and after dry cleaning is given. We found the cleaning to be greatly improved, but not as much as when using thermophoresis, as shown in Figure 2.15 (a).

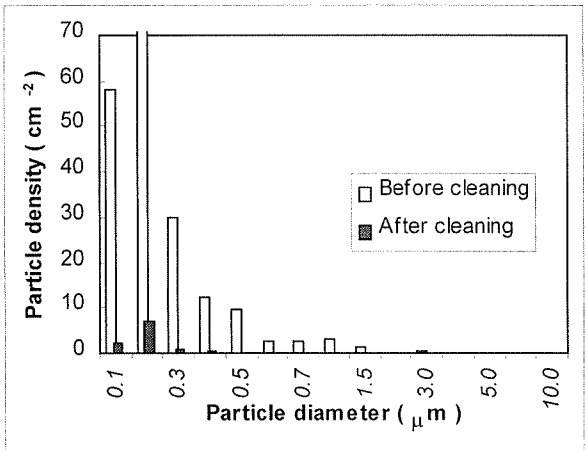

Figure 2.16 The densities of 0.2 μm CML particles before and after laser cleaning. The laser flux was 357 mJ/cm^2, 3 cleaning cycles. The nitrogen flow was 4223 ml/min. The 0.2 μm particle density was 420 cm^{-2}.

From the comparison of different techniques used to reduce particle re-contamination, we found that thermophoresis, induced by heating the wafer, has the greatest cleaning efficiency and its experimental setup is the simplest.

2.4 References

[1] Boughaba S., Wu X., Sacher E. and Meunier M., *J. Adhesion,* **61**, 293 (1997).

[2] Ohyama T., Endoh K., Mikami A. and Mori Y., *Rev. Sci. Instrum.*, **59**, 2018 (1988).

[3] Tam A. C., Leung W. P., Zapka W., and Ziemlich W., *J. Appl. Phys.*, **71**, 3515 (1992).

[4] Batchelor G. K. and Shen C., *J. Colloid Interface Sci.*, **107**, 21 (1985).

[5] Zapka W., Ziemlich W., and Tam A. C., *Appl. Phys. Lett.*, **58**, 2217 (1991).

[6] Heroux J. B., Boughaba S., Ressejac I., Sacher E. and Meunier M., *J. Appl. Phys.*, **79**, 2857 (1996).

[7] Engelsberg A. C., U.S. patents 5 024 968 and 5 099 557.

[8] Donovan R. P. and Menon V. B. in *Handbook of Semiconductor Wafer Cleaning Technology*, Kern W. Ed. (Noyer Publications, Park Ridge, New Jersey, 1993), pp.164-167.

[9] Donovan R. P., Yamanoto T., and Periasamy R., *Mat. Res. Soc. Symp. Proc.*, **315**, 3 (1993).

[10] Ye Y., Pui D. Y., Lui B. Y. H., Opiolka S., Blumhorst S., and Fissan H., *J. Aerosol Sci.*, **22**, 63 (1991).

[11] Tyndall A. M., *Proc. R. Inst.*, **6**, 3 (1870).

[12] Derjuig B. and Yalamov Y., *J. Colloid Interface Sci.*, **22**, 195 (1966).

[13] Batchelor G. K. and Shen C., *J. Colloid Interface Sci.*, **107**, 21 (1985).

[14] Willams M. M. R., *J. Colloid Interface Sci.*, **122**, 110 (1988).

[15] Jayarj S., *Heat Mass Transfer*, **30**, 167 (1995).

[16] Epstein P., *Z. Phys.*, **54**, 537 (1929).

[17] Sears F. W., Zemansky M. W. and Young H. D., College Physics (Addison-Wesley Publishing Co., Reading, Massachusetts, Menlo Park, California, 1982), pp. 254.

Chapter 3

PHOTOACOUSTIC WAVE EMISSION DURING LASER-ENHANCED PARTICULATE REMOVAL

3.1 Introduction

As mentioned previously, laser enhanced semiconductor surface cleaning is chemical-free and environment-friendly. It has shown great potential for removing submicron-sized particles from substrate surfaces [1]. However, the mechanisms for this particle removal process are presently not well understood. The photoacoustic waves (PAW) induced by the laser pulses contain much information about surface vibrations and the induced bubble pressure pulse thought to play the major role in particulate removal [2, 3]. Thus, a study of these waves may aid our understanding of the laser cleaning process. Several techniques have been developed to measure the photoacoustic waves induced by laser pulses [4-6]. The piezoelectric transducer is one of them. It is simple and can monitor surface vibrations during laser cleaning.

3.2 Experimental Arrangement and Procedure

Our experimental arrangement is found in Figure 3.1. We used a broad band piezoelectric transducer (Panametrics, V1091) to measure the PAW signals induced by a single pulse of KrF excimer laser (MPB Technologies, Inc. AQX-150, wavelength:

248 nm, pulse duration: 22 ns) during both dry (direct surface energy transfer to particles) and steam (indirect surface energy transfer to particles through an intervening liquid) laser cleaning. The laser flux could be changed continually by a variable attenuator. The transducer contacted the back side of a 100 mm <100> silicon wafer, using vacuum grease as the coupling agent; PAW signals were amplified by a preamplifier (HP 8447A) and displayed on a 300 MHz digitizing oscilloscope (HP 54201D) before being analyzed by computer. Relative amplitudes of PAW signals under different experimental conditions were used for comparison. Polystyrene latex and

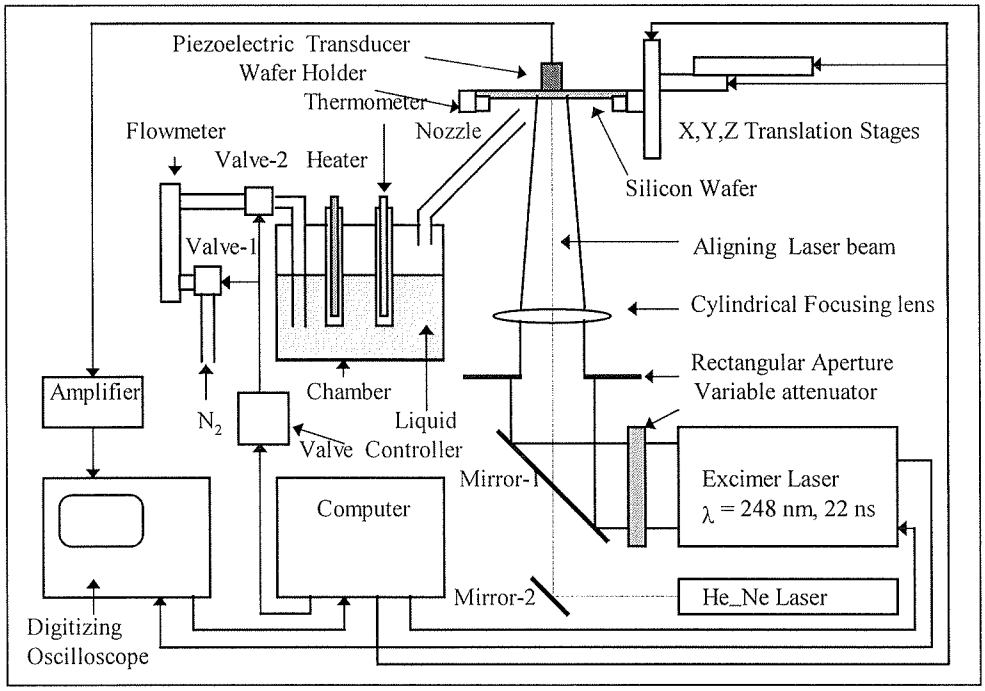

Figure 3.1 Experimental arrangement to demonstrate PAW generation and detection, and removal of PSL and Al_2O_3 particles by dry and steam cleaning.

aluminum oxide particles, 0.1 and 0.2 microns in diameter, respectively, were deposited on the silicon surfaces and cleaned by both dry and steam methods. The laser cleaning efficiency was evaluated by counting the number of particles with a laser scanning surface inspection system (Particle Measuring Systems, Inc., SAS 3600).

3.3 Results and Discussion

During dry laser cleaning, at 248 nm, the silicon substrate strongly absorbed the laser energy, which induced the temperature of the wafer surface to increase rapidly during the laser pulse. A localized temperature rise in the substrate results in a localized thermal expansion which, in turn, generates photoacoustic waves by the thermoelastic effect [7]. Several approaches have been proposed for modeling this thermoelastic process [8-11]. The laser thermoelastic generation of ultrasound is a complex process that involves optical, thermal, thermomechanical, and mechanical phenomena within the material. Here, we only focus on the subject as it relates to laser cleaning.

During steam cleaning, water is transparent to excimer laser, the silicon substrate strongly absorbed the laser energy, the temperature of the surface layer increased in very short time, the water film adjacent to the surface was superheated by energy transfer and

explosively evaporated. The pressure pulse due to bubble generation and collapse induced additional PAW signals at the surface [12].

By moving the transducer to different locations on the back side of silicon wafer during laser cleaning, we found that the PAW signal induced by the laser pulse propagated along the silicon wafer surface, perpendicular to the laser beam, and was reflected at the wafer edge. While a thermoelastic process usually launches all types of acoustic waves in all the directions of the half-space. The features of the laser excitation improve the efficiency of longitudinal wave generation in the direction normal to the impinged surface [11]. The velocity of the longitudinal PAW signal is obtained by

$$V_{PAW} = \Delta x / \Delta t = 5455 \text{ m/s}$$

where Δx and Δt are the distances and PAW signal time delays for pairs of detection points.

Figure 3.2 shows the PAW signals for dry and steam laser cleaning detected by the piezoelectric transducer located at the center of silicon wafer back side, directly opposite the laser beam. The peak value of the PAW signal detected during steam cleaning at a laser energy flux of 187 mJ/cm^2 was about two times greater than that detected during dry cleaning at a similar laser energy flux of 195 mJ/cm^2. It was necessary to use a laser

energy flux of 310 mJ/cm^2 during dry cleaning for the PAW signal to reach the same level as that during steam cleaning at a laser energy flux of 187 mJ/cm^2.

The amplitude of the PAW signal strongly depends upon the incident laser energy, the cleaning method and the distance between laser beam and location of the transducer, as shown in Figures 3.3 and 3.4.

During steam cleaning at low laser fluxes, the temperature increase at the substrate surface due to the laser energy was not high enough to superheat the water film, and no (or few) bubbles were generated. The dominant PAW signal came from the thermoelastic effect at the substrate surface so that the PAW signals for dry and steam cleaning were similar: because of a higher heat loss at the water/substrate interface compared with that at the air/substrate interface, the PAW signal was slightly less during steam cleaning. As the laser flux increased, the PAW signal for steam cleaning increased much faster because the superheated water film created many bubbles: the PAW signal due to the bubble pressure is proportional to the amount of bubbles or the bubbles coverage on the surface. At a laser fluence of 170 mJ/cm^2, the PAW signal during steam cleaning is about two times greater than that during dry cleaning; this is one reason why steam cleaning has a higher cleaning efficiency than dry cleaning [3]. At high laser fluxes, the elevated temperature of the substrate surface induces film boiling of the water

adjacent to the surface [13], and a layer of bubble is generated at the water/substrate interface. The vapor layer isolates the heat transferring from the surface to water. No more bubbles were generated as the laser flux was further increased, saturating the PAW signal.

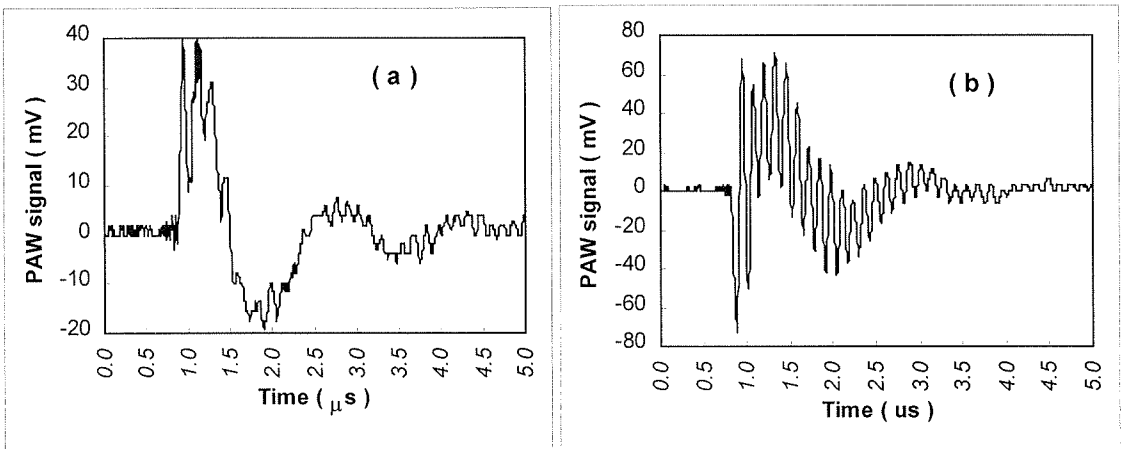

Figure 3.2 The photoacoustic wave signals : (a) dry laser cleaning at a laser energy flux of 195 mJ/cm^2; (b) steam laser cleaning at a flux of 187 mJ/cm^2; (c) dry laser cleaning at a flux of 310 mJ/cm^2.

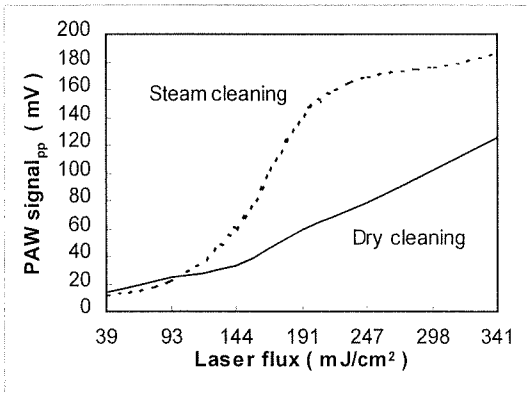

Figure 3.3 The peak-to-peak amplitude of the PAW signal as a function of incident laser flux during dry and steam cleaning.

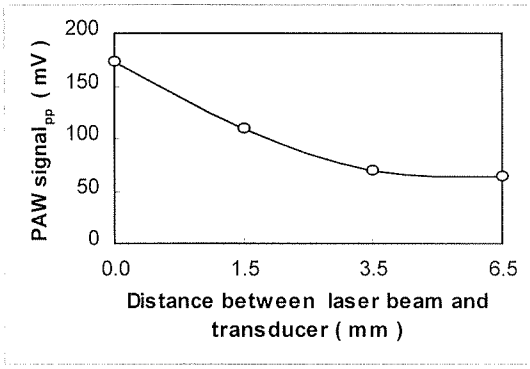

Figure 3.4 The peak-to-peak amplitude of the PAW signal as a function of the distance between the laser beam and the location of the transducer during dry cleaning with a laser flux of 321 mJ/cm^2.

We deposited 0.1 μm PSL particles on the silicon surface. During dry cleaning, the PSL particle cleaning threshold was at a laser flux of 76 mJ/cm^2. From Figure 3.3, we find the PAW signal to be about 20 mV. With the exception of the particles directly irradiated, none of those in the PAW propagation path were removed even though the laser flux reached 326 mJ/cm^2. At this laser flux, the PAW signal 3.5 mm away laser beam was about 80 mV, as shown in Figure 3.4, much stronger than that in the directly irradiated area at a laser flux of 76 mJ/cm^2. These results led us to the conclusion that only the

irradiated area suffers the thermoelastic pulse; it couples much more efficiently with particles at the surface than the PAW which was excited by this thermoelastic pulse and was detected at the back side of the wafer. Therefore, the effective removal of PSL particles by dry cleaning is localized in the laser beam.

Similar phenomenon was found for the removal of Al_2O_3 particles during steam cleaning: only the particles in the directly irradiated area were removed. As mentioned earlier [15], the dominant Al_2O_3 particle removal force during steam cleaning is bubble pressure. The heat diffusion length $(\kappa\tau/\rho C_p)^{1/2}$ of silicon is less than 10 μm, which can be ignored compared with the laser beam width (~ 1 mm). Thus, bubble generation due to superheated of water film adjacent to the substrate surface is confined to the laser beam.

3.4 References

[1] Tam C., Leung W. P., Zapka W. and Ziemlich W., *J. Appl. Phys.* **71**, 3515 (1992).

[2] Wu X., Sacher E. and Meunier M. in *Proc. of Adhesion Society* (Savannah, Georgia, Feb. 1998), Dickie R. A. Ed. p.309.

[3] Wu X., Sacher E. and Meunier M., *J. Adhesion.* **70**, 167 (1999).

[4] Leung W. P. and Tam A. C., *Appl. Phys. Lett.* **60**, 6 (1992).

[5] Tam A. C., Do N., Klees L., Leung P. T. and Leung W. P., *Opt. Lett.* **17**, 1809 (1992).

[6] Yavas O., Leiferer P., Park H. K., Grigoropoulos C. P., Poon C. C., Leung W. P., Do N. and Tam A. C., *Appl. Phys.* **A58**, 407 (1994).

[7] Burgreen D., *Element of Thermal Stress Analysis* (C.P. Press, Jamaica, New York, 1971), pp. 1–28, 89–91.

[8] Doyle P. A., *J. Phys. D: Appl. Phys.*, **19**, 1613 (1986).

[9] McDonald F. A., *Appl. Phys. Lett.,* **54**, 1504 (1989).

[10] Dubois M., Enguehard F. and Bertrand L., *Appl. Phys. Lett.,* **64**, 554 (1994).

[11] Enguehard F. and Bertrand L., *J. Appl. Phys.,* **84**, 1532 (1997).

[12] Yavas O., Schilling A., Bischof J., Boneberg J. and Leiderer P., *Appl. Phys.* **A 64**, 331 (1997).

[13] Stralen S. V. and Cole R., *Boiling Phenomena* (Hemisphere, Washinton, 1979), vol. 1, p.104.

[14] Lazare S. and Gramier V., *Laser Chem.*, **10**, 25 (1989).

[15] Wu X., Sacher E. and Meunier M., *J. Appl. Phys.,* accepted.

Chapter 4

THEORETICAL MODELING OF EXCIMER LASER CLEANING

4.1 Introduction

Modeling is the subject of two papers:

(i) The Effects of Hydrogen Bonds on the Adhesion of Inorganic Oxide Particles on Hydrophilic Silicon Surfaces, published in the Journal of Applied Physics, **86**, 1744 (1999).

(ii) The Modeling of Excimer Laser Particle Removal from Hydrophilic Silicon Surfaces, submitted to the Journal of Applied Physics,

which are found section 4.2 and 4.3 respectively. Here, we introduce the basic ideas of the model.

4.1.1 Dominant adhesion forces between particles and substrate surfaces

In order to explain the laser cleaning and photoacoustic wave experimental results given in chapters 2 and 3, we must understand the interactions between particles and substrate surfaces during laser cleaning. These interactions can be classified into two parts: adhesion interactions and removal interactions induced by the laser pulse. Cleaning becomes efficient when the removal forces become greater that the adhesion forces. First, we will consider the dominant adhesion forces. Several review papers on particle

adhesion to various substrate surfaces [1-3] suggested that van der Waals, capillary and electrostatic forces were involved in holding particles to the substrate surface.

The van der Waals force consists of two terms: one treats the particle as a non-deforming sphere while the other considers particle deformation. The deformation area of the particles can be calculated using the JKR model [4] but this does not appear suitable for PSL particles [5]. The equations used to calculate van der Waals force, deformation area and detail discussion are not given here; they are found in section 4.2, equations (4.4) and (4.5).

Water molecules in air can adsorb onto a solid and form a thin liquid film near the contact area between particle and substrate surface. This liquid film provides a capillary force that can be calculated by [3]

$$F_C = 4\pi r_p \sigma_{liquid}[\sin\alpha \sin(\alpha_C + \theta) + \cos\theta] \tag{4.1}$$

where r_p is the particle radius, σ_{liquid} is the liquid surface tension, θ is the contact angle of the liquid on the particle and α_c is the angle between the point vertically from the center of the particle to the point of the liquid film contact with the particle. We assume that the area of liquid film is approximately equal to the contact area. For PSL particles on hydrophilic silicon surfaces and liquid water, $\alpha_{max} = 30°$, $\theta = 91°$ and $\sigma_{liquid} = 72.75$ mN/cm. For oxide particles, such as SiO_2 and Al_2O_3 particles, $\alpha \approx 0°$ and $\theta = 0°$.

The electrostatic forces include electrostatic image forces and double layer forces at the particle. These two forces are given by [1,2]

$$F_{ei} = 4\pi(\varepsilon_0/\varepsilon)\, U^2\, [0.5772 + 0.5\, ln(2r_p/z_0)] \quad (4.2)$$

$$F_{dl} = 4\pi\varepsilon_0\, U^2\, (r_p/z_0) \quad (4.3)$$

where the dielectric constant of free space $\varepsilon_0 = 8.85 \times 10^{-12}$ F/m, the relative dielectric constant $\varepsilon < 10$, the maximum zeta potential U ~ 0.5 V, and the distance between the particle and the substrate surface $z_0 = 4$ Å . The values of all adhesion forces for 0.2 μm PSL and SiO_2 particles on the silicon surface are given in the Table 4.1 in section 4.2. The electrostatic image forces are two orders of magnitudes smaller than the double layer forces; they are neglected and are not listed in Table 4.1.

From these calculations, we find that the van der Waals force deformation term is predominant for both organic and inorganic oxide particles; in comparison, capillary forces are much smaller, and while electrostatic double layer forces may be neglected. It should be noted that the van der Waals force of PSL is much larger than that of SiO_2 because PSL is a softer material and has a much larger deformation. Based on these calculations, the PSL particles should be more difficult to remove, but the laser cleaning experiments give the opposite results.

We list the possibilities whose may induce the big differences of the cleaning efficiencies between PSL and inorganic particles: melting, ablation and oxide

degradation of PSL particles; and the different removal forces for two kinds of particles. The melting and ablation look like being the most possible because PLS material has low malting point (240 °C) [6] and low ablation threshold for KrF excimer laser (250 mJ/cm^2) [7]. In order to verify these possibilities, we deposited great number of PSL particles on the surface (particle density ~ 10^4 cm^{-2}), then different laser flux were used to scan the wafer surface (100 – 380 mJ/cm^2), we used XPS to analyze the components on the wafer surface. If melting and ablation of PSL particle happened during laser cleaning, the PSL thin film would existed on the wafer surface and great increase of carbon component would be found by XPS. In Figure 4.1, there is no indication of the increase of carbon component.

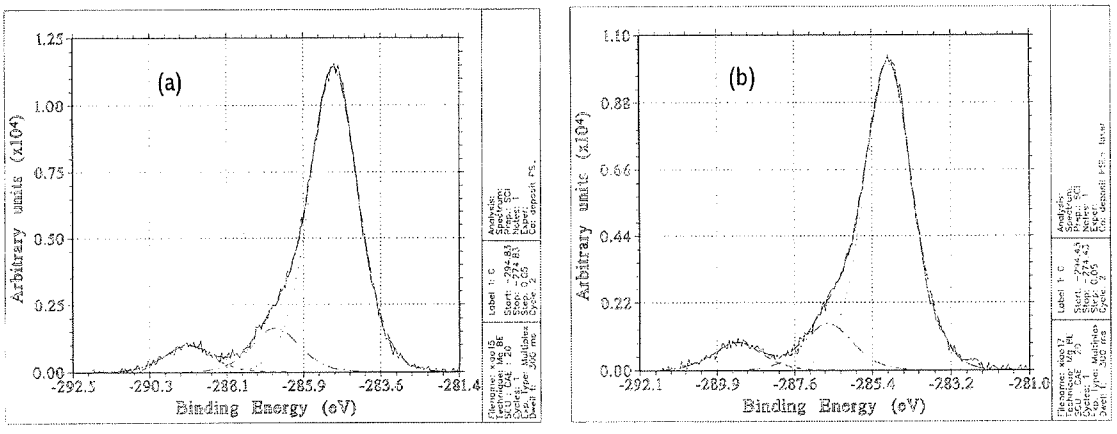

Figure 4.1 XPS spectra of C^{1s} peak, PSL particles deposited on hydrophilic silicon surfaces. (a) before laser cleaning, the concentration of C^{1s} is 25.26% (b) after laser cleaning, laser flux is 220 mJ/cm^2, the concentration of C^{1s} is 21.57%.

The absorption of laser energy of submicron sized particle is weaker than that of plate material, and energy is lost due to poor thermal coupling between the particle and substrate surface. So, the PSL particles cannot reach the melting point and ablation threshold. The possible of oxide degradation of PSL particles is also very low in very short laser pulse duration. The thermal removal forces of organic and inorganic particles will be discussed in the later section. They cannot explain the differences of the cleaning efficiencies between PSL and inorganic particles.

To explain the contradiction of theory and experiment results, we must consider the adhesion force contribution of hydrogen bonding between the hydroxyl groups on the surfaces of inorganic particles and those on the silicon surface [1, 8, 9]. A detailed discussion will be found in section 4.2.

During dry laser cleaning, both particle and substrate absorb laser energy and are heated immediately. Sudden thermal expansions of both particle and substrate then take place over very short time duration, through the thermoelastic effect [10]. This leads to the acceleration and ejection of PSL particles from the surface. During steam laser cleaning, the particles are covered by a thin film of water. In this case, due to electrical shielding [3,11], the van der Waals force is reduced, by about a factor of two; capillary forces are nullified, and any indirect hydrogen bond chain between particle and surface has a significant probability of bonding to free water molecules. This is one reason why SiO_2

particles can only be removed during steam cleaning; the values of the adhesion forces for SiO_2 during steam cleaning are also given in Table 4.1. On laser exposure, the laser energy is transferred to the liquid film except for that fraction used in thermal expansion. This transient heating of the deposited liquid film leads to its explosive evaporation at the interface of water/substrate. Bubble growth generates high-pressure pulses and directs particles away from the substrate surface. In section 4.3, the adhesion and removal forces will be discussed in greater detail.

4.1.2 References

[1] Krupp H., *Advan. Colloid Interface Sci.*, **1**, 111 (1967).

[2] Bowling R. A., *J. Electrochem. Soc.*, **132**, 2209 (1985).

[3] Ranade M. B., *Aerosol Sci. Tech.*, **7**, 161 (1987).

[4] Johnson K. L. and Roberts A. D., *Proc. R. Soc. London,* **A324**, 301 (1971).

[5] Rimai D. S. and DeMejo L. P., *Annu. Rev. Mater. Sci.*, **26**, 21 (1996).

[6] Brandrup J. and Immergut E. H., Eds., *Polymer Handbook* (Wiley-Interscience, New York, 1989), p.v/82.

[7] Paraskevopoulos G., Singleton D. L., Irwin R. S. and Taylor R. S., *J. Appl. Phys.*, **70**, 1938 (1991).

[8] Knozinger H., in *The Hydrogen Bond*, Schuster P., Zandel G. and Sandorfy C., Eds. (North-Holland, New York, 1976), part I.

[9] Sugino R., Okui Y., Okuno M., Shigeno M., Sato Y., Ohsawa A. and Ito T., *IEICE Trans. Electron.,* **E75-C**, 829 (1992).

[10] Burgreen D., *Element of Thermal Stress Analysis* (C.P. Press, Jamaica, New York, 1971), pp. 1–28, 89–91.

[11] Kolomenskii A. K. and Maznev A. A., *J. Appl. Phys.*, **77**, 6052 (1995).

4.2 The Effects of Hydrogen Bonds on the Adhesion of Inorganic Oxide Particles on Hydrophilic Silicon Surfaces

In the previous section, the laser cleaning results for organic and inorganic particles showed that hydrogen bonds might have a dominant effect on the adhesion of inorganic oxide particles, such as SiO_2 and Al_2O_3, to hydrophilic silicon surfaces. An analysis of the adhesion forces due to hydrogen bonds between particle and substrate surfaces has been carried out here , and is used to interpret the efficiencies of removing polystyrene latex (PSL), SiO_2 and Al_2O_3 particles from a hydrophilic silicon surface by laser cleaning. Evidence of the dominant effect of hydrogen bonding was confirmed by using alcohol instead of water during particle deposition. This work has been published in the Journal of Applied Physics, **86**, 1744 (1999).

The Effects of Hydrogen Bonds on the Adhesion of Inorganic Oxide Particles on Hydrophilic Silicon Surfaces

X. WU, E. SACHER and M. MEUNIER

Groupe de Recherche en Physique et Technologie des Couches Minces

Département de Génie Physique

École Polytechnique de Montréal

C.P. 6079, Succursale Centre-Ville,

Montréal, Québec H3C 3A7

Canada

4.2.1 INTRODUCTION

Contamination on wafer surfaces remains a serious problem in semiconductor manufacturing [1]. It is well know that particle contamination decreases device yield drastically [2]. To remove particles from a wafer surface requires knowledge of those adhesion forces that hold the particles to that surface.

The attractive interaction forces between different media are classified as long- and short-range. Long-range forces act to bring the particle to the surface and establish the

adhesion contact area; they include van der Waals and electrostatic forces. Short-range forces can add to adhesion only after the establishment of an adhesive contact area; they include the various types of chemical bonds: metallic, covalent and ionic, as well as hydrogen bonds [3]. Much work has been done to describe adhesion forces between particle and substrate surface [4-7]. This work has led to the conclusion that van der Waals, capillary, and electrostatic adhesion forces are the major contributors. Chemical bonds at the contact area between the adherents are so far accounted for only qualitatively [4, 5, 8, 9], although they may play an important role on the silicon surface, because a quantitative treatment of chemical bonds between particle and substrate surface is very difficult.

It is well know in surface chemistry that many solid surfaces contain potential hydrogen bond donors and acceptors. Because hydrogen bond formation has low activation energy, it occurs at room temperature; therefore, particle-substrate surface interactions via hydrogen bonding are possible [10]. Water viscosity experiments have demonstrated the existence of hydrogen bonds between spherical and flat fused silica surfaces [11]. Although the hydrogen bond is not a strong chemical bond (its bond energy is generally about 5 kcal/mole or 0.22 eV/bond) [3], it is, nonetheless, much stronger than the energy of van der Waals adhesion, typically 1 kcal/mole or 0.043 eV/bond [12]. Thus, hydrogen bonding may play a very important role in the adhesion of particles to substrate surfaces.

This paper discusses the adhesion forces due to hydrogen bonds between both SiO_2 and Al_2O_3 particles and a hydrophilic silicon surface, then uses the chemical adhesion model to explain the experimental laser cleaning results.

4.2.2 EXPERIMENTAL EQUIPMENT AND PROCEDURE

Although the details of particle removal by laser cleaning have been given previously [13], a brief description will be given here. We irradiated the contaminated wafer surface in ambient air with KrF excimer laser pulses (MPB Technologies, Inc. AQX-150, at 248 nm wavelength, with a 22 ns pulse width at half maximum), using both dry and steam laser cleaning techniques. Steam laser cleaning has a high cleaning efficiency, made possible by the use of a thin film of deposited water as an energy transfer medium and adhesion force reduction agent. Dry laser cleaning is simpler, in that no liquid is involved; it is compatible with cluster tools.

Three kinds of particles were deposited onto a silicon wafer surface using a particle generator (Particle Measuring System, Inc.). The particles were: 0.1 μm polystyrene latex (PSL) from Particle Measuring System, Inc., and 0.1–0.2 μm agglomerated SiO_2 and 0.1 μm Al_2O_3 from Beta Diamond Corp. The particle generator used a diaphragm pump to force air through a filter. Filtered air then moved through a nebulizer having about 0.007% monodisperse particles suspended in deionized (DI) water. The flow then

passes through a drying chamber where the water droplets evaporated. Finally, the particle-laden air was sprayed onto the wafer surface through a long tube with a moveable nozzle.

4.2.3 LASER CLEANING RESULTS

Figure 4.2 shows the particle densities for each kind of particle, before and after laser cleaning. We found that, for dry cleaning, KrF excimer laser radiation effectively removed all the PSL particles from the silicon surface but, for SiO_2 and Al_2O_3 particles,

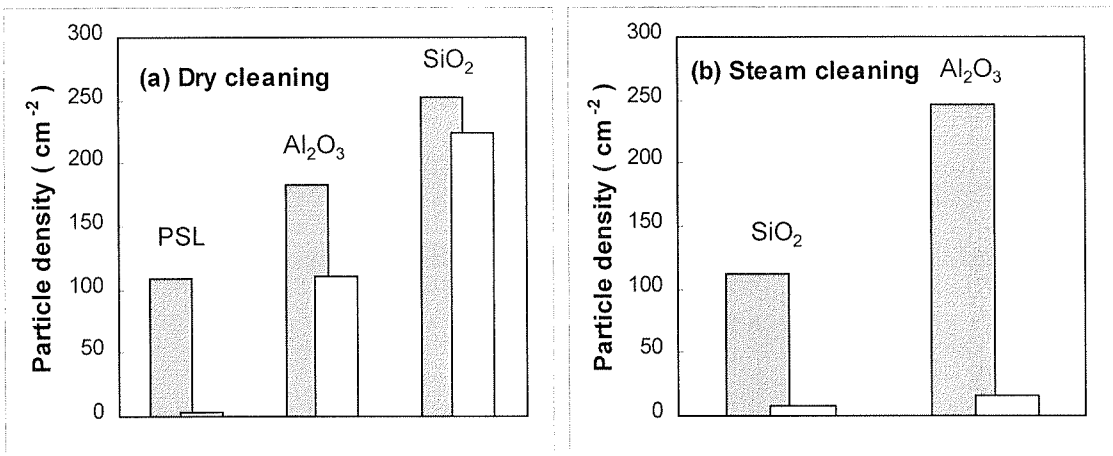

Figure 4.2 0.1 μm PSL, SiO_2 and Al_2O_3 particle densities before (gray bar) and after (white bar) laser cleaning. (a) During dry laser cleaning, the laser energy fluxes were 326, 314 and 326 mJ/cm^2, respectively, and 2, 4 and 4 cleaning scanning cycles, respectively were used. (b) During steam cleaning, the laser energy fluxes were 180 and 154 mJ/cm^2, respectively, and 5 and 4 cleaning scanning cycles were used, respectively.

the particle densities were not much reduced. For steam laser cleaning, both SiO_2 and Al_2O_3 particles were removed with high efficiencies.

A second set of experiments was used to verify the effect of hydrogen bonds on the adhesion of particles to hydrophilic silicon surfaces. This was achieved by using two different alcohols (methanol and ethanol) instead of DI water during particle deposition. On alcoholic steam cleaning, which immediately followed particle deposition and had experimental conditions identical to those of steam cleaning except for a larger laser flux, the cleaning efficiencies of SiO_2 and Al_2O_3 particles were drastically reduced, as shown in Figure 4.3.

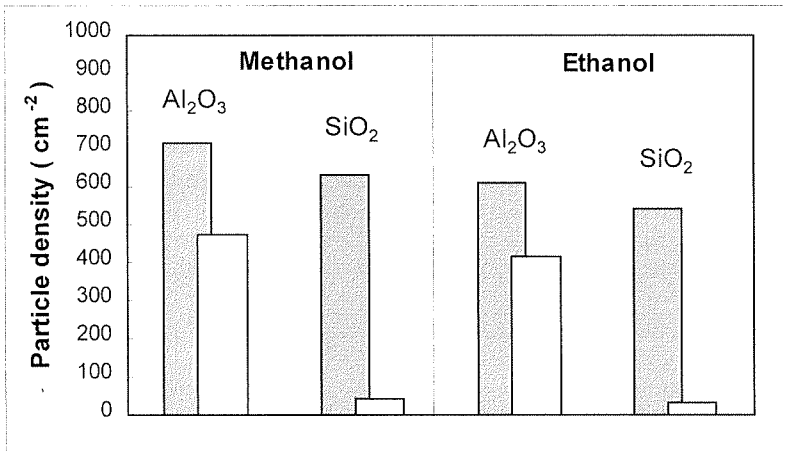

Figure 4.3 0.1 μm SiO_2 and Al_2O_3 particle densities before (gray bar) and after (white bar) steam laser cleaning, using methanol and ethanol instead of DI water during particle deposition. The laser energy flux was 204 mJ/cm^2, and 5 cleaning scanning cycles were used.

4.2.4 CHEMICAL BONDS AND ADHESION FORCES

A summary of our previous discussion of adhesion forces between PSL and SiO_2 particles and a hydrophilic silicon surface [13], is given in Table 4.1. There, the van der Waals force was shown to dominate capillary and electrostatic forces for submicron sized particles attached to the silicon surface. It can be expressed as [5]

$$F^{V} = F_{0}^{V} + F_{Deformation}^{V} = \frac{h\varpi_{132} r_{P}}{8\pi z_{0}^{2}} + \frac{h\varpi_{132} a^{2}}{8\pi z_{0}^{3}} \qquad (4.4)$$

Table 4.1. The adhesion forces of 0.2 μm PSL and SiO_2 particles on the silicon surface.

	Dry Cleaning		Steam Cleaning
Adhesion Forces	PSL Particles (0.2 μm)	SiO_2 Particles (0.2 μm)	SiO_2 Particles (0.2 μm)
van der Waals (deformation)	160 mdyn	9.9 mdyn	3.2 mdyn
van der Waals (non-deformation)	1.4 mdyn	1.5 mdyn	0.5 mdyn
Capillary	4.7 mdyn	9.0 mdyn	0
Electrostatic	0.004 mdyn	0.004 mdyn	0.35 mdyn
Chemical Bonds	none	surface hydroxyl	surface hydroxyl

The first term of equation (4.4) is the van der Waals forces between a sphere and a plane, and the second term is due to elastic or plastic deformation. $h\varpi_{132}$ is the Lifshitz-van der

Waals constant, r_p is the particle radius, z_0 is the separation distance between particle and substrate, which is not measurable but assumed to range from 4 to 10 Å [4] (we used $z_0 = 4$ Å), a is the deformation contact radius of particle on the surface, which can be calculated using the JKR model [14] for rigid particles (SiO_2 and Al_2O_3) :

$$a^3 = \frac{9}{2} W \pi r_p^2 \left(\frac{1 - \nu_1^2}{E_1} + \frac{1 - \nu_2^2}{E_2} \right) \tag{4.5}$$

where W is the work of adhesion of the particle on the substrate surface which approaches the value of $2(\gamma^s_1 \gamma^s_2)^{1/2}$, γ^s_1 and γ^s_2 being the surface free energies of particle and substrate, respectively; ν and E are Poisson's ratio and Young's modulus for particle and substrate. For PSL particles, the contact radius is not a function of the particle radius to the 2/3 power but, rather, to the 1/2 power [15]. The softer the particle, the larger both the contact radius and the adhesion force. Based on these calculations, PSL particles should be more difficult to remove than the two inorganic particles, but the laser cleaning experiments give the opposite results.

To explain this contradiction, we consider the short-range adhesion forces from hydrogen bonds between hydroxyl groups on the inorganic oxide particle surfaces and on the hydrophilic silicon surface. PSL particles, having no surface oxide, do not produce such hydroxyl groups.

A key characteristic of the SiO_2 surface is that it becomes covered with silanol (SiOH) groups at room temperature [16]. The concentration of SiOH groups on the silica surface is about the same for different type of silica [17]; the results of several methods agree very well and give an average value of 4.6 ± 0.2 OH/nm^2 for a fully hydroxylated silica surface [10, 16]. This average number of silanol groups very nearly corresponds to the number of silicon atoms on a silica surface. The metal-oxygen bond of many metal oxides is more ionic in character than that of silica. The oxygen ions of an alumina surface seem to be effective hydrogen bond acceptor sites; further, alumina surfaces which were previously exposed to water vapor or moist air are terminated by a monolayer of hydroxyl groups, each occupying about 0.08 nm^2 on the surface, corresponding to 12.5 OH/nm^2 [17].

Our hydrophilic silicon surface was hydroxylated during SC1 pretreatment [13]. SiO_2 and Al_2O_3 particles were kept in air and immersed in water for deposition, so their surfaces were also hydroxylated. Water, which has both hydrogen bond donor and acceptor properties, has a pronounced tendency to interact with the OH groups on hydroxylated surfaces through hydrogen bonding. Figure 4.4 shows several examples of how a water molecule may be bound to a hydroxylated surface [18-21].

An operational definition commonly used [22] states that a hydrogen bond between two groups X–H and Y exists when there is evidence of interaction between X-H and Y. The

distance between atoms X and Y (in our case, the hydrogen bond is O–H---O) is comparable with the van der Waals contact distance (~ 3.4 Å) [23] so, when the particles are deposited on the substrate surface, they may be bonded to the surface either (a) indirectly, through hydrogen bonding with water molecules adjacent to the contact area, or (b) directly, through hydrogen bonding of the hydroxyl groups of particle and substrate in the deformation area [24], as shown in Figure 4.5. Absorbed water molecules can be retained around the contact area up to a temperature of 180 °C [25].

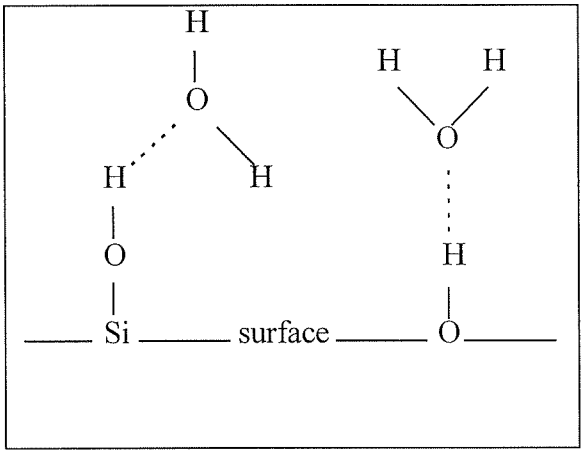

Figure 4.4 Several examples of water hydrogen bonded to hydroxylated surfaces. The dashed lines are hydrogen bonds.

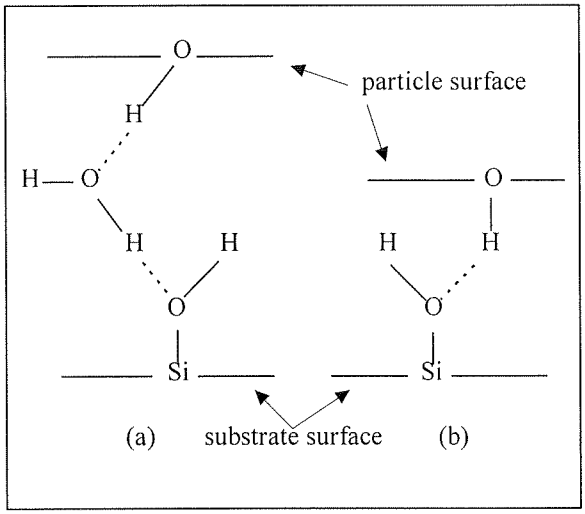

Figure 4.5 Indirect (a) and direct (b) hydrogen bonding between particle and substrate surfaces. The dashed lines are hydrogen bonds.

In order to calculate the adhesion force due to hydrogen bonding, we must know the total bond energy E_{total} which is calculated as

$$E_{total}=DSE_{bond} \tag{4.6}$$

where $\boldsymbol{D}$ is the OH group density, $\boldsymbol{S}$ and $\boldsymbol{E_{bond}}$ are the total interaction area and the hydrogen bonding interaction energy between particle and substrate. $\boldsymbol{E_{bond}}$ depends on the natures of the surfaces, in particular on their degrees of hydroxylation and on the electronic structure of the materials. The average bonding energy of the O–H---O hydrogen bond is about 5 kcal/mole (~ 0.22 eV/bond) [27]. In the case of dry cleaning, the interaction area is

$$S = \pi a^2 + 2\pi r_p \Delta z\, b \tag{4.7}$$

where the first term is the deformation area of the particles and the second term is the ring area cut at a height Δz near the contact point with the probability $\boldsymbol{b}$ that particle and surface form a hydrogen bond.

In general, the total O–H---O bond length is 2.72 Å and the length of a hydrogen bond H---O is 1.7 Å [28]. The X–H---O bond angle was set at 120° [23]. The length of the O–Si bond is 1.66 Å [29], and we used 0.96 Å as the length of the O–H bond in a water molecule and a surface silanol group [29]. According to the hydrogen bond structure in Figure 4.4, Δz is approximately equal to the total length of the hydrogen bond chain. If there is only one water molecule involved, the chance of this water molecule connecting

particle and surface is 50% ; if two water molecules participate, the possibility reduced to 25%, and so on. For SiO_2 particles, Δz_b is ~ 7.21 Å and, for Al_2O_3, it is ~ 7.05 Å. During steam cleaning, a water film covers the particle surface, the hydrogen bond has a 50 % probability of connecting the particle to the surface or connecting the free water molecules in the film, so the second term in equation (4.7) is reduced by half. To break the hydrogen bonds between particle and substrate, the work done by the cleaning force must be larger than the total adhesion energy of hydrogen bonding. To simplify the problem, we assume the adhesion force of a hydrogen bond as being uniform and existing in the range from its potential minimum to the dissociation distance d_{bond}. Finally, we obtain the adhesion force due to hydrogen bonding:

$$F_{H\text{-}bond} = E_{total} / d_{bond} \tag{4.8}$$

To our knowledge, there are few studies on the dissociation length of the hydrogen bond. Fliszar [30] studied the dissociation energies of chemical bonds as a function of bond electron density. He noted that the loss of one millielectron at each atom forming a single bond translates into a bond weakening of less than 1 kcal/mole (0.043 eV). When two ground state molecules, A and B, associate to form a hydrogen bond, they do not lose their chemical identities: some charge transfer is generally to be expected into the A---B bond, but it is much less than that in forming a normal chemical bond. Thus, during the dissociation process, the electron loss is expected to be smaller and the dissociation distance, longer. The force constant of the H-O---H hydrogen bond is 0.69×10^5 dynes/cm [31]. According to our assumption of a uniform energy change with

bond length, a change of 0.1 Å in the length of a hydrogen bond would take less than 0.022 eV. Therefore, in order to break the hydrogen bond or, in other words, to overcome the 0.22 eV hydrogen bond energy, the dissociation distance should be near 1Å. We arbitrarily selected this value as the dissociation distance in our calculation.

Using equations (4.6)–(4.8), we have calculated the adhesion forces due to hydrogen bonding between particle and substrate for both dry and steam cleaning, as shown in Figure 4.5. The van der Waals forces, calculated from equations (4.4) and (4.5), are also shown in Figure 4.6, for comparison with the hydrogen bonding forces. It appears that the adhesion force due to hydrogen bonding is much larger than that due to van der Waals interaction. For PSL particles, there are no surface groups capable of participating in hydrogen bonding, so only van der Waals forces play a role. Hydrogen bonding is the reason why SiO_2 and Al_2O_3 particles have lower dry cleaning efficiencies than PSL particles.

The dissociation distance can have a substantial effect on the calculated results of the adhesion force due to hydrogen bonds. For example, bond lengths 30% shorter in dissociation distance will cause a 40% increase in the calculated adhesion force. There are other parameters that can induce calculation errors, such as the degrees of hydroxylation on particle and substrate surfaces and the presence of asperities on the surfaces. Here we use 100% hydroxylation although, in practice, it may be less. The

presence of asperities on particle and substrate surfaces can greatly reduce the adhesion forces [4], a subject that will be considered in a subsequent paper.

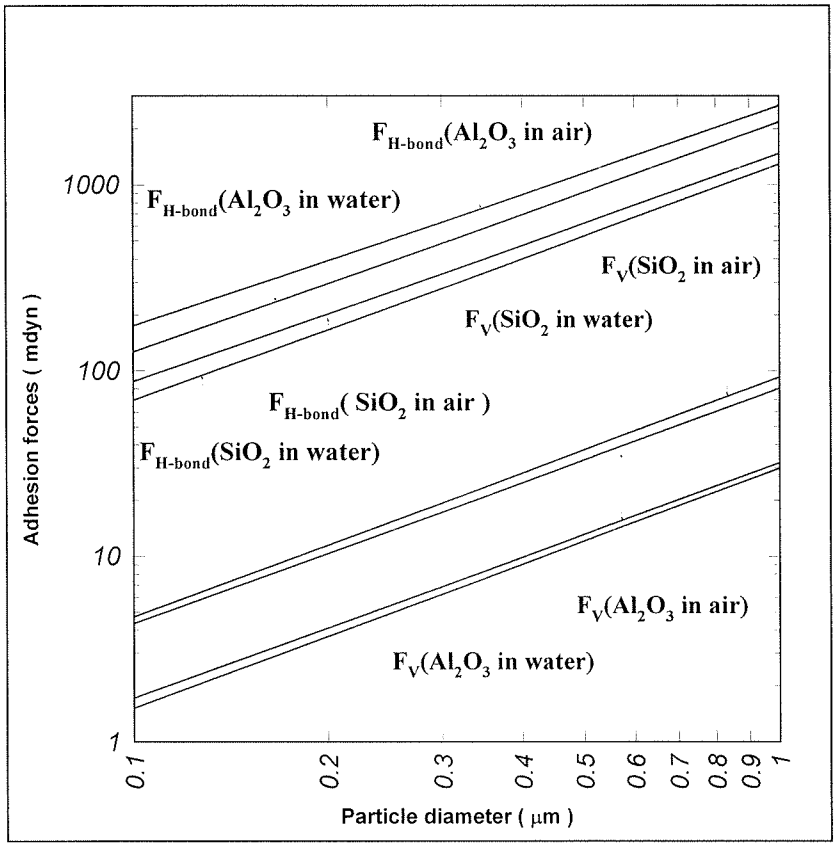

Figure 4.6 $F_{H\text{-}bond}$ and $F_{van\ der\ Waals}$ as a function of particle diameters for SiO_2 and Al_2O_3 particles on the silicon surface during dry and steam cleaning.

When we used methanol and ethanol instead of water during particle deposition, we expected similar adhesion behavior for the hydroxylated particle surfaces because their OH groups can also act as hydrogen bond participants [32]. Examples of alcohol

molecules on SiO_2 and Al_2O_3 surfaces are shown in Figure 4.7 [10, 33–35]. When the particles deposit on the hydrophilic silicon surface, alcoholic hydroxyl groups adsorbed on the particle surfaces bond with hydroxyl groups on the substrate surface. The interaction energy of H---O–R is about 7 kcal/mole for silica [33, 35] and about 14 kcal/mole [35] for alumina, so that the order of the interaction energies between particle and surface with the different deposition liquids is: Al_2O_3/ROH > SiO_2/ROH > Al_2O_3/H_2O > SiO_2/H_2O. During steam cleaning, free water molecules have difficulty replacing the alcohol molecules involved in indirect hydrogen bonds because the alcohols have larger interaction energies than water. Therefore, the order of laser cleaning efficiencies is expected to be Al_2O_3/ROH < SiO_2/ROH < Al_2O_3/H_2O < SiO_2/H_2O, as found experimentally.

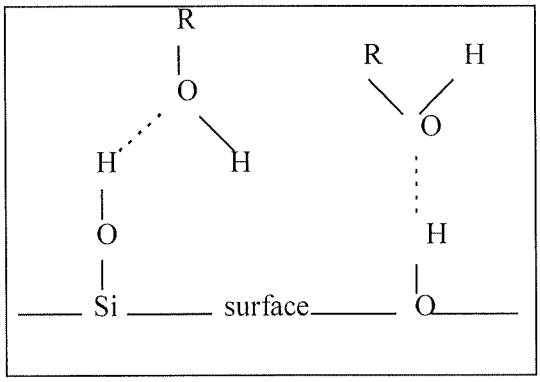

Figure 4.7 Postulated ways in which alcohol molecules may form hydrogen bonds with hydroxyl groups on SiO_2 and Al_2O_3 surfaces.

4.2.5 CONCLUSIONS

The hydroxylated surfaces of inorganic oxide particles and hydrophilic silicon wafers can interact to form hydrogen bonds. A simple model has been developed to calculate the adhesion forces due to such hydrogen bonds. The values of the adhesion forces calculated according to our model can rationalize the experimental results of laser cleaning, in which PSL particles were easily removed by dry cleaning but SiO_2 and Al_2O_3 particles were not. When we used alcohol as a dispersal agent instead of water during particle deposition, the cleaning efficiencies of SiO_2 and Al_2O_3 particles were greatly reduced during the steam cleaning which followed because the hydrogen bonds formed with alcohol molecules have stronger interaction energies and are more difficult to replace by free water molecules during steam cleaning.

4.2.6 ACKNOWLEDGMENTS

The authors thank J. P. Lévesque for his technical assistance. This work was supported by the Natural Sciences and Engineering Research Council of Canada.

4.2.7 REFERENCES

[1] Kern W. and Tolliver D., in *Handbook of Semiconductor Wafer Cleaning Technology.* Kern W. Ed. (Noyes Publications, Park Ridge, New Jersey, 1993), pp. 3, 68 and 595.

[2] Kern W., *J. Electrochem. Soc.*, **137,** 1887 (1990).

[3] Pauling L., *The Natural of the Chemical Bond and the Structure of Molecules and Crystal* (Cornell Univ. Press, New York, 1960), Chap. 12.

[4] Krupp H., *Advan. Colloid Interface Sci.*, **1**, 111 (1967).

[5] Bowling R. A., *J. Electrochem. Soc.*, **132**, 2209 (1985).

[6] Ranade M. B., *Aerosol Sci. Tech.*, **7**, 161 (1987).

[7] Donovan R. P., Yamamoto T. and Periasamy R., *Mat. Res. Soc. Symp. Proc.*, **315**, 3 (1993).

[8] Kitchener J. A., *J. Soc. Cosmet. Chem.*, **24**, 709 (1973).

[9] Bhattacharya S. and Mittal K. L., *Surf. Technol.*, **7**, 413 (1978).

[10] Knozinger H., in *The Hydrogen Bond*, Schuster P., Zandel G. and Sandorfy C., Ed. (North-Holland, New York, 1976), Chap. 27.

[11] Peschel G. and Aldfinger K. H., *J. Colloid Interface Sci.*, **34**, 505 (1970).

[12] Israelachvili J., *Intermolecular and Surface Forces* (Academic, New York, 1991), Chap. 8.

[13] Wu X., Sacher E. and Meunier M., *J. Adhesion*, accepted.

[14] Johnson K. L., Kendall K. and Roberts A. D., *Proc. R. Soc. London,* **A324**, 301 (1971).

[15] Rimai D. S. and DeMejo L. P., *Annu. Rev. Mater. Sci.*, **26**, 21 (1996).

[16] Iler P. K., The Chemistry of Silica (Wiley-Interscience, New York, 1970), Chap. 6

[17] Kipling J. J. and Peacall D. B., *J. Chem. Soc.*, **182**, 834 (1957).

[18] Kiselev A. V. and Lygin V. I., *Russ. Chem. Rev.*, **31**, 175 (1962).

[19] Morimoto T., Nayao M. and Imai J., *Bull. Chem. Soc. Japan*, **44**, 1282 (1971).

[20] Peri J. B., *J. Phys. Chem.*, **69**, 211 (1965).

[21] Della Gatta G., Fubini B. and Venturello G., *J. Chim. Phys. Chem.*, **70**, 64 (1973).

[22] Pimentel G. C. and McClellan A. L., *The Hydrogen Bond* (Freeman, San Francisco, 1960).

[23] Olovsson I. and Jonsson P. in *The Hydrogen Bond*, Schuster P., Zandel G. and Sandorfy C., Ed. (North-Holland, New York, 1976), chap. 8.

[24] Depasse J. and Watillon A., *J. Colloid Interface Sci.*, **33**, 43 (1970).

[25] Okkerse C., in *Physical and Chemical Aspects of Adsorbents and Catalysis*, Linsen B. G. Ed. (Academic, New York, London, 1970), p. 251.

[26] Schuster P. in *The Hydrogen Bond*, Schuster P., Zandel G. and Sandorfy C., Ed. (North-Holland, New York, 1976), p. 108.

[27] Iler P. K., The Chemistry of Silica (Wiley-Interscience, New York, 1970), p. 387.

[28] Joesten M. D. and Schaad L. J., *Hydrogen Bonding* (Marcel Dekker, Inc., New York, 1974), p. 36.

[29] Lide D. R. and Frederikse H. P. R. Ed. *CRC Handbook of Chemistry and Physics* (CRC Press, New York, 1996), p. 9.

[30] Fliszar S., in *Chemistry and Physics of Energetic Materials*, Bulusu S. N. ed. (Kluwer Academic Publishers, Amsterdam, 1990), p. 143.

[31] Schuster P., in *The Hydrogen Bond*, Schuster P., Zandel G. and Sandorfy C., Ed. (North-Holland, New York, 1976), p. 40.

[32] Greenler R. G., *J. Chem. Phys.*, **37**, 2094 (1962).

[33] Sewell P. A. and Morgan A. M., *J. Am. Ceram. Soc.*, **52**, 136 (1969).

[34] Borell E., Zechina A. and Morterra C., *J. Phys. Chem.*, **71**, 2945 (1967).

[35] Jeziorowski H., Knozinger H., Meye W. and Muller H. D., *JCS Faraday* **I 69**, 1774 (1973).

4.3 The Modeling of Excimer Laser Particle Removal from Hydrophilic Silicon Surfaces

We summarize experimental results on the removal of submicron-sized polystyrene latex (PSL), carboxylate-modified latex (CML), SiO_2 and Al_2O_3 particles from hydrophilic silicon surfaces by excimer laser, using both dry and steam cleaning. The cleaning thresholds have also been determined for these particles. These results are theoretically explained by an ideal sphere particle adhesion model which includes van der Waals forces and hydrogen bonding, and an ideal sphere particle removal model which includes rapid thermal expansion of the substrate due to the thermoelastic effect and the pressure shock due to bubble generation in the condensed water film. The situation of practical (i. e., rough, irregularly shaped) particles has been considered, and the theoretical analysis includes the effects of both asperities on the particle surface and particle aggregation. The results of the calculations show that particle surface roughnesses which are small compared with the particle dimension can cause large reductions in both adhesion and thermoelastic removal forces, consistent with the experimental observations. This work has been submitted to the Journal of Applied Physics.

The Modeling of Excimer Laser Particle Removal from Hydrophilic Silicon Surfaces

X. WU, E. SACHER and M. MEUNIER

Groupe de Recherche en Physique et Technologie des Couches Minces

Département de Génie Physique et de Génie des Matériaux

École Polytechnique de Montréal

C.P. 6079, Succursale Centre-Ville,

Montréal, Québec H3C 3A7

Canada

4.3.1 INTRODUCTION

The interaction of an excimer laser with a silicon surface can lead to the removal of submicron-sized contaminant particles [1, 2]. This technique is efficient, simple, fast and chlorofluorocarbon-free, a considerable environmental advantage over standard cleaning techniques. Laser cleaning may be dry, meaning that no energy transfer liquid is present on the sample surface during laser exposure; dry laser cleaning is compatible with cluster tools. However, to increase particle removal efficiencies, steam laser cleaning may be used, where the laser energy is absorbed by the substrate surface and the surface

temperature rises rapidly; the heat from the substrate surface is efficiently coupled to a liquid energy transfer medium, such as water, which is condensed on the silicon surface just prior to the arrival of the laser pulse [3-5], resulting the explosive evaporation of the liquid.

The particle removal efficiency of laser cleaning depends on two major factors: the adhesion forces holding the particles to the substrate surface and the laser-induced particle removal forces. It is well established that the efficiency of laser cleaning increases with increasing laser fluence [5] but, at higher laser fluences, substrate surfaces are easily damaged by laser irradiation [5-7]. Determining the optimal laser cleaning conditions and clearly understanding the interaction mechanisms between particle and substrate surface are the goals of our modeling of the laser cleaning process.

Many studies have been carried out to unravel the interactions that occur in particulate adhesion and removal [8-14]. Most of them considered adhesion and removal separately. In our present study, we summarize the experimental results of the removal of submicron-sized particles, such as SiO_2, Al_2O_3, polystyrene latex (PSL) and carboxylate-modified latex (CML), from hydrophilic silicon surfaces by pulsed excimer laser irradiation. The cleaning thresholds of the particles were determined during both dry and steam cleaning. In order to obtain a total picture of both particle adhesion and removal by laser cleaning, these experimental results are rationalized on the basis of an analysis

of adhesion forces, including van der Waals, capillary and chemical forces, and a similar analysis of removal forces, including rapid thermal expansion and bubble generation pressure forces. By comparing the cleaning results of two kinds of SiO_2 particles having different surface roughnesses, we found that particle surface asperities have a substantial effect on the cleaning efficiency. Because surface roughness is known to play an important role in determining the adhesion and removal of particles, our theoretical models on adhesion and removal include these effects.

4.3.2 SUMMARY OF EXCIMER LASER CLEANING RESULTS AND PHOTOACOUSTIC WAVE MEASUREMENTS

Details of the excimer laser cleaning and photoacoustic wave (PAW) measurement systems have been described elsewhere [15, 16]. A KrF excimer laser (MPB Technologies, Inc., AQX-150) operating at 248 nm, with a 22 ns pulse full width at half maximum (FWHM) and a fluence of 200 mJ, was used to irradiate the hydrophilic silicon surfaces [7] on which 0.1 μm SiO_2, 0.1 μm Al_2O_3, 0.1 μm PSL or 0.2 μm CML particles were deposited. The particle densities on the wafer surfaces, before and after laser cleaning, were determined by a laser scanning surface inspection system (Particle Measuring Systems, Inc., SAS 3600). The PAW signals were detected by a broad band piezoelectric transducer (Panametrics, V1091) which contacted the backside of the silicon wafer, They were amplified by a preamplifier (HP 8447A) and displayed on a

300 MHz digitizing oscilloscope (HP 54201D), before being analyzed by computer using the fast Fourier transform (FFT) technique.

Removal of particles is localized only in the laser beam during dry and steam cleaning. Figure 4.8 shows the particle densities, before and after laser irradiation, for both dry and steam cleaning. The results show that the organic particles, PSL and CML, were

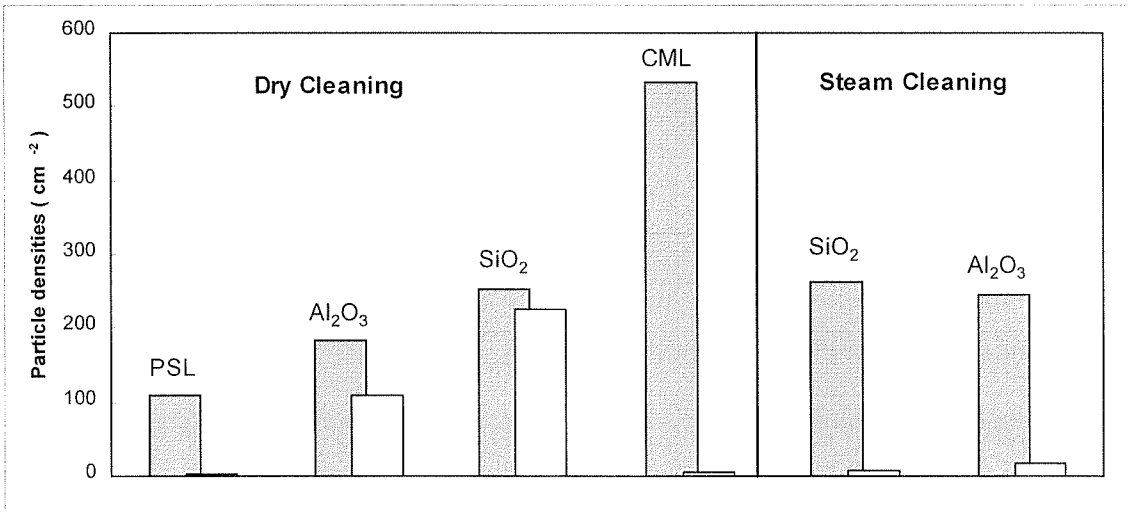

Figure 4.8 Particle densities before (gray bar) and after (white bar) laser cleaning. During dry laser cleaning, the laser energy fluxes for PSL, SiO_2, Al_2O_3 and CML were 326, 314, 326 and 353 mJ/cm^2, respectively, and 2, 4, 4 and 2 cleaning scanning cycles were used, respectively. During steam cleaning, the laser energy fluxes for SiO_2 and Al_2O_3 were 180 and 154 mJ/cm^2, respectively, and 5 and 4 cleaning scanning cycles were used, respectively.

effectively removed by dry cleaning with a laser flux near 320 mJ/cm^2. However, the inorganic particles, SiO_2 and Al_2O_3, of the same size, were much less efficiently cleaned. They were removed with high cleaning efficiencies only on steam cleaning. The particles remaining after laser cleaning may be due to several sources: strongly adhering particles, recontamination by the ejected particles near the surface, a transfer from adjacent uncleaned areas and contamination by the cleaning system.

The PAW signal induced by the laser pulse propagates along the silicon wafer surface, perpendicular to the long axis of the laser beam, and is reflected at the wafer edge. The amplitude of the PAW signal strongly depends on the incident laser energy, the cleaning method and the distance between the laser beam and the location of the transducer, as shown in Figure 4.9 and Figure 4.10. It should be noted that the PAW signal cannot be measured where the laser beam strikes, and the values these are clearly much larger than what we measure.

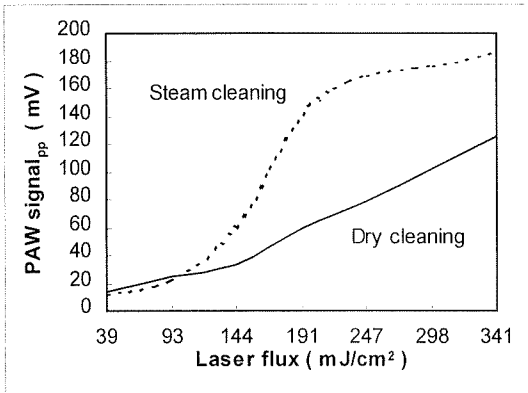

Figure 4.9 The peak-to-peak amplitude of the PAW signal as a function of incident laser flux during dry and steam cleaning.

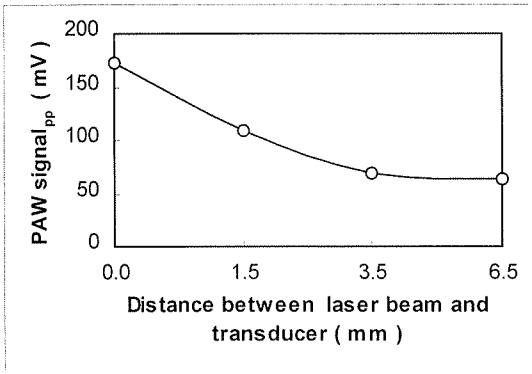

Figure 4.10 The peak-to-peak amplitude of the PAW signal as a function of the distance between the laser beam and the transducer located at the backside of the silicon wafer during dry cleaning with a laser flux of 321 mJ/cm^2.

4.3.3 LASER CLEANING THRESHOLDS

There is no common definition for the laser cleaning threshold because it strongly depends on the particle diameter and the initial particle density on the substrate surface. In our study, the particle diameter was 0.1 μm and the initial particle density was about 200 cm^{-2} which is similar with that of a heavily contaminated wafer. The cleaning threshold is defined as the removal of 50% of the particles from the substrate surface. In Table 4.2, we list the cleaning and damage thresholds, during dry and steam cleaning, for PSL, SiO_2 and Al_2O_3.

Table 4.2 Laser cleaning and damage thresholds, during dry and steam cleaning, for PSL, SiO_2 and Al_2O_3 particles.

Particles	PSL (0.1 μm)	SiO_2 (0.1 μm)	Al_2O_3 (0.1 μm)
Laser cleaning method	Dry	Steam	Steam
Laser cleaning threshold	76 mJ/cm^2	143 mJ/cm^2	143 mJ/cm^2
Laser damage threshold	380 mJ/cm^2	200 mJ/cm^2	

The cleaning threshold of PSL during dry cleaning, 76 mJ/cm^2, was much lower than the optimal cleaning condition, 340 mJ/cm^2. To obtain a high cleaning efficiency, more laser energy is needed to remove those particles more tenaciously held at the surface, to eject the particles more farther away and to reduce the number of multiple scans necessary to avoid recontamination.

It is interesting to note that SiO_2 and Al_2O_3 particles have the same cleaning thresholds during steam cleaning, 143 mJ/cm^2. It was at this flux that we observed the onset of explosive evaporation of the water film, very close to the optimal cleaning flux of 150 mJ/cm^2. This phenomenon demonstrates that bubble pressure plays an important role in the removal of inorganic oxide particles. To explain the large differences between dry and steam cleaning, and between particle types and cleaning thresholds, we quantitatively analyze the adhesion and removal forces between particles and substrate surfaces.

4.3.5 THEORETICAL MODELS OF AN IDEAL SPHERICAL PARTICLE ON A SMOOTH SURFACE

4.3.4.1 Adhesion model

The interaction forces between solids, which cause the adhesion of particle to substrate surface, can be classified into long- and short-range [8]. Long-range forces, which act to bring the particle to the surface and establish the adhesive contact area, include van der

Waals, capillary, electrostatic and double-layer forces. Short-range forces, which can add to adhesion only after the establishment of an adhesive contact area, include the various types of chemical bonds: metallic, covalent and ionic, as well as hydrogen bonds. In our previous study [15, 17], it was demonstrated that, for submicron-sized particles on hydrophilic silicon surfaces, the dominant long-range adhesion force is the van der Waals interaction, while hydrogen bonding makes the most important short-range contribution to inorganic oxide particles.

The following discussion assumes that particles are ideal sphere and already in contact with a smooth substrate surface, assumes also that there is no aggregation. Van der Waals attractive forces can be calculated using a macroscopic approach [18], in which the material properties are related to the Lifshitz-van der Waals constant. For a spherical particle and a smooth flat substrate surface, it can be expressed as [10]:

$$F^{V} = F_{0}^{V} + F_{Deformation}^{V} = \frac{h\varpi_{132} r_{P}}{8\pi z_{0}^{2}} + \frac{h\varpi_{132} a^{2}}{8\pi z_{0}^{3}} \qquad (4.9)$$

The first term of equation (4.9) is the van der Waals forces between a sphere and a flat surface before deformation, and the second term is the force acting on the contact area due to elastic or plastic deformation. $h\varpi_{132}$ is the Lifshitz-van der Waals constant, r_p is the particle radius, z_0 is atomic separation distance between particle and substrate, which is not measurable but assumed to range from 4 to 10 Å [8] (we used $z_0 = 4$ Å), a is the

radius of the deformation area on the particle which can be calculated for rigid particles (SiO_2 and Al_2O_3) using the JKR model [19].

$$a^3 = \frac{9}{2} W \pi r_p^2 \left(\frac{1 - \nu_1^2}{E_1} + \frac{1 - \nu_2^2}{E_2} \right) \tag{4.10}$$

where W is work of adhesion of the particle on the substrate surface which approaches the value of $2(\gamma_1^s \gamma_2^s)^{1/2}$, γ_1^s and γ_2^s are the surface free energies of particle and substrate, respectively. ν and E are Poisson's ratio and Young's modulus, respectively, and their subscripts refer to particle and substrate. For PSL particles, the contact radius is not a function of the particle radius to the 2/3 power but, rather, is a function of the square root of the particle radius [20]. The PSL contact radius slowly increases with residence time [21]; we ignored these changes in our calculations because the residence time was less than three hours in our experiments, too short to cause a noticeable change. During steam cleaning, particles were covered with a condensed water film. The shielding effect of the liquid greatly reduces the van der Waals forces [8]; for example, the Lifshitz-van der Waals constant of Al_2O_3 particles on silicon surfaces is reduced from 5.62 eV to 2.23 eV [11].

The adhesion force due to hydrogen bonding between inorganic particles and the hydrophilic silicon surface has been discussed in our previous study [17]. It was given by:

$$F_{H\text{-}bond} = DE_{bond}(\pi a^2 + 2\pi r_p \Delta z b)/d_{bond} \tag{4.11}$$

where $\boldsymbol{D}$ is the OH group density on the particle surface (12.5 OH/nm^2 for Al_2O_3 [22]) and $\boldsymbol{E_{bond}}$ is the hydrogen bonding interaction energy between particle and substrate. $\boldsymbol{E_{bond}}$ depends on the natures of the surfaces, in particular on their degrees of hydroxylation and on the electronic structures of the materials [23]. The average energy of the O–H---O hydrogen bond is about 5 kcal/mole (~ 0.22 eV/bond) [23], πa^2 is the deformation area of the particles, $2\pi r_p \Delta z$ is the ring area cut at a height Δz near the contact point and $\boldsymbol{b}$ is the probability that particle and surface are bonded by a chain of water molecules; for Al_2O_3 on dry cleaning, $\Delta z\ \boldsymbol{b}$ is ~ 7.05 Å [17, 24–26]. During steam cleaning, free water molecules may break the hydrogen bond chain connecting the particle to the surface, so the probability $\boldsymbol{b}$ is reduced to say, 50%.

$\boldsymbol{d_{bond}}$ is hydrogen bond dissociation distance. We assume that the force of hydrogen bond remain constant as the bond length elongating. The force constant of OH---H hydrogen bond is 0.69×10^5 dyn/cm [27]. The energy cost to separate a hydrogen bond is equal to the half of product of the force constant and the square of the bond length change, 0.1 Å length change of hydrogen bond will cost less than 0.022 eV. Therefore, to break the hydrogen bond or, in other words, to overcome the 0.22 or so eV hydrogen bond energy, the dissociation distance should be near 1Å [17, 28]. 1 Å is a reasonable selection for the dissociation distance in our calculation. The dissociation distance can greatly affect the calculated results of the total adhesion force due to hydrogen bonds. It may, for example,

be shorter than 1Å; a dissociation distance 30% shorter will increase the calculated adhesion force about 40%. There are other parameters that can induce calculation errors, such as the degrees of hydroxylation on particle and substrate surfaces and the presence of asperities on the surfaces. Here, we use complete hydroxylation although, in practice, it may be less than 100%. For PSL particles, there are no surface groups capable of participating in hydrogen bonding, so only van der Waals forces play a role.

Using equations (4.9)–(4.11), we calculated the adhesion forces as a function of particle diameter for a typical organic particle, PSL, and for a typical inorganic oxide particle, Al_2O_3, contacting a hydrophilic silicon surface; this was done for both dry and steam cleaning, and is shown in Figure 4.11. It appears that the adhesion forces are almost a linear function of particle diameter; they are greatly reduced during steam cleaning, and hydrogen bonding between Al_2O_3 particles and hydrophilic silicon surfaces becomes much stronger than van der Waals interactions. This, and not the van der Waals force, causes the large difference in cleaning efficiencies of Al_2O_3 and PSL particles during dry laser cleaning. Indeed, the van der Waals forces acting on the Al_2O_3 particles are much less than those acting on the PSL particles, due to their smaller deformation.

4.3.4.2 Model for dry laser cleaning

On laser pulse irradiation during dry cleaning, the particle and silicon substrate absorb laser energy and are rapidly heated. The thermoelastic effect [29] causes an extremely

rapid thermal expansion of the substrate and particle, which ejects the particles from the surface. In order to calculate the thermoelastic removal force, we must first know the temperature increase of both particles and silicon substrate due to the laser irradiation.

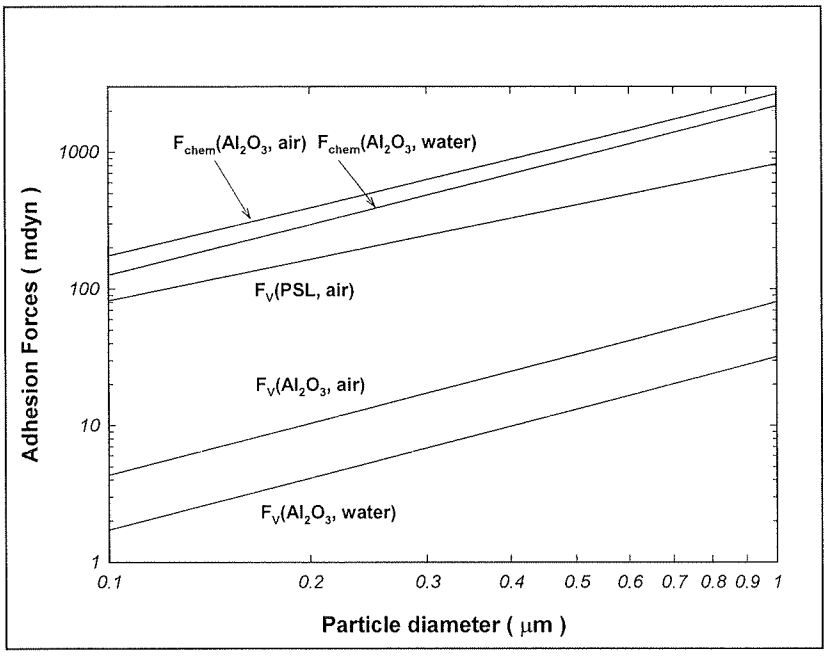

Figure 4.11 Adhesion forces (van der Waals F_v and hydrogen bonding F_{chem}) of PSL and Al_2O_3 particles on hydrophilic silicon surface during dry and steam cleaning, as a function of particle diameter.

At the KrF excimer laser wavelength of 248 nm, the photon absorption length α^{-1} (5.5 nm [30]) and the heat diffusion length $(\kappa\tau / \rho C_p)^{1/2}$ (4.3 μm [31, 32]) of silicon are much smaller than both the thickness of the wafer (0.5 mm) and the dimension of the laser

beam (0.8 mm × 18 mm), where α, κ, ρ, C_p and τ are the optical absorption coefficient, the thermal conductivity, the density, the specific heat of the substrate material and the laser pulse duration, respectively. Thus, the semi-infinite, one-dimensional heat equation is a good approximation. The temperature distribution in the substrate can be described by [31]:

$$\rho C_p(T)\frac{\partial}{\partial t}T(z,t) = \frac{\partial}{\partial z}\left[\kappa(T)\frac{\partial}{\partial z}T(z,t)\right] + (1-R)\alpha I_0(t)e^{-\alpha z} \qquad (4.12)$$

where z is the coordinate normal to the substrate surface ($z = 0$), t is the time following the laser pulse arrival, T is the temperature, R is surface reflectivity and $I_0(t)$ is the laser intensity. The spatial dependence of $I_0(t)$ is neglected because the particles of interest are much smaller than the laser spot. Heat conduction from the substrate surface to the ambient air is very slow, and the radiation losses are much smaller than the incident laser energy. For example, at a surface temperature of 850 K and laser flux of 310 mJ/cm^2, the power flux flowing into the substrate is $J_{in} = -\kappa\,(dT/dz) = 1.45 \times 10^9$ W/m^2 [33] but the power flux lost by radiation is $J_{rad} = 5.67 \times 10^4\ T_s^4 = 2.32 \times 10^4$ W/m^2 [33] and by convection with the ambient air, $J_{conv} = h_c(T_s - T_0) = 2 \times 10^4$ W/m^2 [33], where T_s and T_0 are the surface temperature and the room temperature, h_c is the unit thermal conductance (5 – 25 W/m^{2}K for air convection [33]). Thus, over the short time scale considered, heat losses at the substrate surface may be neglected. The boundary and initial conditions thus become:

$$\left.\frac{\partial T(z,t)}{\partial z}\right|_{z=0} = 0 \qquad (4.13)$$

$$T(z,t)\big|_{z=\infty} = T(z,0) = T_0 \qquad (4.14)$$

where T_0 is the room temperature. Because the optical absorption coefficient α of crystalline silicon is very large (1.81×10^6 cm^{-1} [30]), and α and R do not change much with temperature, we employed their room temperature values in our calculation. The thermal properties of crystalline silicon strongly depend on the temperature. Using a nonlinear regression of experimental data [32] of crystalline silicon thermal properties, $\kappa(T)$ and $C_p(T)$ of crystalline silicon can be expressed as:

$$\kappa(T) = 2.99 \times 10^4 / (T - 99) \quad \text{W/mK} \qquad (4.15)$$

$$C_p(T) = 863.3 + 0.09923T - 6369e^{-0.01216T} \quad \text{J/kgK} \qquad (4.16)$$

The one-dimensional conductive heat transfer equation (4.12) was solved numerically by an implicit finite difference algorithm [34]. The peak surface temperature of the silicon substrate as a function of laser energy densities is shown in Figure 4.12.

The calculation of the temperature distribution in particles is a very complex problem because of the non-uniform surface absorption due to small particle Mie-type scattering [35] and the difficulty of solving the three-dimensional, spherical coordinate, heat diffusion equation. Fortunately, the optical absorption lengths α^{-1} of the particles considered are $10–10^2$ μm [36-38], much larger than the dimensions of the particles.

This means that the particles absorb laser energy weakly. The heat transfer from the substrate to the particles can be ignored because of poor coupling between them. So, the temperature increase in the particle during laser irradiation is not significance, and we can assume that the submicron-sized particles maintain a constant temperature during laser irradiation.

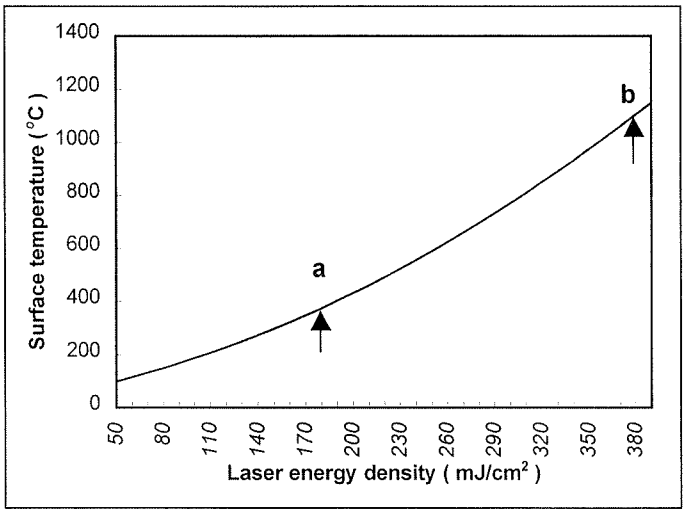

Figure 4.12 Surface temperature of silicon substrate as a function of laser energy density. Points **a** and **b** give the laser damage thresholds for dry and steam cleaning, respectively.

The rapid temperature rise in the substrate, induced by the laser pulse, generates stresses and strains in the irradiated area. These strains cause some particle displacement. From the point of view of the particles, their resistance of these strains subjects them to ejection forces from the substrate surface equal to the stresses in the substrate [39]. If the

particles are to be detached from the surface, they must experience a real displacement. Based on the relationship between stresses and strains [29], an expression for the thermal removal force on the particles produced by substrate thermal expansion can be obtained:

$$F_{thermal} = \gamma E \pi a^2 \Delta T \tag{4.17}$$

where γ, E, ΔT are the linear thermal expansion coefficient, the elastic modulus and the temperature increase at the substrate surface. πa^2 is the deformation area of the particle. The equation shows that the thermal removal force depends on the deformation area of the particle. Soft particles such as PSL should suffer much stronger removal forces from the substrate than hard particles, such as SiO_2 and Al_2O_3. Figure 4.13 shows the removal forces on PSL and Al_2O_3 particles due to the thermoelastic effect under dry cleaning conditions (the incident laser energy density is about 320 mJ/cm^2) and cleaning threshold for PSL particles (the incident laser energy density is 76 mJ/cm^2) as a function of the particle diameter. The dominant adhesion forces are also included in Figure 4.13 for comparison purposes. It is apparent in Figure 4.13 that the thermal removal force is large enough to overcome the adhesion forces for PSL particles under these cleaning condition but is much less than the hydrogen bonding forces, in the case of Al_2O_3 particles. The removal force for PSL at the cleaning threshold is slightly lower than the adhesion force; only those particles, which are loosely held at the surface, can be removed. These predictions are consistence with the laser cleaning experiments.

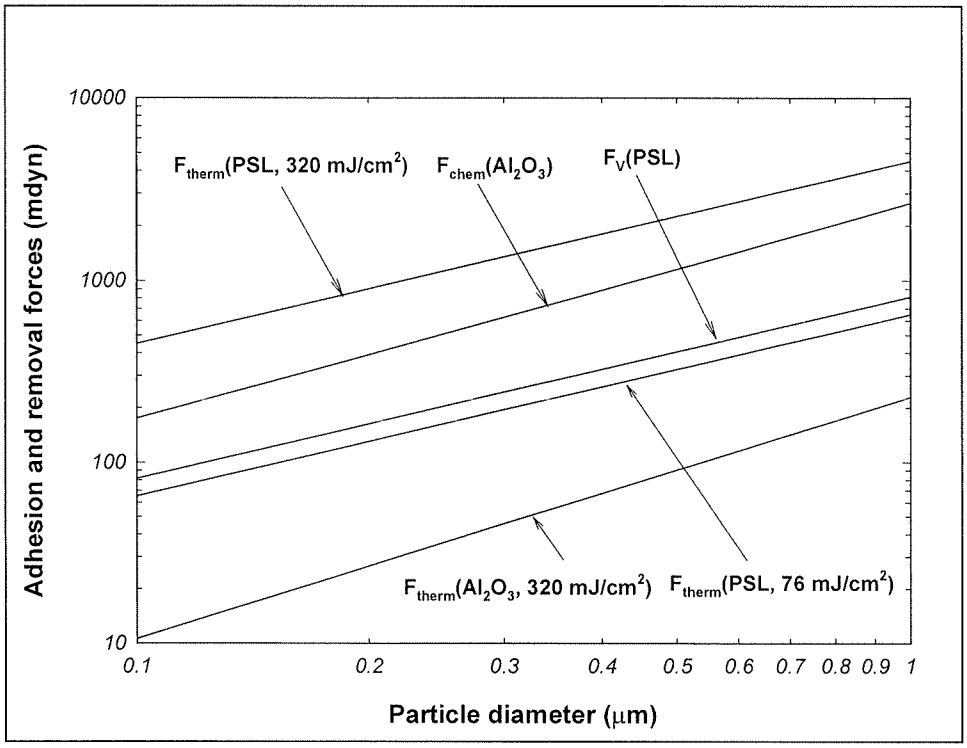

Figure 4.13 Thermal removal forces F_{them} and dominant adhesion forces (van der Waals F_v and hydrogen bonding F_{chem}) as a function of particles diameter for PSL and Al_2O_3 particles during dry cleaning at laser flux of 320 mJ/cm^2 and 76 mJ/cm^2 (dry cleaning threshold for PSL particles).

The localized removal of PSL particles during dry cleaning is due to the facts that, in irradiated area, the amplitude of thermoelastic pulse and coupling of stress and strain into particles are much stronger than those of PAW which excited by this thermoelastic pulse and detected at the backside of the wafer. Therefore, the effective removal of PSL particles by dry cleaning is localized in the laser beam.

4.3.4.3 Model for steam laser cleaning

In the case of steam cleaning, the water film is transparent to the excimer laser. The laser energy is absorbed only by the substrate. The rapidly heated substrate surface superheats the water layer adjacent to it, causing nucleation [40]; this is followed by the creation of a dense population of bubbles which coalesce in large numbers and, in this way, an insulating vapor layer at the water/substrate interface is generated. The phenomenon is called film boiling [40]. A detailed description of the explosive evaporation of the water film is extremely difficult, due to the formation of a superheated liquid, the thermal instability of the bubbles and the development of nucleation centers [41]. The incident laser energy density (10^2 J/cm^2) is much larger than the heat energy density needed to heat liquid water to boiling (10^{-3} J/cm^2) and to vaporization (10^{-2} J/cm^2) [42]. The vapor layer isolates the heat continuously transferring from substrate to liquid water, so that the temperature distribution in the substrate is approximately the same as that during dry cleaning.

The generation of substantial pressure, due to bubble collapse, often causing undesired cavitation damage on propeller blades, pumps, and hydraulic machines, has been known for many years [43] and can also be used to remove particles from solid surface [44]. In the ablation of a liquid film by a short-pulsed laser, the pressure production is ascribed to the explosive growth of bubbles by instantaneous heating [45,46]. This explosive growth of bubbles can be considered as a phenomenon in which the explosion in the fluid

medium generates an explosive blast wave. The shock front of the blast wave is normal to the direction of the wave motion. The pressure jump associated with this shock is from atmospheric pressure P_{atm} to the shock-generated pressure P_{shock}. The pressure increment $P_{shock} - P_{atm}$ is termed the overpressure P_{over}. When a blast wave impinges at head-on incidence onto an unyielding surface, the movement of the shock front is terminated abruptly, normal reflection occurs and the entire front is instantly subjected to a reflected overpressure $P_{reflect}$ which is substantially greater than the overpressure P_{over} in the immediate surrounding. The reflected overpressure is given by [47]

$$P_{reflect} = P_{shock}(8P_{shock} - P_{atm})/(P_{shock} + 4P_{atm}) \quad (4.18)$$

During steam cleaning, the blast wave generated in explosive growth of bubbles imposes a dynamic load on the particles in this field. The dynamic load is characterized by a rapidly reached peak value, the reflected overpressure [47], and then a decay that accompanies the decay in the blast wave, itself.

We have made several assumptions in calculating the removal force due to bubble generation, in order to simplify the problem: (1) the shock-generated pressure is approximately equal to the vapor pressure in the vapor layer at the water/substrate interface, i.e. $P_{shock} \approx P_v(T)$; T is the temperature in the vapor layer, the values of $P_v(T)$ and P_{atm} can be found in reference [42]; (2) the temperature in the vapor layer is approximately equal to the temperature of the substrate surface; (3) the vapor pressure inside the vapor layer is taken as the saturation vapor pressure of the superheated vapor

layer due to the non-uniform temperature distribution in the liquid film [48]; (4) the vapor layer thickness, limited by the thickness of the superheated liquid layer, may exceed the particle radius since the thermal penetration depth in water is of the order of 1 μm. The upper limit of the removal force due to bubble generation is then given by:

$$F_{bubble} = \pi r_p^{\,2} P_{reflect} \tag{4.19}$$

where r_p is the radius of the particle.

Lu et al [14] have proposed a different equation to calculate the removal force induced by bubble generation, based on the several assumptions (i) bubble generation is inertial-controlled process; (ii) in the region near liquid/substrate interface, the vapor layer created by evaporation of liquid acts as a plane piston, compressing its adjacent liquid and generating stress waves; (iii) the value of the volume fraction of the vapor inside the superheated liquid layer is less that 1; (iv) the expansion velocity of the vapor layer is equal to the growth velocity of the bubbles; (v) same as (3) above, They deduced the pressure of the stress wave from its average energy at a unit area vapor/liquid interface, and then obtained the cleaning force induced by bubble generation:

$$F_C = \{(8/3)c^2 \rho f^2 [P_V(T) - P_\infty]^3\}^{1/4} \pi r_p^2 \tag{4.20}$$

where c is the transmission speed of the stress wave, ρ is the density of the liquid, f is the volume fraction of the vapor, and P_v and P_∞ are the vapor pressure inside the bubble and the ambient liquid pressure. From this equation, they could predict the laser fluence

cleaning threshold and interpret the experimental results of the removal of alumina particles from a nickel-phosphorus surface, using isopropyl alcohol.

The removal forces due to bubble generation, as calculated by both models, as a function of the Al_2O_3 particle diameter, under steam cleaning conditions (the incident laser energy density is about 150 mJ/cm^2), are given in Figure 4.13, where we take $f = 1$, and the transmit speed of the stress wave $c = 1465$ m/s, the speed of sound in water, because they are close if the stress pressure is less than 10^8 Pa [49]. Both removal forces due to the thermoelastic effect and the dominant adhesion forces due to hydrogen bonding are also shown in Figure 4.14.

The removal forces of the two models for 0.1 μm particle, as function of the laser energy density, are given in Figure 4.15. The inflection in Figure 15, at laser fluence 180 mJ/cm^2, was due to reaching of the critical temperature of water vapor and the phase transition from water vapor to ideal gas. It shows that the removal force of the explosion model is about two times greater than Lu's under steam laser cleaning conditions. This difference may be due to the different assumptions of these two models: in Lu's model, bubble generation is considered as a reversible piston process; in the explosion model, it is clearly irreversible. For lower vapor pressures, meaning at lower laser flux and surface temperature, bubble generation is farther away from the explosive process and the values of the two models are closer. The actual bubble generation process is probable

somewhere between these two models, closer to the explosion model under steam laser cleaning conditions.

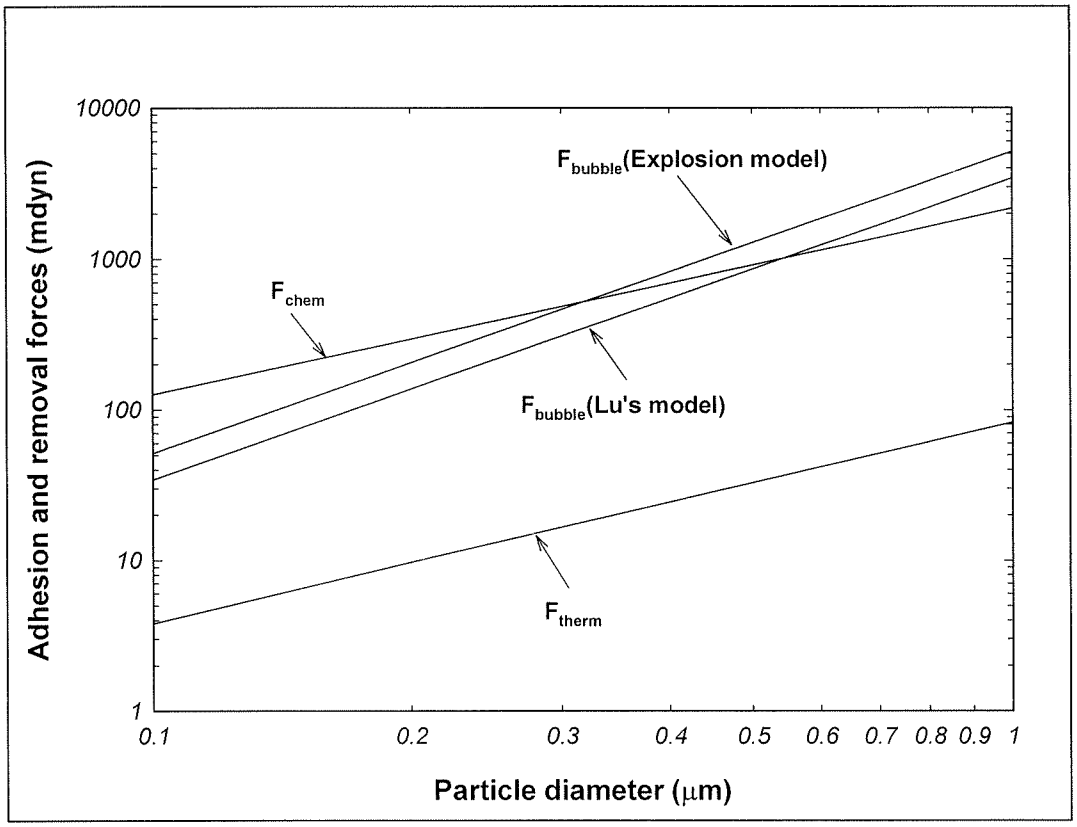

Figure 4.14 Thermal removal force F_{them}, bubble removal force F_{bubble} and dominant adhesion force F_{chem} as functions of the particle diameter, for Al_2O_3 particles during steam cleaning with a laser flux of 150 mJ/cm^2.

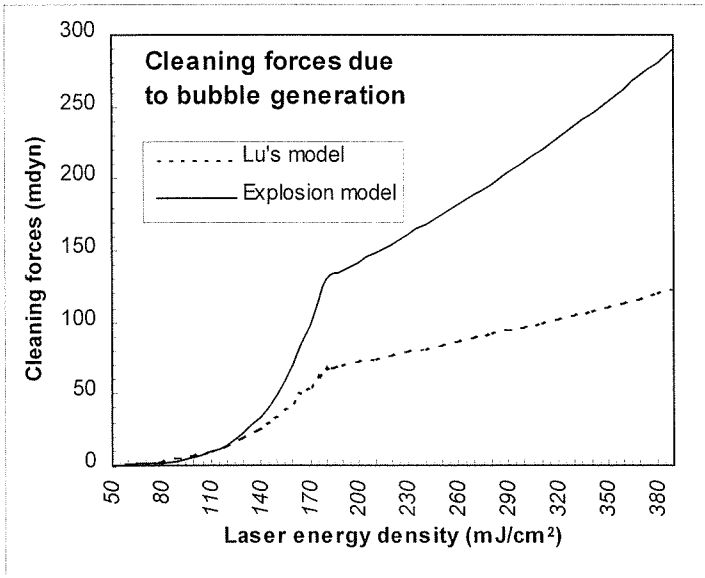

Figure 4.15 The bubble generation cleaning forces of Lu's model and the explosion models for 0.1 μm particles as function of the laser energy density

It is clear from Figure 4.14 that the explosive evaporation of the water film generates a strong removal force, much greater than the thermal expansion force since, first, the bubble pressure has a much larger interaction area on the particle surface (8×10^{-3} μm^2, as compared to 6×10^{-5} μm^2 in the purely thermoelastic regime, for 0.1 μm Al_2O_3 particles) and, second, bubble generation has a much higher energy conversion efficiency (0.0015%, as compared to 0.00036% in the purely thermoelastic regime [50]). This analysis explains the high cleaning efficiencies of Al_2O_3 particles during steam cleaning. Because the heated area is located in the laser beam where the liquid film can explosively evaporate, only the particles in the laser beam experience the bubble pressure removal force.

A similar phenomenon was found for the removal of Al_2O_3 particles during steam cleaning: only the particles in the directly irradiated area were removed. As mentioned earlier, the dominant Al_2O_3 particle removal force during steam cleaning is bubble pressure. The heat diffusion length $(\kappa\tau/\rho C_p)^{1/2}$ of silicon is less than 10 μm, which can be ignored compared with the laser beam width (~ 1 mm). Thus, bubble generation due to superheated of water film adjacent to the substrate surface is confined to the laser beam.

From Figure 4.14, we find that the removal forces due to bubble generation are still lower than the hydrogen bonding adhesion force for the particles smaller than 0.4 μm. In the next section, we will discuss the influence of surface roughness on the cleaning efficiency, whose effect is to greatly reduce the adhesion forces.

In earlier papers [15,16], we noted that the excimer laser energy, 5 eV, is much higher than the strength of a hydrogen bond, ~ 0.2 eV, and could conceivably participate in bond breaking. However, further consideration has led us to the fact that the quantized annihilation of a photon must be matched to another process (or series of processes, as in XPS) which entirely use the energy released. A review of possible processes (internal electronic transitions, ionization potentials) does not reveal a match, effectively excluding the participation of photons in hydrogen bond breaking.

4.3.5 THEORETICAL MODELS OF PRACTICAL PARTICLES ON A PRACTICAL SILICON SURFACE

4.3.5.1 Surface roughness and particle aggregation

The previous particle adhesion and removal models were based on the assumption that particles are ideal spheres and that substrates have smooth, flat surfaces. However, we have found that many types of particles have irregular shapes and that substrate surfaces have certain roughnesses; it has been shown that the surface roughness of a particle markedly decreases the adhesion forces [8, 51-53]. We measured the surface roughnesses of silicon wafers by AFM (TopoMetrix TMX2010), and found that the average roughness was about 0.33 nm and the rms roughness was about 0.4 nm, both much smaller than the dimensions of particle asperities; thus, the substrate surface can be considered to be smooth. It is very difficulty to measure the surface roughness of submicron-sized particles, and different particles have different surface topographies. The scanning electron microscope (SEM) and transmission electron microscope (TEM) are useful tools in determining particle surface topography. SEM and TEM photomicrographs of PSL, SiO_2 and Al_2O_3 particles are shown in Figure 4.16. We can see that the PSL particles have smooth surfaces and may be considered as almost perfect spheres, but SiO_2 and Al_2O_3 particles have irregular shapes. The radii of curvature of asperities r_e are much smaller than the overall radius of the particle r_p , 10% of the particle radius being a reasonable assumption for the upper limit of the asperity curvature radius, i.e. $r_e = 0.1\ r_p$.

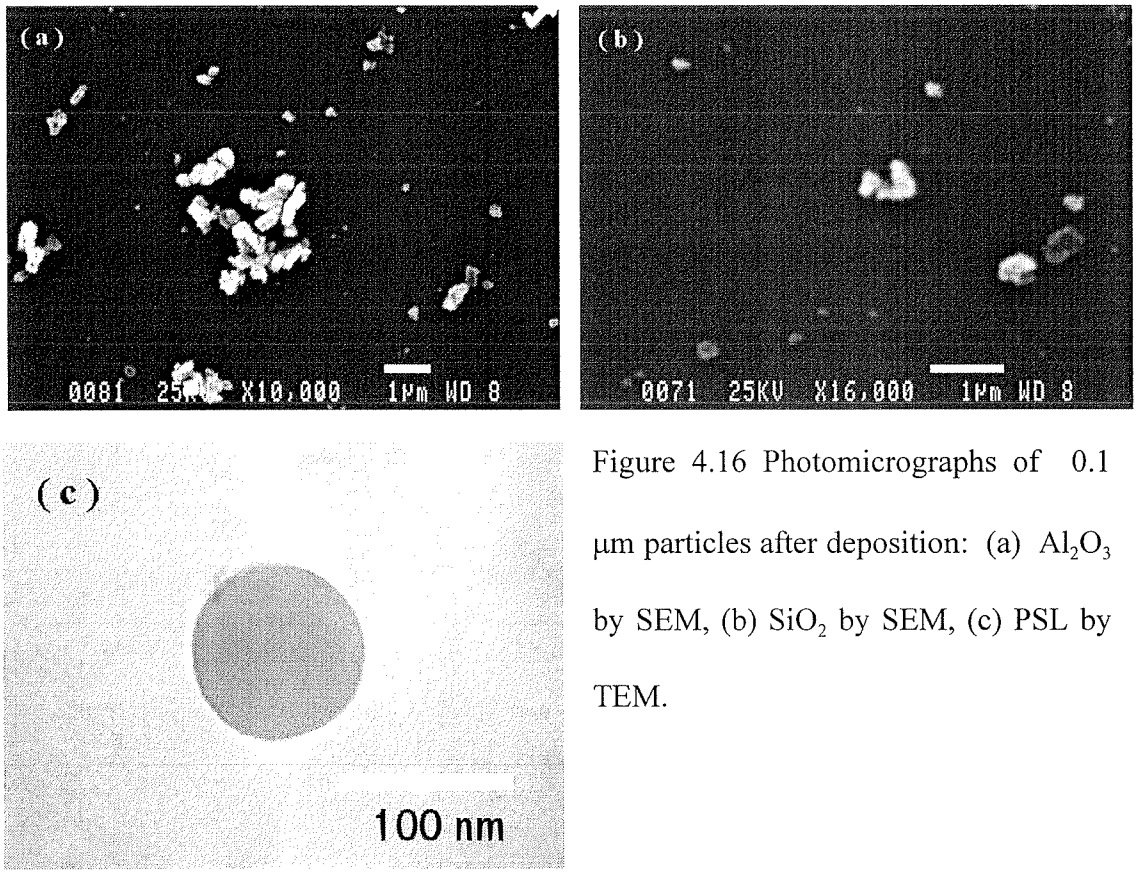

Figure 4.16 Photomicrographs of 0.1 μm particles after deposition: (a) Al_2O_3 by SEM, (b) SiO_2 by SEM, (c) PSL by TEM.

We also see that larger SiO_2 and Al_2O_3 particles form clusters with smaller ones. This aggregation has been considered to be the result of van der Waals attraction and hydrogen bonding, which hold particles together at the moment of contact during particle deposition [23]. The aggregation of Al_2O_3 particles is more significant than that of SiO_2 because Al_2O_3 has stronger hydrogen bonds (127 mdyn for 0.1 μm Al_2O_3 particles in water, 69 mdyn for 0.1 μm SiO_2 particles in water), and can form stronger and more stable links between particles. This is why the Al_2O_3 particles have a broader size distribution than SiO_2 after deposition of nominal 0.1 μm particles, as shown in

Figure 4.17. The peak maximum for 0.1 μm Al_2O_3 particles appears at 0.2 μm, and may be due to particle aggregation during the deposition process or to the measurement error of the laser scanning surface inspection system: any difference between the actual and measured sizes of these particles may be attributed to the calculation method used by the laser scanning surface inspection system which is calibrated by comparing with 0.1 μm standard polystyrene latex particles [54].

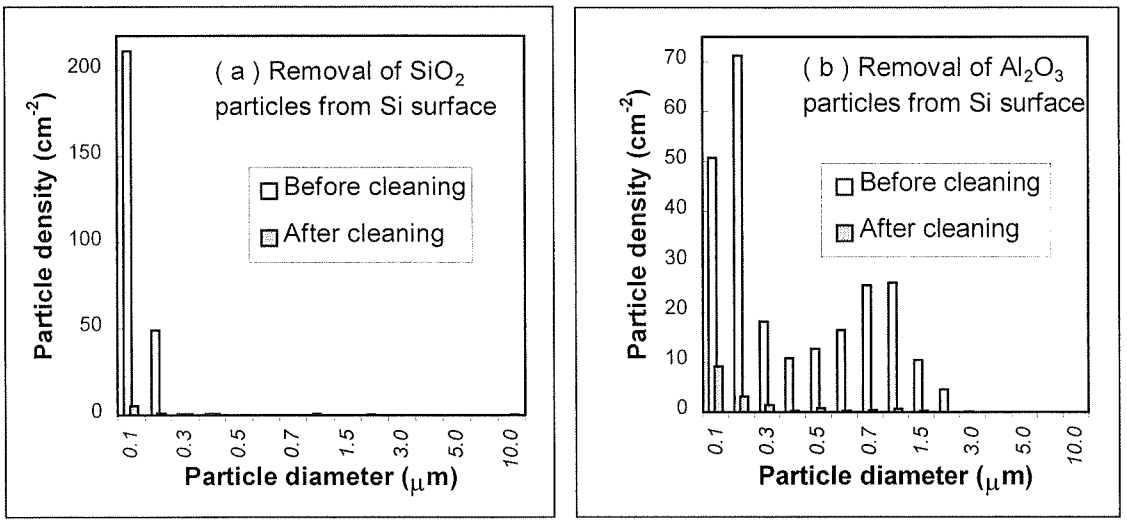

Figure 4.17 Particle densities before and after steam laser cleaning. (a) SiO_2 particles, laser energy flux of 180 mJ/cm^2, 5 cleaning cycles. (b) Al_2O_3 particles, laser energy flux of 154 mJ/cm^2, 4 cleaning cycles.

4.3.5.2 Modified adhesion and laser cleaning models

It is generally recognized that surface roughness acts to reduce the adhesion between two solids. When the radii of the asperities at the particle surface are much greater than the particle-substrate separation, the effective particle radius and contact area that appear in equations (4.9)–(4.11) and (4.17), must be decreased. This is because the dominant component of the force between particle and substrate surface acts only at the contact point and the surrounding area. In general, there is no predictable relationship between the geometry of the surface asperities and the overall particle radius. To simplifying the problem, the rough particle is modeled by a spherical solid core having uniformly distributed spherical asperities on the surface, all with the same radius of curvature and height. In the stable state of a single particle contacting the substrate, there are either three or four asperities contact with the substrate surface. We selected average 3.5 contact points.

In the case of 0.1 μm Al_2O_3 particles, the larger particle sizes are assumed to be aggregates of 0.1 μm particles. The total number of asperities contacting with the substrate surface depends on the number of components and the structure of the cluster. It is very difficult to calculate the total number of contact points because the aggregation of small particles depends on random contact processes and the possibility of forming clusters of all shapes, varying with cluster growth in a way too complex to simulate or

image. The determination of the actual dimensions of the clusters is another problem [55], the laser scanning surface inspection system only giving the equivalent spherical diameter of a PSL particle. The contact area between the cluster and substrate surface is determined directly by the dimensions and shapes of the clusters.

The simplest and calculable case is for a single 0.1 μm particle with asperities on the substrate surface. The equations to calculate the adhesion and the thermoelastic removal forces, (4.9)–(4.11) and (4.17), are modified as follows:

$$F^{V} = \left(\frac{h \varpi_{132} r_e}{8 \pi z_0^2} + \frac{h \varpi_{132} a^2}{8 \pi z_0^3} \right) n \tag{4.21}$$

$$a^3 = \frac{9}{2} W \pi r_e^2 \left(\frac{1 - \nu_1^2}{E_1} + \frac{1 - \nu_2^2}{E_2} \right) \tag{4.22}$$

$$F_{H\text{-}bond} = De_{bond}(\pi a^2 + 2\pi r_e \Delta z b) n / d_{bond} \tag{4.23}$$

$$F_{thermal} = \gamma E \pi n a^2 \Delta T \tag{4.24}$$

$$n = 3.5 \tag{4.25}$$

where r_e is the effective radius of the particles (asperity radius), which is 0.005 μm in our case, and n is the average number of contact points between particle and substrate surface. The bubble removal force would not be affected by asperities or by aggregation because it acts over the entire bottom half of the particle; this means that equation (4.19) does not need to be changed. Using these equations, we recalculated the adhesion and

removal forces for a 0.1 μm irregular Al_2O_3 or SiO_2 particle on a silicon surface, during steam cleaning with a laser flux of 150 mJ/cm^2, and the results are shown in Table 4.3.

One can easily see from Table 4.3 that when asperities and aggregation are considered, the adhesion and thermoelastic removal forces are significantly decreased. The dominant adhesion force is still hydrogen bonding, the thermoelastic removal force is larger than the van der Waals force but much smaller than the hydrogen bonding force. During steam cleaning, the removal force induced by bubble generation is great enough to overcome the adhesion forces and eject particles from the substrate surface. The difference in magnitude between the bubble pressure removal force and the adhesion force increases with particle diameter, and may explain why larger particles are much easier to remove from the substrate surface when asperities and aggregation are present.

Colloidal SiO_2 particles were employed in the steam cleaning experiments to confirm the influences of asperities on the cleaning efficiency. They have smooth surfaces and a more spherical shape than powdered SiO_2 particles, as seen in Figure 4.18. The aggregation of colloidal SiO_2 particles in the picture is due to very high particle deposition density (about 1000 time higher than that under cleaning conditions) in order to catch particles under SEM.

Table 4.3 The adhesion and removal forces for a single 0.1 μm irregular Al_2O_3 or SiO_2 particle on a silicon surface during steam cleaning with a laser flux of 150 mJ/cm^2.

Particles / Forces	SiO_2		Al_2O_3	
	With asperities	Ideal Sphere	With asperities	Ideal Sphere
F^V	0.87mdyn	1.5 mdyn	0.4 mdyn	1.7 mdyn
$F_{H\text{-}bond}$	14.7 mdyn	69.6 mdyn	29.8 mdyn	126 mdyn
$F_{thermal}$	1 mdyn	6.7 mdyn	0.7 mdyn	3.8 mdyn
F_{bubble}	51.4 mdyn			

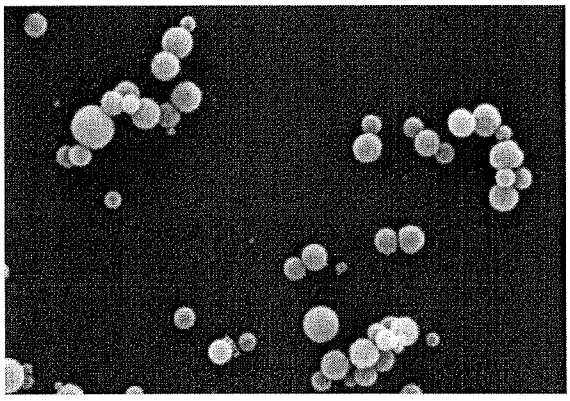

Figure 4.18 SEM photomicrographs of 0.1 μm colloidal SiO_2 particles.

Colloidal SiO_2 particle densities before and after steam cleaning are seen in Figure 4.19. It was found that the steam cleaning efficiency of colloidal SiO_2 particles was much

lower than that of powdered SiO_2.as seen in Figure 4.17 (a). The dominant size of colloid and powder SiO_2 particles is 0.1 μm. Roughly 64% of colloidal SiO_2 particles were removed compared to 97% of the powdered SiO_2 particles (with asperities), under similar conditions (see Figure 4.17 (a)). The theoretical predictions given earlier are in good agreement with these experimental results.

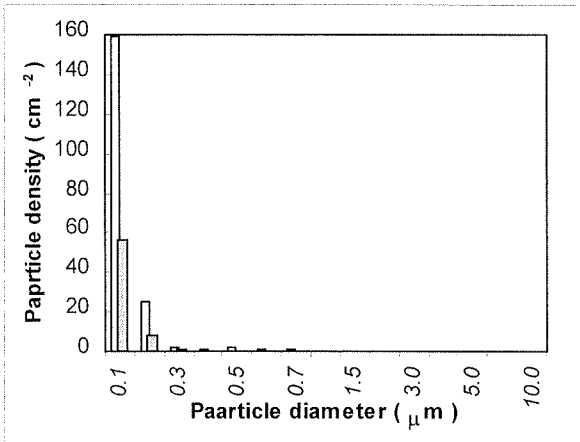

Figure 4.19 Colloidal SiO_2 particle densities before and after steam laser cleaning with a laser energy flux 215 mJ/cm^2, 6 cleaning cycles.

The contact area of a cluster with a surface involves only some of the component particles and there is an average 3.5 asperities for each contacting component. Thus, the adhesion forces of clusters are also greatly reduced but, since the bubble removal force will not be affected, the cleaning efficiency for clusters will also be greatly improved.

4.3.6 CONCLUSIONS

Theoretical models of particle adhesion and removal are used to explain our excimer laser cleaning results. The following main points are included in the models:

(1) The dominant adhesion force holding organic particles, such as PSL, to the surface is the van der Waals force with deformation. Hydrogen bonding between inorganic oxide particles, such as Al_2O_3, and the substrate is the dominant contribution to adhesion forces there. A deposited water film greatly reduces the adhesion forces due to the shielding effect of the van der Waals force and to the interruption of the hydrogen bond chain between particle and surface.

(2) The one-dimensional heat transfer equation is used to calculate the temperature distribution at the substrate. The temperature increase of the particles, and the heat convection and radiation losses at the substrate surface are neglected.

(3) The laser-generated thermoelastic pulse of the heated substrate gives rise to the removal force on the particles during both dry and steam cleaning. During steam cleaning, an additional removal force, due to bubble pressure, is created, by energy transfer to the liquid layer; it is larger than that due to the thermoelastic effect. Two models for the bubble removal force, the explosion and the Lu's model, are discussed and compared. Explosion model is more suitable for laser cleaning conditions.

(4) In the area illuminated by the laser beam, rapidly thermal expansion of the substrate and bubble generation contribute to localized cleaning.

(5) Both particle surface asperities and particle aggregation will markedly decrease the adhesion and thermoelastic removal forces, although the bubble pressure removal force is not affected. In this situation, the effective radius of the particle and the multiple contact area must be included in the theoretical models.

(6) The models which describe the laser cleaning process take into account the particle shape; they predict that particles with different surface roughnesses and shapes will have substantially different cleaning efficiencies during steam laser cleaning. The results of these calculations are found to fit the experimental results well.

4.3.7 ACKNOWLEDGMENTS

The authors thank J. P. Lévesque for his technical assistance. This work was supported by the Natural Sciences and Engineering Research Council of Canada.

4.3.8 REFERENCES

[1] Zapka W., Ziemlich W. and Tam A. C., *Appl. Phys. Lett.*, **58**, 2217 (1991).

[2] Imen K., Lee S. J. and Allen S. D., *Appl. Phys. Lett.*, **58**, 203 (1991).

[3] Tam A. C., Leung W. P., Zapka W. and Ziemlich W., *J. Appl. Phys.*, **71**, 3515 (1992).

[4] Kelley J. D., Stuff M. I., Hovis F. E. and Linford G. J., *SPIE Proc.*, **1415**, 211 (1991).

[5] Park H. K., Grigoropoulos C. P., Leung W. P. and Tam A. C., *IEEE Trans. Com. Pack. Manuf. Technol.*, **A17**, 631 (1994).

[6] Heroux J. B., Boughaba S., Ressejac I., Sacher E. and Meunier M., *J. Appl. Phys.*, **79**, 2857 (1996).

[7] Boughaba S., Wu X., Sacher E. and Meunier M., *J. Adhesion,* **61**, 293 (1997).

[8] Krupp H., *Advan. Colloid Interface Sci.*, **1**, 111 (1967).

[9] Kitchener J. A., *J. Soc. Cosmet. Chem.*, **24**, 709 (1973).

[10] Bowling R. A., *J. Electrochem. Soc.*, **132**, 2209 (1985).

[11] Ranade M. B., *Aerosol Sci. Tech.*, 7, 161 (1987).

[12] Kelley J. D. and Hovis F. E., *Microelectron. Eng.*, **20**, 159 (1993).

[13] Lu Y. F., Song W. D., Ang B. W., Hong M. H., Chan D. S. H. and Low T. S., *Appl. Phys.*, **A65**, 9 (1997).

[14] Lu Y. F., Zhang Y., Song W. D., and Chan D. S. H., *Jpn. J. Appl. Phys.*, **37**, L1330 (1998).

[15] Wu X., Sacher E. and Meunier M., *J. Adhesion*, accepted

[16] Wu X., Sacher E. and Meunier M., *Proc. 22nd Annu. Mtg. Adhesion Soc.* (Adhesion Society, Blacksburg, VA, 1999), p. 277.

[17] Wu X., Sacher E. and Meunier M., *J. Appl. Phys.*, accepted

[18] Lifshitz E. M., *Sov. Phys. JETP,* **2**, 73 (1956).

[19] Johnson K. L., Kendall K. and Roberts A. D., *Proc. R. Soc. London,* **A324**, 301 (1971).

[20] Rimai D. S. and Demejo L. P., *Annu. Rev. Mater. Sci.,* **26**, 21 (1996).

[21] Krishnan S., Busnaina A. A., Rimai D. S. and Demejo L. P., *J. Adhesion Sci. Technol.*, **8**, 1357 (1994).

[22] Kipling J. J. and Peacall D. B., *J. Chem. Soc.*, **182**, 834 (1957).

[23] Iler P. K., *The Chemistry of Silica* (Wiley-Interscience, New York, 1970), pp. 373 and 387.

[24] Lide D. R. and Frederikse H. P. R. Eds. *CRC Handbook of Chemistry and Physics* (CRC Press, New York, 1996), p. 9-22.

[25] Joesten M.D. and Schaad L. J., *Hydrogen Bonding* (Marcel Dekker, Inc., New York, 1974), pp 36 and 38.

[26] Olovsson I. and Jonsson P. in *The Hydrogen Bond*, P. Schuster, Zandel G. and. Sandorfy C, Eds. (North-Holland, New York, 1976), Chap. 8.

[27] Schuster P., in *The Hydrogen Bond*, Schuster P., Zandel G. and Sandorfy C., Eds. (North-Holland, New York, 1976), p. 40.

[28] Israelachvili J., *Intermolecular and Surface Forces* (Academic, New York, 1991), Chap. 8.

[29] Burgreen D., *Elements of Thermal Stress Analysis* (C. P. Press, Jamaica, New York, 1971). pp. 77, 129 and 179.

[30] Aspnes D. E. and Studna A. A., *Phys. Rev.*, **B 27**, 985 (1983).

[31] Baeri P. and Campisano S. U. in *Laser Annealing of Semiconductors*, Poate J. M. and Mayer J. W., Eds. (Academic Press, Now York, 1982), chap. 4.

[32] Touloukian Y. S. Ed. *Thermophysical Properties of Matter* (IFI/ Plenum, New York-Washington, 1970, 1973, 1977), Vol. 4, 5 and 13.

[33] Holman J. P., Heat Transfer (McGraw-Hill, New York, 1997), pp. 2, 12, 13.

[34] Ozisik M. N., *Boundary Value Problem of Heat Conduction* (International Textbook, Scranton, Pennsyvania, 1968), pp. 402-405

[35] Hulst H., *Light Scattering by Small Particles* (Wiley, New York, 1957).

[36] Lazare S. and Gramier V., *Laser Chem.*, **10**, 25 (1989).

[37] Awazu K., Kawazve H. and Muta K., *J. Appl. Phys.*, **68**, 4183 (1991).

[38] Evans B. D., *J. Appl. Phys.*, **70**, 3995 (1991).

[39] Lu Y. F., Song W. D., Ye K. D., Lee Y. P., Chan D. S. H. and Low T. S., *Jpn. J. Appl. Phys.*, **36**, L1304 (1997).

[40] Stralen S. V. and Cole R., *Boiling Phenomena* (Hemisphere, Washington, 1979), vol. 1.

[41] Lyamshev L. M. and Naugol'nykh K. A., *Sov. Phys. Acoust.*, **27**, 357 (1982)

[42] Lide D. R. and Frederikse H. P. R. Eds. *CRC Handbook of Chemistry and Physics* (CRC Press, New York, 1996), pp. 6-10 and 6-16.

[43] Trevena D. H., *Cavitation and Tension in Liquids* (Adam Hilger, Bristol, 1987).

[44] Bardina J., in *Particles on Surface 1: Detection, Adhesion, and Removal*, Mittal K. L., ed. (Plenum Press, New York, 1988), pp. 329.

[45] Park H. K., Kim D., Grigoropoulos C. P. and Tam A. C., *J. Appl. Phys.*, **80**, 4072 (1996).

[46] Yavas O., Schilling A., Bischof J., Boneberg J. and Leiderer P., *Appl. Phys.*, **A64**, 331 (1997).

[47] Kinney G. F., *Explosive Shocks in Air* (Macmillan, Ney York, 1962).

[48] Carey V. P., *Liquid-Vapor Phase-Change Phenomena* (Hemisphere, Washington, 1992), p. 193.

[49] Davidson G. P. and Emmony D. C., *J. Phys. E: Sci. Instrum.*, **13**, 92 (1980).

[50] Paraskevopoulos G., Singleton D. L., Irwin R. S. and Taylor R. S., *J. Appl. Phys.*, **70**, 1938 (1991).

[51] Schaefer D. M., Carpenter M., Gady B., Reifenberger R., Demejo L. P. and Rimai D. S., *J. Adesion Sci. Technol.*, **9**, 1049 (1995).

[52] Fuller K. N. G. and Tabor D., *Proc. R. Soc. Lond.*, **A.345**, 327(1975).

[53] Czarnecki J. and Dabros T., *J. Colloid Interface Sci.*, **78,** 25(1980).

[54] Ohomori M., Yasutake M. and Wakiyama S., *J. Electrochem. Soc.*, **143**, 4125 (1996).

[55] Fujino N., Karino I., Kobayashi J. and Kuromoto K., *J. Electrochem. Soc.*, **143**, 4125 (1996).

Chapter 5

CONCLUSIONS AND FUTURE DIRECTIONS

In the first chapter of this thesis, we presented an overview of various aspects of semiconductor wafer contamination, discussing the contaminants types, origins and effects on semiconductor device quality and yield. An understanding of the principles underlying these various disciplines is, therefore, important for successfully solving wafer cleaning problems in the laboratory and during microelectronics fabrication. Several important technologies that are directly associated with wafer cleaning have been briefly reviewed. These technologies include both chemical and physical methods. Their advantages and disadvantages (or limitation) have also been presented.

The development of a new approach of wafer cleaning, laser cleaning, was reviewed in the first chapter also. Pulsed Nd:YAG, Er:YAG, CO_2 and excimer lasers have been used to remove micron- or even submicron-sized particles from a solid surface during dry or steam cleaning. These act on different materials, such as particle, substrate or coated liquid film, depending on the laser wavelength and material absorption. Among these laser cleaning techniques, excimer steam laser cleaning is the most efficient for the cleaning of small particles. A review of the theoretical studies on particle adhesion and removal were presented. The adhesion forces which hold the particles on the substrate

include van der Waals forces, electrostatic forces, capillary forces and chemical bonds. Chemical bonds are believed to play an important role in particle adhesion on silicon surfaces. However, a quantitative analysis of chemical bonding forces in particle adhesion is lacking. The removal forces come from the thermoelastic effect and liquid film explosive evaporation during steam cleaning. There are few direct descriptions of the removal force arising from liquid bubble generation. The goal of our research is also given in this chapter which is the development of experimental methods and theoretical models for the fundamental understanding of particle adhesion and removal during laser cleaning.

In the second chapter, we demonstrated the detail experimental procedure of removal of 0.1 μm PSL, 0.2 μm CML, 0.1 μm SiO_2 and Al_2O_3 particles from hydrophilic silicon surfaces by both dry and steam cleaning. Remarkable cleaning efficiencies have been achieved for 0.1 μm PSL and 0.2 μm CML particles during dry laser cleaning. High efficiencies for the laser cleaning of 0.1 μm SiO_2 and Al_2O_3 particles are observed only on steam cleaning, because the adhesion forces are greatly reduced, and the explosive evaporation of the deposited liquid film generates additional removal forces through bubble growth and collapse. A new technique, thermophoresis, used to prevent emitted particle recontamination, is introduced. While both gravity and laminar flow have been used to keep the emitted particles away from the cleaned surface, the calculations show

that the thermophoretic force acting on the particles smaller than 0.5 μm in a temperature gradient field is much greater that gravity. Thus, we calculate that the major recontamination mechanism, air flow fluctuation, can be overcome to a larger extent, and a larger fraction of the emitted particles will be kept from recontaminating the cleaned surface. The experimental results verify this theoretical prediction, permitting the cleaning efficiency to be greatly improved for dry cleaning. A comparison between thermophoresis and laminar flow techniques is carried out. Thermophoresis, whose temperature gradient is created by heating the wafer with an infrared lamp, has the advantages of being simple to set up and having a high cleaning efficiency.

In the third chapter, detailed Photoacoustic wave (PAW) measurements were presented. PAW measurements were performed to monitor the surface vibrations induced by the laser pulses during both dry and steam cleaning. It was found that steam laser cleaning generates higher PAW signals. These results help us to understand the mechanisms of laser cleaning. From the variations of the PAW signal amplitude with laser flux and distance between detection point and laser beam, we are led to suggest that the amplitude of the thermoelastic pulse in irradiated area is much stronger than that of PAW which was exited by this thermoelastic pulse and was detected at the backside of the wafer, the energy coupling from this thermoelastic pulse to the particles is more efficient than that from PAW at other places, the removal of PSL particles during dry cleaning is confined

in the laser beam. Localized removal during steam cleaning was explained by local bubble generation in the laser beam.

In the fifth chapter, brief calculation has show that the van der Waals forces between oxide particles and silicon surface are smaller than those of PSL particles because they have smaller contact area. These are in contradiction to the experimental results of cleaning efficiencies for dry and steam cleaning. This led us to consider hydrogen bonding adhesion forces between inorganic oxide particles and the hydrophilic silicon surface.

In the second section, we developed a model to calculate the adhesion forces due to hydrogen bonds between the hydroxylated surfaces of inorganic oxide particles and hydrophilic silicon surfaces. In this model, the particles can be directly bonded to the surface, by a single hydrogen bond, or indirectly, by a chain of hydrogen bonds. During steam cleaning, the chain of hydrogen bonds may be interrupted by water molecules, reducing the adhesion forces due to hydrogen bonding. The adhesion forces calculated according to our model can rationalize the experimental results of laser cleaning, in which PSL particles were easily removed by dry cleaning but SiO_2 and Al_2O_3 particles were not; high cleaning efficiencies for oxide particles were obtained only by steam cleaning. When we used alcohol as a dispersal agent instead of water, the cleaning efficiencies of SiO_2 and Al_2O_3 particles were greatly reduced during steam cleaning

because the hydrogen bonds formed with alcohol molecules have stronger interaction energies and are more difficult to interrupt by free water molecules during steam cleaning.

In the third section, the experimental results on the removal of submicron-sized polystyrene latex (PSL), carboxylate-modified latex (CML), SiO_2 and Al_2O_3 particles from hydrophilic silicon surfaces by excimer laser, using both dry and steam cleaning, were summarized. Then, cleaning thresholds were determined for these particles. The cleaning threshold for 0.1 μm PSL particles during dry cleaning is 76 mJ/cm^2, much lower than the optimal cleaning condition, 340 mJ/cm^2. During steam cleaning, 0.1 μm SiO_2 and Al_2O_3 particles have the same cleaning threshold, 143 mJ/cm^2, which is very close to optimal cleaning conditions and is the value of the lowest laser flux to induce the explosive evaporation of the liquid film deposited on the surface.

Several theoretical models of particle adhesion and removal were used to explain our excimer laser cleaning results in this chapter. The dominant adhesion force holding organic particles, such as PSL, to the surface is the van der Waals force with deformation. Hydrogen bonding between inorganic particles, such as Al_2O_3, and the substrate is the dominant contribution to adhesion forces for oxide particles. A deposited water film greatly reduces the adhesion forces due to the shielding effect of the van der Waals force and the breaking of the hydrogen bond chain between particle and surface.

The one-dimensional heat transfer equation was used to calculate the temperature distribution at the substrate; the temperature increase of the particles, and both heat convection and radiation losses at the substrate surface, were neglected because the particles have weak absorption at the excimer laser wavelength and energy losses at the surface are, therefore, much smaller than the incident laser energy. The laser pulse-generated thermoelastic effect of the heated substrate gives rise to the removal force on the particles during both dry and steam cleaning. During steam cleaning, an additional removal force, that due to bubble pressure, is created. Two models for the bubble removal force, the explosion and Lu model, are discussed and copared. We think that the explosion model is closer to the actual processing under steam laser cleaning conditions. A calculation for the bubble generated removal force is given which show that it is larger than that due to the thermoelastic effect.

Both particle surface asperities and particle aggregation markedly decrease the adhesion and the thermoelastic removal forces, although the bubble pressure removal force is not affected. Both the effective particle radius and multiple contact areas have been included in the theoretical models to take account of this situation. The models that describe the laser cleaning process consider the particle shape; they predict that particles with different surface roughnesses and shapes will have substantially different cleaning efficiencies during steam laser cleaning. The results of these calculations are found to fit our experimental results well.

The work contained in this thesis has resulted in the following papers and presentations:

(1) Boughaba S., Wu X., Sacher E. and Meunier M., Liquid Explosive Evaporation Removal of Submicron- sized particles from Silicon Surfaces, *Proc. 19th Annu. Mtg. Adhesion Soc.,* (Blacksburg, VA, 1996) p. 509.

(2) Boughaba S., Wu X., Sacher E. and Meunier M., Liquid Explosive Evaporation Removal of Submicron- sized particles from Silicon Surfaces, *J. Adhesion,* **61**, 293 (1997).

(3) Wu X., Sacher E. and Meunier M., Excimer Laser Induced Removal of Particles from Silicon Surfaces: Effects of Photoacoustic Waves, *Proc. 21th Annu. Mtg. Adhesion Soc.,* (Blacksburg, VA, 1998) p. 309.

(4) Wu X., Sacher E. and Meunier M., Excimer Laser induced Removal of Particles from Hydrophilic Silicon Surfaces, *J. Adhesion,* **70**, 167 (1999).

(5) Wu X., Sacher E. and Meunier M., Photoacoustic Waves Emission during Laser Enhanced Particle Removal, *Proc. 22th Annu. Mtg. Adhesion Soc.,* (Blacksburg, VA, 1999) p. 309.

(6) Invited talk, Wu X., Sacher E. and Meunier M., Photoacoustic Waves Emission during Laser Enhanced Particle Removal, Adhesion Sociaty Meeting, Panania City Beach, FL, Feb. 21-24, 1999.

(i) Wu X., Sacher E. and Meunier M., The Effects of Hydrogen Bonds on the Adhesion of Inorganic Oxide Particles On Hydrophilic silicon Surfaces, J. Appl. Phys., **86**, 1744 (1999).

(7) Wu X., Sacher E. and Meunier M., The Modeling of Excimer Laser Particle Removal from Hydrophilic Silicon Surfaces, J. Appl. Phys., submitted.

(8) Meunier M., Wu X., Sacher E., Beaudoin F., Simard-Normandin M., Excimer Laser Cleaning for Microelectronics: Modeling, Applications and Challenges, SPIE proceedings (Conference, San Jose, January 1999).

Finally, we will suggest some possible future research directions. We know that, even though the laser cleaning techniques have many advantages over traditional methods, they are still limited to the laboratory because the cleaning mechanisms are not clearly understood and some kinds of inorganic particles cannot be removed by laser cleaning. In our studies, we found that hydrogen bonds are the dominant adhesion force holding inorganic particles on silicon surfaces. Thus, future research should focus on finding some chemical materials (gas or liquid) which can break or weaken the hydrogen bonds before cleaning. In the fabrication of semiconductor microelectronics devices, the particles may deposit at only a few sites on the wafer. Scanning the total wafer surface to remove these particles is not the best method: it will take longer to clean, may damage uncontaminated area or increase the possibilities of recontamination during the laser cleaning processing. One solution to this problem is a combined laser cleaning and laser scanning surface inspection system to cleaning the contaminated area. When particles on the devices are to be cleaned, the damage to delicate parts induced by the laser cleaning

must be considered. The optimal cleaning conditions and procedures should be determined.

BIBLIOGRAPHY

Aspnes D. E. and Studna A. A. (1983). Dielectric functions and optical parameters of Si, Ge, GaP, GaAs, GaSb, InP, InAs, and InSb from 1.5 to 6.0 eV. Phys. Rev., B 27, 985-1009.

Awazu K., Kawazve H. and Muta K. (1991). Simulataneous geration of the 7.6-eV optical absorption band and F_2 molecule in fluorine doped silica glass under annealing. J. Appl. Phys., 69, 4183-4192.

Baeri P. and Campisano S. U. (1982). Heat flow calculation. Laser Annealing of Semiconductors, Poate J. M. and Mayer J. W., Eds. Academic Press, Now York, chap. 4.

Bardina J. (1988). Methods for surface particle removal: a comparative study. Particles on Surface 1: detection, Adhesion, and Removal. Mittal K. L., ed. Plenum Press, New York, 329-338.

Batchelor G. K. and Shen C. (1985). Thermophoretic deposition in gas flowing over cold surfaces. J. Colloid Interface Sci., 107, 21-37.

Bhattacharya S. and Mittal K. L. (1978). Mechanics of removing glass particulates from a solid surface. Surf. Technol., 7, 413-425.

Boughaba S., Wu X., Sacher E. and Meunier M. (1997). Liquid explosive evaporative removal of submicron particles from hydrophilic oxidized silicon surfaces. J. Adhesion, 61, 293-307.

Bowling R. A. (1985). An analysis of particle adhesion on semiconductor surfaces. J. Electrochem. Soc., 132, 2208-2214.

Brandrup J. and Immergut E. H., Eds. (1989). Polymer Handbook, Wiley-Interscience, New York, v/82.

Burgreen D. (1971). Element of Thermal Stress Analysis, C.P. Press, Jamaica, New York, 1–28, 77, 89–91, 129 and 179.

Busnaina A. A. Kashkoush I. I. And Gale G. W. (1995). An experimental study of megasonic cleaning of silicon wafers. J. Electrochem. Soc., 142, 2812-2817.

Carey V. P., *Liquid-Vapor Phase-Change Phenomena* (Hemisphere, Washington, 1992), p. 193.

Czarnecki J. and Dabros T. (1980). Attenuation of the van der waals attraction energy in the particle/semi-infinite medium system due to the roughness of the particle surface. J. Colloid Interface Sci., 78, 25-30.

Davidson G. P. and Emmony D. C. (1980). A schlieren probe method for the measurement of the refractive index profile of a shock wave in a fluid. J. Phys. E: Sci. Instrum., 13, 92-97.

Della Gatta G., Fubini B. and Venturello G. (1973). Water vapourheats of adsorption on η Al_2O_3. J. Chim. Phys. Chem., 70, 64-71.

Depasse J. and Watillon A. (1970). The stability of amorphous colloidal silica. J. Colloid Interface Sci., 33, 430-438.

Donovan R. P. and Menon V. B. (1993). Particle deposition and adhesion. Handbook of Semiconductor Wafer Cleaning Technology, Kern W. Ed. Noyer Publications, Park Ridge, New Jersey, 164-167.

Donovan R. P., Yamamoto T. and Periasamy R. (1993). Particle deposition, adhesion and removal. Mat. Res. Soc. Symp. Proc., 315, 3-23.

Doyle P. A. (1986). On epicentral waveforms for laser-generated ultrasound. J. Phys. D: Appl. Phys., 19, 1613-1623.

Dubois M., Enguehard F. and Bertrand L. (1994). Modeling of laser thermoelastic generation of ultrasound in an orthotropic medium. Appl. Phys. Lett., 64, 554-556.

Engelsberg A. C. (1988). Removal of surface contaminants by irradiation from a high-energy source. U.S. patents 5024968 and 5099557.

Enguehard F. and Bertrand L. (1997). Effects of optical penetration and laser pulse duration on laser generated longitudinal acoustic waves. J. Appl. Phys., 84, 1532-1538.

Evans B. D. (1991). Optical transmission in undoped crystalline α-Al_2O_3 grown by several techniques. J. Appl. Phys., 70, 3995-3997.

Fliszar S. (1990). On the dissociation of chemical bonds. Chemistry and Physics of Energetic Materials, Bulusu S. N. ed. Kluwer Academic Publishers, Amsterdam, 143-155.

Frank A. M. and Lovoi P. A. (1986). Method of and apparent for the removal of paint and the like from a substrate. U. S. Patent No. 4588885.

Fujino N., Karino I., Kobayashi J. and Kuromoto K. (1996). First observations of 0.1 μm size particles on Si wafers using atomic force microscopy and optical scattering. J. Electrochem. Soc., 143, 4125-4128.

Fuller K. N. G. and Tabor D. (1975). The effect of surface roughness on the adhesion of elastic solids. Proc. R. Soc. Lond., A345, 327-342.

Hattori T. (1990). Contamination control problems and prospects. Solid State Tech. July, S1-S8.

Heroux J. B., Boughaba S., Ressejac I., Sacher E. and Meunier M. (1996). CO_2 laser-assisted removal of submicron particles from solid surfaces. J. Appl. Phys., 79, 2857-2862.

Holman J. P. (1997). Heat Transfer, McGraw-Hill, New York, 2, 12 and 13.

Hulst H. (1957). Light Scattering by Small Particles, Wiley, New York.

Iler P. K., The Chemistry of Silica (Wiley-Interscience, New York, 1970), pp. 373, 387 and Chap. 6.

Imen K., Lee S. J. and Allen S. D. (1991). Laser-assisted micron scale particle removal. Appl. Phys. Lett., 58, 203-205.

Israelachvili J. (1991). Intermolecular and Surface Forces, Academic, New York, Chap. 8.

Jayarj S. (1995). Thermophoresis in laminar flow over cold inclined plates with variable properties. Heat Mass Transfer, 30, 167-173.

Joesten M.D. and Schaad L. J. (1974). Hydrogen Bonding, Marcel Dekker, Inc., New York, 36 and 38.

Johnson K. L., Kendall K. and Roberts A. D. (1971). Surface energy and the contact of elastic solid. Proc. R. Soc. London, A324, 301-313.

Kelley J. D. and Hovis F. E. (1993). A thermal detachment mechanism for particle removal from surfaces by pulsed laser irradiation. Microelectronic. Eng., 20, 159-170.

Kelley J. D., Stuff M. I., Hovis F. E. and Linford G. J. (1991). Removal of small particles from surfaces by pulsed laser irradiation: observations and a mechanism. SPIE Proc., 1415, 211-219.

Kern W. and Puotinen D. (1970). Cleaning solutions based on hydrogenperoxide for use in silicon semiconductor technology. RCA Rev., **32**, 187-207.

Kern W. (1993). Overview and evolution of semiconductor wafer contamination and cleaning technology. Handbook of Semiconductor Wafer Cleaning Technology. Kern W. Ed. Noyes Publications, Park Ridge, New Jersey, 3, 6-8 and 68.

Kern W. (1990). The evolution of silicon wafer cleaning technology. J. Electrochem. Soc., 137, 1887-1892.

Kinney G. F. (1962). Explosive Shocks in Air, Macmillan, New York.

Kitchener J. A. (1973). Surface forces in the deposition of small particles. J. Soc. Cosmet. Chem., 24, 709-725.

Knozinger H. (1976). Hydrogen bonds in systems of adsorbed molecules. The Hydrogen Bond, Schuster P., Zandel G. and Sandorfy C., Eds. North-Holland, New York, Chap. 27.

Kolomenskii A. K. and Maznev A. A. (1995). Propagation of laser-generated surface acoustic waves visualized by shake-off of fine particles. J. Appl. Phys., 77, 6052-6054.

Krishnan S., Busnaina A. A., Rimai D. S. and Demejo L. P. (1994). The adhesion-induced deformation and the removal of submicrometer particles. J. Adhesion Sci. Technol., 8, 1357-1370.

Krupp H. (1967). Particle adhesion theory and experiment. Advan. Colloid Interface Sci., 1, 111-239.

Lee S. J., Imen K., and Allen S. D. (1992). CO_2 assisted particle removal threshold measurements. Appl. Phys. Lett., 61, 2314-2316.

Leung W. P. and Tam A. C. (1992). Noncontact monitoring of laser ablation using a miniature piezoelectric probe to detect photoacoustic pulses in air. Appl. Phys. Lett., 60, 23-25.

Lide D. R. and Frederikse H. P. R. Eds. (1996). CRC Handbook of Chemistry and Physics, CRC Press, New York, 6-10, 6-16 and 9-22.

Lu Y. F., Song W. D., Ang B. W., Hong M. H., Chan D. S. H. and Low T. S. (1997). A theoretical model for laser removal of particles from solid surfaces. Appl. Phys., A65, 9-13.

Lu Y. F., Song W. D., Ye K. D., Lee Y. P., Chan D. S. H. and Low T. S. (1997). Acleaning model for removal of particles due to laser-induced thermal expansion of substrate surface. Jpn. J. Appl. Phys., 36, L1304-L1306.

Lu Y. F., Zhang Y., Song W. D., and Chan D. S. H. (1998). A theoretical model for laser cleaning of microparticles in a thin liquid layer. Jpn. J. Appl. Phys., 37, L1330-L1332.

Magee T. J. and Leung C. S. (1991). Scannin UV laser removal of contaminants from semiconductor and optical surface. Particles on Surfaces 3, Mittal K. L. ed. Plenum Press, New York, 307-317.

Mayer A. and Shwartzman S. (1979). Megasonic cleaning: a new cleaning and drying system for use in semiconductor processing. J. Electron. Mater., 8, 885-894.

McDonald F. A. (1989). Practical quantitative theory of photoacoustic pulse generation. Appl. Phys. Lett., 54, 1504-1506.

Menon V. B., Michaels L. D., Donovan R. P., and Ensor D. S. (1989). Effects of particulate size, composition, and medium on silicon wafer cleaning. Solid State Technol., 32, 57-62.

Moslehi M. M., Chapman R. A., Wong M., Paranipe A., Najm H. N., Kuene J., Yeakley R. L. and Davis C. J. (1992). RTP for advanced CMOS process integration. IEEE Trans. Electron Dev., 39, 4-32.

Ohomori M., Yasutake M. and Wakiyama S. (1996). First observation of 0.1 μm size particles on Si wafers using atomic force microscopy and optical scattering. J. Electrochem. Soc., 143, 4125-4128.

Ohyama T., Endoh K., Mikami A. and Mori Y. (1988). Optical interferometry for measuring instantaneous thickness of transparent solid and liquid films. Rev. Sci. Instrum., 59, 2018-2022.

Okkerse C. (1970). hysical and Chemical Aspects of Adsorbents and Catalysis, Academic, New York, London, 251.

Olovsson I. and Jonsson P. (1976). X-ray and neutron difraction studies of hydrogen bonded systems. The Hydrogen Bond, P. Schuster, Zandel G. and. Sandorfy C, Eds. North-Holland, New York, 393-456.

Ozisik M. N. (1968). Boundary Value Problem of Heat Conduction, International Textbook, Scranton, Pennsyvania, 402-405.

Paraskevopoulos G., Singleton D. L., Irwin R. S. and Taylor R. S. (1991). Time-resolved reflectivity as a probe of the dynamics of laser ablation of organic polymers. J. Appl. Phys., 70, 1938-1946.

Park H. K., Grigoropoulos C. P., Leung W. P. and Tam A. C. (1994). A pratical excimer laser-based cleaning tool for removal of surface contaminants. IEEE Trans. Com. Pack. Manuf. Technol., A17, 631-643.

Park H. K., Kim D., Grigoropoulos C. P. and Tam A. C. (1996). Pressure generation and measurement in the rapid vaporization of water on a pulsed-laser-heated surface. J. Appl. Phys., 80, 4072-4081.

Pauling L. (1960). The Natural of the Chemical Bond and the Structure of Molecules and Crystal, Cornell Univ. Press, New York, Chap. 12.

Peschel G. and Aldfinger K. H. (1970). Viscosity anomalies in liquid surface zones IV: The apparent viscosity of water in thin layers adjacent to hydroxylated fused silica surfaces. J. Colloid Interface Sci., 34, 505-510.

Pimentel G. C. and McClellan A. L. (1960). The Hydrogen Bond, Freeman, San Francisco.

Ranade M. B. (1987). Adhesion and removal of fine particles on surface. Aerosol Sci. Tech., 7, 161-176.

Rimai D. S. and Demejo L. P. (1996). Physical interactions affecting the adhesion of dry particles. Annu. Rev. Mater. Sci., 26, 21-41.

Schaefer D. M., Carpenter M., Gady B., Reifenberger R., Demejo L. P. and Rimai D. S. (1995). Surface roughness and its influence on particle adhesion using atomic force techniques. J. Adesion Sci. Technol., 9, 1049-1062.

Schuster P. (1976). Energy surfaces for hydrogen bonded systems. The Hydrogen Bond, Schuster P., Zandel G. and Sandorfy C., Ed. North-Holland, New York, 40-108.

Sears F. W., Zemansky M. W. and Young H. D. (1982). College Physics, Addison-Wesley Publishing Co., Reading, Massachusetts, Menlo Park, California, 254.

Shwartzman S., Mayer A. and Kern W. (1985). megasonic particle removal from solid-state wafers. RCA Rev., 46, 81-105.

Stowers I. F. and Patton H. G. (1979). Surface Contamination: Genesis, Detection, and Control, Plenum Press, New York, Vol. 1, 341-349.

Stralen S. V. and Cole R. (1979). Boiling Phenomena. Hemisphere, Washinton, vol. 1, 104.

Sugino R., Okui Y., Okuno M., Shigeno M., Sato Y., Ohsawa A. and Ito T. (1992). Removal of Fe and Al on a silicon surface using UV-excited dry cleaning. IEICE Trans. Electron., E75-C, 829-833.

Tam A. C., Leung W. P., Zapka W. and Ziemlich W. (1992). Laser-cleaning techniques for removal of surface particulates. J. Appl. Phys., 71, 3515-3525.

Tipton C. M. and Bowlig R. A. (1992). in Proc. First Intern. Symp. On Cleaning Technol. In Semicond. Dev. Manufacturing, Pennington, N. J., Ruzyllo J. and Novak R., eds, 170-178.

Tolliver D. (1993). Trace chemical contamination on silicon surface. Handbook of Semiconductor Wafer Cleaning Technology. Kern W., ed. Noyes Publications, Park Ridge, New Jersey, 68-69.

Touloukian Y. S. Ed. (1970, 1973, 1977). Thermophysical Properties of Matter, IFI/ Plenum, New York-Washington, Vol. 4, 5 and 13.

Trevena D. H. (1987). Cavitation and Tension in Liquids, Adam Hilger, Bristol.

Willams M. M. R. (1988). The thermophoretic force between a sphere and a plane surface. J. Colloid Interface Sci., 122, 110-119.

Wu X., Sacher E. and Meunier M. (1998). Excimer laser-induced removal of particles from silicon surfaces: effects of photoacoustic waves. Proc. of Adhesion Society, Savannah, Georgia, Feb. Dickie R. A. Ed., 309-311.

Wu X., Sacher E. and Meunier M. (1999). Excimer laser induced removal of particles from hydrophilic silicon surfaces. J. Adhesion, 70, 167-178.

Wu X., Sacher E. and Meunier M. (1999). The effects of hydrogen bonds on the adhesion of inorganic oxide particles on hydrophilic silicon surfaces. J. Appl. Phys., 86, 1744-1748.

Wu X., Sacher E. and Meunier M. (1999). Photoacoustic wave emission during laser-enhanced particulate removal. Proc. 22nd Annu. Mtg. Adhesion Soc., Adhesion Society, Blacksburg, VA, 277-279.

Yavas O., Leiferer P., Park H. K., Grigoropoulos C. P., Poon C. C., Leung W. P., Do N. and Tam A. C. (1994). Optical and acoustic study of nucleation and growth of bubble at

a liquid-solid interface induced by nanosecond-pulsed-laser heating. Appl. Phys., A58, 407-415.

Yavas O., Schilling A., Bischof J., Boneberg J. and Leiderer P. (1997). Bubble nucleation and pressure generation during laser cleaning of surfaces. Appl. Phys., A64, 331-339.

Ye Y., Pui D. Y., Lui B. Y. H., Opiolka S., Blumhorst S., and Fissan H. (1991). Thermophoretic effect of particle deposition on a free standing semiconductor wafer in a clean room. J. Aerosol Sci., 22, 63-72.

Zapka W., Ziemlich W. and Tam A. C. (1991). Efficient pulsed laser removal of 0.2 μm sized particles from a solid surface. Appl. Phys. Lett., 58, 2217-2219.

Zapka W., Ziemlich W., Leung W. P., and Tam A. C. (1993). Laser cleaning removes particles from surface. Microelectronic. Eng., 20, 171-183.

Appendix: Physical and chemical Properties of Si, SiO_2, Al_2O_3 and PSL

Properties	Si	SiO_2	Al_2O_3	PSL
Water contact angle θ	0°	0°	0°	91°
Lifshitz-van der Waals constant $h\varpi_{132}$ (eV, on Si, in air)	6.76	3.88	5.62	3.59
Lifshitz-van der Waals constant $h\varpi_{132}$ (eV, on Si, in water)	3.49	1.25	1.62	1.01
Surface free energy γ^s (mJ/m^2)	825	700	665	52
Younh's modulus E (GPa)	162	73	400	1.26
Poisson's ratio ν	0.22	0.17	0.24	0.33
Hydroxyl groups density D (OH/nm^2)	-	4.6 ± 0.2	12.5	0
Average length of hydrogen bond chain Δz_b (⊕)	-	7.21	7.05	-
Optical absorption coefficient at 248 nm α (cm^{-1})	1.81×10^6	5	10	6.3×10^3
Surface reflectivity at 248 nm	0.675	0.04	0.075	0.03
Density ρ (g/cm^3)	2.33	2.65	3.99	1.12
Specific heat C_p (KJ/KgK)	0.7	0.8	0.9	1.2
Thermal conductivity κ (W/Km)	148	10.4	46	0.11
Linear thermal expansion coefficient γ (K^{-1})	4.68×10^{-6}	1.0×10^{-5}	5.5×10^{-6}	7.0×10^{-5}